JPL D-18911/CL#04-2084
EOS MLS DRL 601 (part 8)
ATBD-MLS-08

Earth Observing System (EOS)

Microwave Limb Sounder (MLS)

EOS MLS Level 3 Algorithm Theoretical Basis

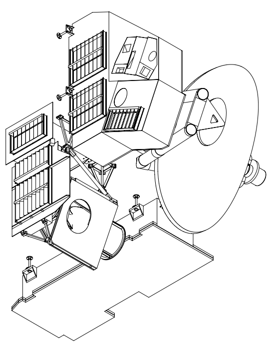

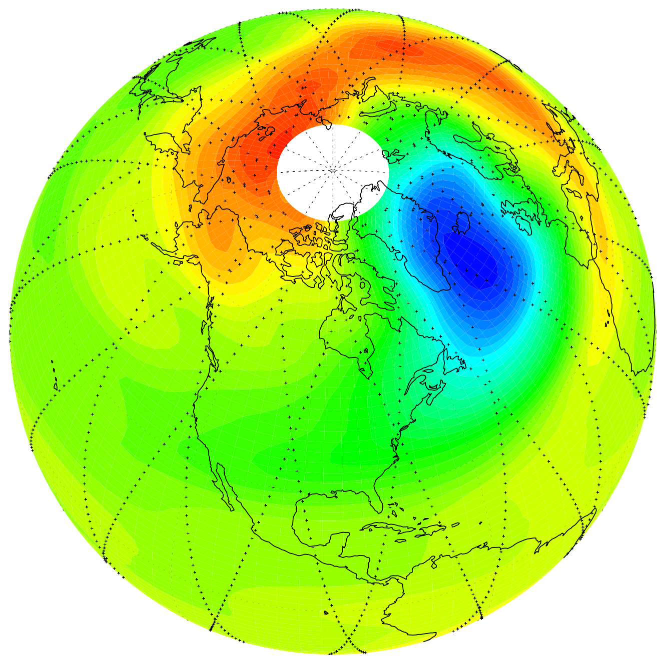

Yibo Jiang

Version 1.0

June 21, 2004

Jet Propulsion Laboratory
California Institute of Technology
Pasadena, California 91109-8099

Release Record

Version	date released	comments
1.0	June 21, 2004	Initial Release

TABLE OF CONTENTS

1. INTRODUCTION 1

1.1 The EOS MLS Experiment 1

1.2 The purpose of this document 3

1.3 EOS MLS data products for which this document applies 3

1.3.1 Level 3 daily map products 3

1.3.2 Level 3 daily zonal mean products 3

1.3.3 Level 3 monthly map products 3

1.3.4 Level 3 monthly zonal mean products 4

2. OVERVIEW OF EOS MLS LEVEL 3 DATA PROCESSING 5

3. EOS MLS LEVEL 3 DATA PROCESSING ALGORITHMS 8

3.1 Daily map products 8

3.1.1 Algorithms for converting Level 2 data to nominal latitude grids 8

3.1.2 Algorithms for producing daily maps 9

3.1.2.1 Introduction 9

3.1.2.2 Discrete Fourier transform and aliasing 11

3.1.2.3 Sampling geometry and coordinate rotation 13

3.1.2.4 Fast Fourier synoptic mapping 16

3.1.2.5 Explicit formulation of FFSM in *combined* mode 19

3.1.2.6 Explicit formulation of FFSM in *single* mode 22

3.1.2.7 Uncertainty Estimate 23

3.1.2.8 Procedure and data processing 26

3.1.2.9 Issues and limitations 30

3.1.2.10 Algorithm testing 31

3.1.2.11 Diagnostics 31

3.2 Daily zonal mean products 34

3.2.1 Algorithms 34

3.2.2 Diagnostics 34

3.3 Monthly map products 35

3.3.1 Algorithms 35

3.3.2 Diagnostics 35

3.4 Monthly zonal mean products 35

3.4.1 Algorithms 35

3.4.2 Diagnostics 35

4. ADDITIONAL TOPICS 36

4.1 Tuning of algorithms and strategy for post-launch operations 36

4.2 Quality control, exception handling and related issues 36

4.2.1 Quality of products 36

4.2.2 Bad or missing data 36

4.2.3 Numerical exceptions 36

4.3 Validation of Level 3 algorithms and data products 37

4.4 Data volumes 37

APPENDIX A. USER INPUT FILE INFORMATION 38

APPENDIX B. DATA VOLUME ESTIMATES 40

B.1 Output files of daily maps, diagnostics, and their FFSM spectra 40
B.2 Output files of monthly maps 40
B.3 Output files of daily zonal means and monthly zonal means 40

APPENDIX C. DERIVATION OF CERTAIN FORMULAE 44

C.1 Derivation of Eqn. (3-10) 44
C.2 Derivation of Eqn. (3-13) 44
C.3 Derivation of Eqn. (3-21) 45
C.4 Derivation of Eqn. (3-22) 46

APPENDIX D. EXAMPLES OF RESULTS FROM LEVEL 3 SOFTWARE 48

D.1 Daily Maps 48
D.1.1 Daily Maps from Synthetic Wave Patterns 48
D.1.2 Daily Maps from Edinburgh University SLIMCAT Chemical Transport Model 50
D.1.3 Daily Maps vs. Input Window Size 53

APPENDIX E. EXAMPLES OF LEVEL 3 DATA INSPECTION PLOTS 55

E.1 Daily Maps 55
E.1.1 Polar Projections (1 page) and Cylindrical Projections (1 page) of Level 2 Residuals and Reconstructed Fields 55
E.1.2 Longitude-Height Cross Sections (1 page) 55
E.1.3 Curtain Plots of Residual between Level 2 and Reconstructed Level 2 (1 pages) 55
E.1.4 Polar Projections (1 page) and Cylindrical Projections (1 page) of Level 3 Precision Estimates 55
E.1.5 Spectra Plots 56
E.1.6 Spectra Plots of Precision Estimates 56

E.2 Monthly Maps 57
E.2.1 Polar Projections (1 page) and Cylindrical Projections (1 page) 57
E.2.2 Longitude-Height Cross Sections (1 page) 57

E.3 Daily Zonal Means 57
E.3.1 Longitude-Height Cross Sections (1 page) 57

E.4 Monthly Zonal Means 57
E.4.1 Longitude-Height Cross Sections (1 page) 57

REFERENCES 120

1. Introduction

1.1 The EOS MLS Experiment

EOS MLS is an experiment on the NASA EOS Aura satellite mission currently scheduled for launch in early 2004, with an operational period extending 5 years or longer after launch. The overall objective of EOS MLS is to help provide measurements and information that are needed for improving understanding of global change in Earth's stratosphere, upper troposphere and mesosphere

EOS MLS is a greatly enhanced version of the Upper Atmosphere Research Satellite (UARS) MLS experiment. It provides measurements of several stratospheric chemical species (O_3, H_2O, OH, HO_2, CO, HCN, N_2O, HNO_3, HCl, HOCl, ClO, BrO, volcanically-injected SO_2), temperature and geopotential height. It measures upper tropospheric H_2O, temperature, O_3, CO, HCN, N_2O, HCl, cloud ice and geopotential height. Mesospheric temperature, H_2O, OH, HO_2, O_3, HCl, CO and geopotential height are measured to provide information on this higher region of Earth's atmosphere.

The EOS Aura orbit is sun-synchronous at 705 km altitude with a 98^o inclination and 1:45 p.m. ascending equator-crossing time. MLS performs observations with the instrument fields-of-view scanning the limb in the orbit plane to provide 82^o N to 82^o S latitude coverage on each orbit.

The limb scans for nominal operation are synchronized to the orbit (using the node-crossing signal from the spacecraft), with the number of scans per orbit an integer multiple of 4, and phased such that limb scan locations occur over the equator. This gives the same latitude sampling in the northern and southern hemispheres, and on the ascending and descending portions of the orbit. MLS nominal operations have 240 limb scans per orbit to give 1.5^o (165 km) along-track separation between adjacent limb scans; this separation is well-matched to the along-track resolution expected for upper tropospheric water vapor measurements. Figure 1-1 shows the locations of measurements with this scan pattern for one 24-hour period.

Figure 1-1. EOS MLS measurement locations for a 24 hour period. Each cross gives the location of the tangent points for individual limb scans. The continuous line is the suborbital track, which is slightly displaced from the tangent points because of Earth's rotation during the time in which the satellite moves forward to the tangent point latitude. The ascending portions of the orbit are those with the southeast-northwest tilt. Daily coverage at high latitudes in the Southern Hemisphere is analogous to that of the Northern Hemisphere shown here. R.R. Lay prepared this figure.

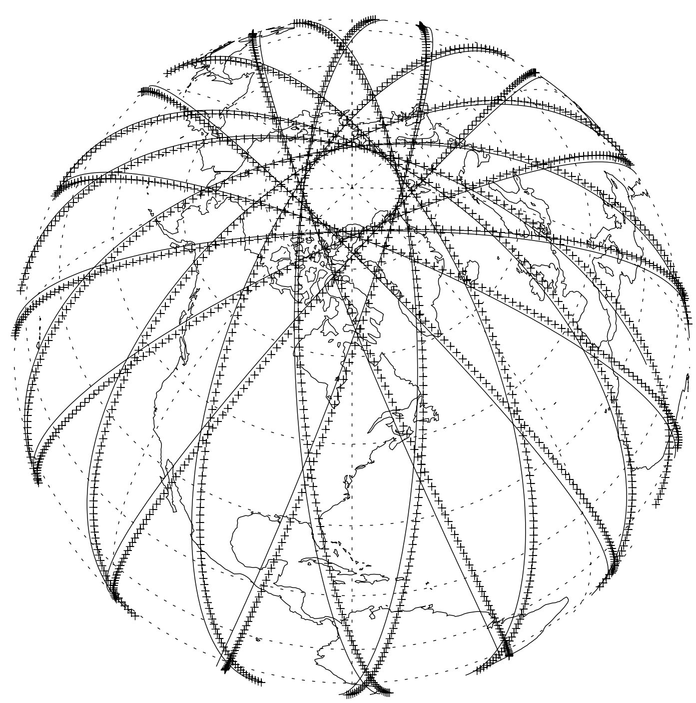

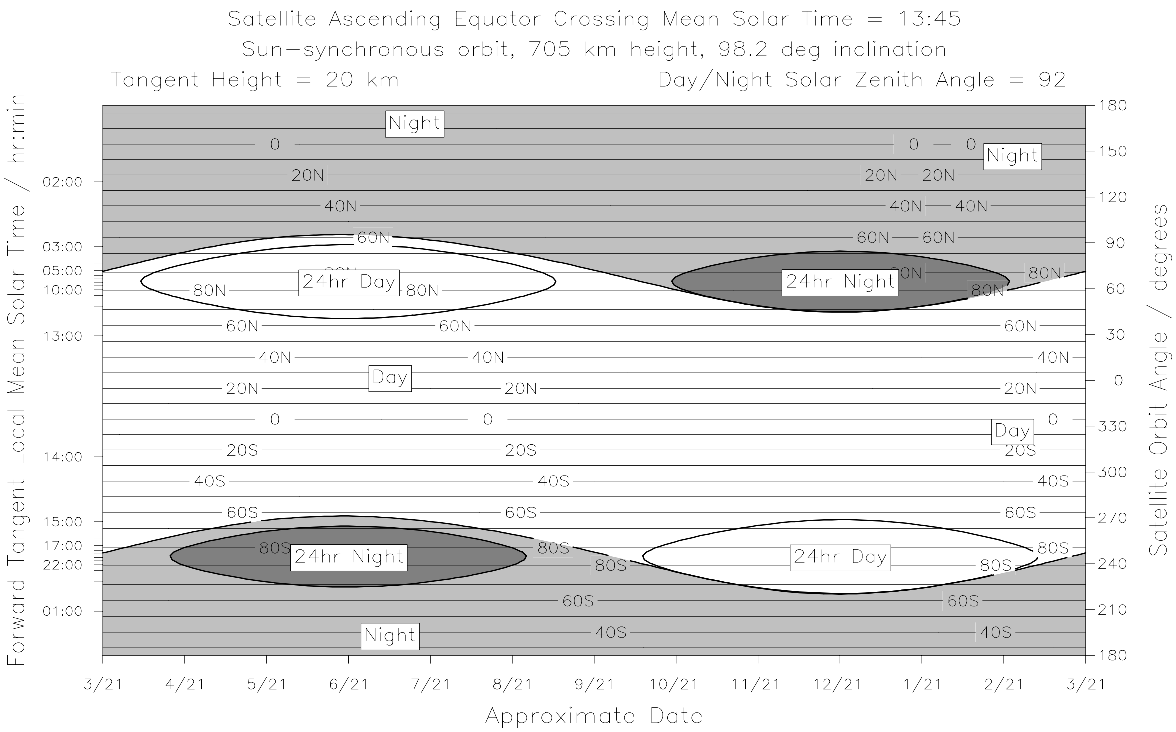

Figure 1-2. Variation, over an annual cycle, of the latitude range where MLS measurements are in day and in night. The horizontal axis gives the approximate date. The right hand vertical axis gives the orbit angle (defined as zero when the satellite is over the equator); the left hand vertical axis gives the corresponding local mean solar time at the (forward) tangent point of MLS observations. Horizontal lines give the latitude of the MLS tangent point, and the day-night boundary is defined as 92^{o} local solar zenith angle. M.J. Filipiak prepared this figure.

As the EOS Aura orbit is sun-synchronous (i.e., the orbit plane has a constant orientation relative to the Earth-Sun line), MLS observations at a given latitude on either the ascending (north-going) or descending (south-going) portions of the orbit have the same local solar time throughout the mission as indicated in Figure 1-2. The local solar zenith angle at a given latitude, and the boundaries between the day and night portions of the orbit, vary around an annual cycle as shown in Figure 1-2.

Data from EOS MLS are routinely processed to various 'Levels' as follow

- 'Level 1' data are calibrated radiances and engineering data from the instrument, with ancillary data such as time, location, satellite attitude, etc. The Level 1B data are in daily files, each covering 0-24 hours GMT. Jarnot [2004] gives the theoretical basis for the EOS MLS Level 1 data processing algorithms.
- 'Level 2' data are vertical profiles of geophysical parameters (and their uncertainties) retrieved at the nominal limb scan locations, along with ancillary and diagnostic data such as time, location, local solar time, solar zenith angle, etc. The Level 2 data are in daily files, each covering 0-24 hours GMT. Livesey and Snyder [2004] give the theoretical basis for the retrieval processes algorithms used in EOS MLS Level 2 data processing.
- Level 3' data are 'gridded' products that include:
  (1) daily global maps for measurements having sufficiently high signal to noise,
  (2) monthly mean global maps for all Level 2 geophysical products,
  (3) daily zonal means for all Level 2 geophysical products, and
  (4) monthly zonal means for all Level 2 geophysical products.

The EOS MLS 'Overview' document [*Waters*, 2004] gives additional overall information on the EOS MLS experiment.

1.2 The purpose of this document

The purpose of this document is to give the theoretical basis for algorithms used to produce all Level 3 products for those EOS MLS measurements that have sufficiently high signal-to-noise to produce useful daily maps. These products are listed in section 1.3, and will be produced using only the MLS Level 2 data files as inputs.

Algorithms for producing MLS Level 3 products from the other MLS measurements, the 'noisy' measurements, are described in Livesey and Snyder [2004]. Those Level 3 products are produced directly from the MLS Level 1 data

It should be noted that, although the algorithms described here are developed for those MLS measurements with sufficiently high signal-to-noise, they can also be used with *any* MLS Level 2 file as input. This provides needed flexibility for producing daily maps for MLS measurements whose signal-to-noise may be better than now expected. It also provides cross-checking of the zonal mean and monthly mean maps to be routinely produced using the other algorithms mentioned above for 'noisy' measurements.

1.3 EOS MLS data products for which this document applies

1.3.1 Level 3 daily map products

Table 1-1 gives the currently-planned EOS MLS Level 3 routine daily map products for which this document applies. Separate maps for data from the ascending and descending portions of the orbit will be made for the diurnally-varying species ClO, OH, and O_3 at higher altitudes. These maps are produced at the 2^o latitude by 4^o longitude grid.

1.3.2 Level 3 daily zonal mean products

Daily zonal mean products, using algorithms described in this document, will be produced for all the daily map products listed in Table 1-1. Current plans are to produce separate zonal means for the ascending (mostly day) and descending (mostly night) portions for each product, and the full latitudinal resolution of the corresponding Level 2 product is maintained (i.e., a zonal mean is produced for each of the nominal Level 2 latitudes), which gives better latitude resolution at high latitudes than in the Level 3 daily maps. The value and estimated precision in the daily zonal mean are included in the data files. Ancillary data included with the geophysical parameters are latitude, local solar time and local solar zenith angle.

1.3.3 Level 3 monthly map products

Level 3 monthly map products, using algorithms described in this document, will be produced for all the daily map products listed in Table 1-1. These maps represent average conditions for the month and are produced at the 2^o latitude by 4^o longitude grid used for the Level 3 daily maps. Separate maps for the ascending and descending sides of the orbit will be produced for diurnally-varying species, as done for the daily maps. The 'months' for these maps are calendar months.

Table 1-1. Level 3 Daily Map Products. The number of pressure surfaces, and volumes, assume the maximum 6 retrieval points per decade pressure, and 4-byte words for the value and precision at each grid point. GPH is geopotential height, IWC is ice water content, and RHI is relative humidity with respect to ice.

product name	units	vertical range				number of pressure surfaces	volume for one day / Megabytes
		pressure / hPa		~ height / km			
		max	min	min	max		
TEMPERATURE	K	464	0.01	0	80	56	6.20
CO	Vmr	464	0.01	0	80	56	6.20
H2O	Vmr	464	0.01	0	80	56	6.20
HNO3	Vmr	100	1	15	50	24	4.39
O3	Vmr	316	0.316	9	55	36	4.65
O3_ascending	Vmr	3.16	0.01	40	80	30	4.65
O3_descending	Vmr	3.16	0.01	40	80	30	4.65
HCl	Vmr	100	0.1	15	65	36	5.11
N2O	Vmr	215	1	9	50	28	4.57
ClO_ascending	Vmr	100	1	15	50	24	4.08
ClO_descending	Vmr	100	1	15	50	24	4.08
OH_ascending	Vmr	10	0.1	15	65	24	4.08
OH_descending	Vmr	10	0.1	15	65	24	4.08
HCN	Vmr	215	22	9	25	12	3.55
GPH	km	464	0.01	0	80	56	6.20
IWC	$g \bullet m^{-3}$	1000	46	0	20	9	6.20
RHI	%	1000	46	0	20	9	6.20
O3_STRAT_COLUMN	DU	not applicable					0.06
total daily volume							85.15

1.3.4 Level 3 monthly zonal mean products

Level 3 monthly zonal mean products, using algorithms described in this document, will be produced for all the daily map products listed in Table 1-1. As in the daily zonal mean products, current plans are to produce separate zonal means for the ascending (mostly day) and descending (mostly night) portions of the orbit, with the full latitudinal resolution of the corresponding Level 2 product. The value and estimated precision in the monthly zonal mean are included in the data files. Ancillary data included with the geophysical parameters are latitude, and maximum and minimum values of the local solar time and local solar zenith angle for the measurement over the course of the month.

2. Overview of EOS MLS Level 3 Data Processing

Fast Fourier Synoptic Mapping (FFSM) techniques, initially developed by Salby [1982 a, b] will be used to produce 'synoptic' maps as the Level 3 daily map product for measurements with sufficiently high signal-to-noise. This technique, which yields the exact transform of the data with no distortions of fast-moving waves or aliasing from high-frequency components of non-sinusoidal features, has been found to be robust under reasonable conditions of randomly varying signals, sampling errors and missing data points. It has been applied previously to map data from the stratospheric sounding unit (SSU) [*Lait and Stanford*, 1988ab], as well as to measurements of various UARS instruments [*Elson and Froidevaux*, 1993; *Elson et al.*, 1994; *Canziani et al*., 1994; *Sassi and Salby*, 1998, *Limpasuvan and Wu*, 2003]. FFSM is distinguished from other approaches [e.g., *Hartmann*, 1976; *Rodgers*, 1976; *Chapman* and *McGregor*, 1978; *Hayashi*, 1983] by its sole reliance on the asynoptic measurements and their sampling in space and time. It presumes nothing of the behavior to be determined nor of the governing equations of the fields that determine the observed behavior. This procedure recovers the actual synoptic structure and evolution as long as the field property being observed is adequately sampled [*Salby and Hayashi*, 1985]. The current plan is for a map output grid of 4^o longitude by 2^o latitude (between 82 N and 82 S), and with the daily maps produced for a time corresponding to 12:00 UT.

Since this technique requires at least several days of measurements to produce a map for a single day, the MLS Science Team has decided to do the Level 3 processing on a monthly basis. This allows all the Level 3 products (including monthly maps and zonal means) to be produced during the same processing step. 'Quick-look' algorithms used by the MLS team for near-real-time inspection will be developed, whose description is not within the scope of this document, for use on the MLS Science Computing Facility (SCF) to produce maps needed for 'quick-look' inspection of the Level 2 data.

Figure 2-1 shows an overview of the MLS Level 3 processing. The principal component of the Level 3 data processing to produce daily maps is the FFSM algorithm mentioned above and described later in section 3.1. The monthly map, and daily and monthly zonal means, will be produced by other algorithms discussed in section 3.2, 3.3, and 3.4. Special algorithms for producing zonal means of 'noisy products' are discussed by Livesey and Snyder [2004]. Inputs to the Level 3 processing are (1) the MLS Level 2 data and (2) a user input file which contains parameters that control the processing (see Appendix A).

The MLS Level 2 dataset is first interpolated to two pre-set latitude grids, with the 2-D interpolation in time and space domain. One grid has points at the latitudes that will be used for the Level 3 maps. The other is a grid at the nominal Level 2 latitudes, which is needed for producing zonal means at the full Level 2 latitude resolution. There are three processing steps from here: 1) daily maps on nominal Level 3 latitude and longitude grid; 2) monthly maps on nominal Level 3 latitude and longitude grid; and 3) daily and monthly zonal means at nominal Level 2 latitudes. In all the processes, the entire aggregate of species (both dynamical and chemical) and vertical levels can be processed in parallel.

Before the FFSM is invoked, the Level 2 data for each latitude and pressure level are 'initialized'. This process includes sorting data into chronological order and into ascending and descending sequences, and data preprocessing (such as interpolation and missing data handling). These preprocessed data are then fed into FFSM modules. The outputs from FFSM are Fourier coefficients for longitude and time for all products at each latitude and pressure level. The final step is to calculate fields for the daily maps and daily zonal mean from the FFSM output, and monthly maps and monthly zonal mean from averaging one month data from Level 2, and appropriate diagnostic information.

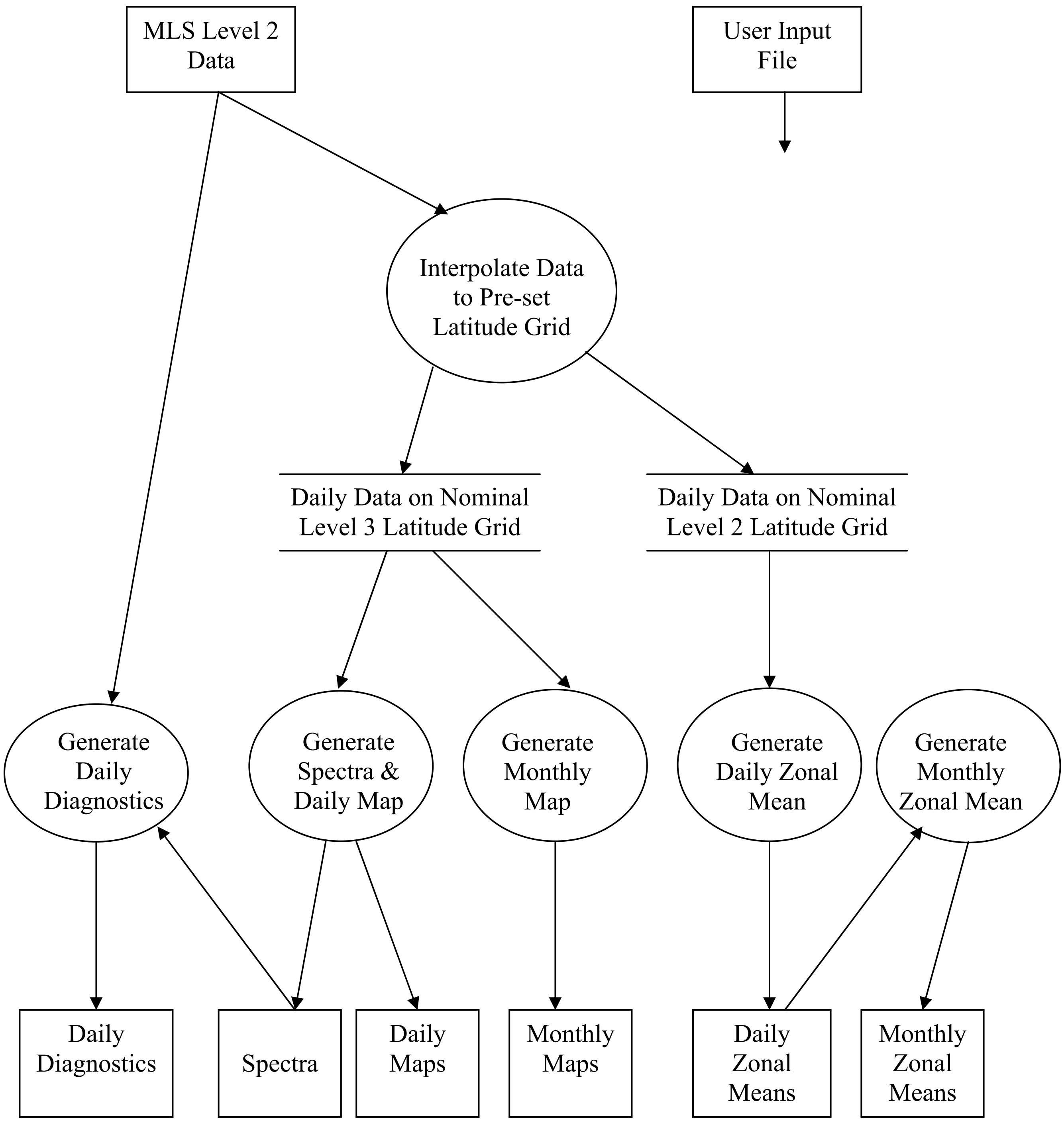

Figure 2-1. Overview of the EOS MLS Level 3 data processing whose algorithms are described in this document.

3. EOS MLS Level 3 Data Processing Algorithms

In this section, the details of the Fast Fourier Synoptic Mapping (FFSM) technique are described. We demonstrate the technique by using simple theoretical fields and atmospheric model data. We also discuss the implementation and efficiency of the algorithm. Finally, some limitations of the technique are discussed.

3.1 Daily map products

3.1.1 Algorithms for converting Level 2 data to nominal latitude grids

As mentioned earlier the EOS MLS Level 2 data are nominally produced every 1.5 degrees along the suborbital path. The Level 2 latitude spacing thus varies from approximately 1.5 degrees at the equator to only a few tenths of degree near the orbit 'turn around' points (near 82 degree latitude), as shown in Figure 3-1.

The Level 2 data must be interpolated to the nominal latitudes (0, ±2, ±4, ... degrees) for the Level

orbit_inclination = 98.2 degrees
no_scans_per_orbit = 240
_spacing_along_track = 1.5 degrees

index	orbit angle	latitude	latitude spacing
1	0.0	0.0	1.48
2	1.5	1.5	1.48
3	3.0	3.0	1.48
4	4.5	4.5	1.48
5	6.0	5.9	1.48
6	7.5	7.4	1.48
7	9.0	8.9	1.48
8	10.5	10.4	1.48
9	12.0	11.9	1.48
10	13.5	13.4	1.48
11	15.0	14.8	1.48
12	16.5	16.3	1.48
13	18.0	17.8	1.48
14	19.5	19.3	1.48
15	21.0	20.8	1.48
16	22.5	22.3	1.48
17	24.0	23.7	1.48
18	25.5	25.2	1.48
19	27.0	26.7	1.48
20	28.5	28.2	1.48
21	30.0	29.7	1.48
22	31.5	31.1	1.48
23	33.0	32.6	1.48
24	34.5	34.1	1.48
25	36.0	35.6	1.48
26	37.5	37.1	1.48
27	39.0	38.5	1.48
28	40.5	40.0	1.47
29	42.0	41.5	1.47
30	43.5	42.9	1.47
31	45.0	44.4	1.47
32	46.5	45.9	1.47
33	48.0	47.4	1.47
34	49.5	48.8	1.47
35	51.0	50.3	1.46
36	52.5	51.7	1.46
37	54.0	53.2	1.46
38	55.5	54.7	1.46
39	57.0	56.1	1.45
40	58.5	57.6	1.45
41	60.0	59.0	1.44
42	61.5	60.4	1.44
43	63.0	61.9	1.43
44	64.5	63.3	1.43
45	66.0	64.7	1.42
46	67.5	66.1	1.41
47	69.0	67.5	1.40
48	70.5	68.9	1.38
49	72.0	70.3	1.37
50	73.5	71.6	1.35
51	75.0	73.0	1.32
52	76.5	74.2	1.29
53	78.0	75.5	1.26
54	79.5	76.7	1.21
55	81.0	77.8	1.14
56	82.5	78.9	1.06
57	84.0	79.9	0.95
58	85.5	80.7	0.80
59	87.0	81.3	0.62
60	88.5	81.7	0.39
61	90.0	81.8	0.14

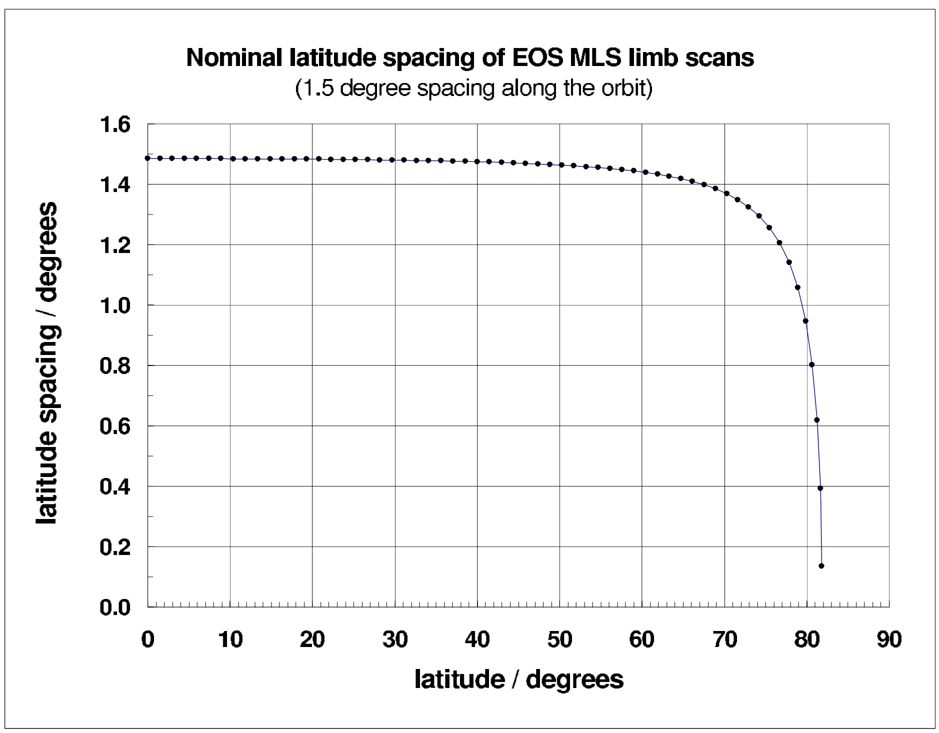

latitude = arcsin(sin(orbit inclination)*sin(orbit angle, where 0 orbit angle is at equator))

Figure 3-1. Latitude spacing between adjacent Level 2 data. Latitude of a measurement is related to the orbit angle α (defined as zero when measurement point is over the equator) by $\theta = \sin^{-1}\{\sin\beta \times \sin\alpha\}$, where β is the orbit inclination (98.2 degrees for EOS CHEM). Nominal latitudes for the EOS MLS Level 2 data are given in the third column of the table to the left of the plot.

3 maps, and also – for the zonal means – to the nominal Level 2 latitudes to account for any (expected small) differences between the actual and nominal Level 2 latitudes.

Missing or 'bad' Level 2 data must be 'filled in' in order to provide a continuous data set for use by the mapping algorithms described in section 3.1.2. Interpolating isolated missing points along the orbital track is straightforward by using linear or cubic spline interpolation method. But when a large gap (e.g., more than 20 orbits) exists in an orbit, however, interpolation along that orbit must be abandoned. Through numerical experimentation with transforms of artificial data and white noise, Lait and Stanford [1988a] found that interpolation using a linear fit yields good results when the gap is larger, while cubic spline fit gives reasonable results when less than 5 points are missing. Therefore, the procedure dealing with missing data is to first interpolate missing data points along an orbit track. Then after data have been sorted into descending and ascending series at fixed latitudes, missing points in those series may be interpolated by linear or cubic spline which will avoid suppressing high frequencies in the small gaps and avoid unrealistic peaks in the large gaps.

The Level 2 data can also be interpolated to Level 3 nominal grids by using Fourier transform techniques along the track if the missing points have been filled in by using linear or cubic spline fit method. The 'along-track' spectra will likely prove useful for analyses of small scale structure seen in the data.

3.1.2 Algorithms for producing daily maps

3.1.2.1 Introduction

Two categories (asynchronous and geosynchronous) of orbital platforms have dominated Earth observations from space [*Salby*, 1989]. Fixed with respect to the Earth, geosynchronous satellites observe a single region all the time. Geostationary satellites provide measurements with higher temporal resolution than possible with asynchronous polar-orbiting satellites. However, geostationary satellites provide limited coverage and distortion at the limb of the field of view. For these reasons asynchronous satellites have been widely used for the monitoring of the Earth's atmosphere. Of these, polar-orbiting platforms (sun-synchronous in particular) are widely used today. An inherent advantage of this orbital geometry is nearly complete global coverage. High inclination orbits such as those of sun-synchronous satellites provide measurements nearly pole to pole, covering all longitudes in approximately a day, or in half a day when both dayside and nightside measurements can be made.

Although having advantages in coverage and vertical resolution, measurements taken from non-geosynchronous satellite are asynoptic: different regions are observed at different times. No information on the field's behavior is observed between the locations and times where measurements are taken. Because of these data voids, and because approximately a day passes before the full range of longitudes is sampled, certain classes of behavior will escape observation.

The asynoptic nature of asynchronous satellite measurements is especially important for variability that involves space and time scales comparable to those of the sampling. Fluctuations on small space and time scales are inherent to the climate system. Undersampling of such behavior will lead to larger scales signals being aliased. Sampling properties are thus an important aspect of satellite data. The discrete sampling in space and time is a key consideration that must be addressed in interpreting such observations.

A few approaches for estimating synoptic maps from asynoptic observations have been developed. A full review of different techniques can be found in Salby [1982 a, b] and Lait and Stanford [1988a]. As stated by Lait and Stanford [1988a]: "Currently, the most common, although crudest, analysis procedure is to interpolate the data in space and time by some means to a synoptic, regularly spaced grid. While adequate for examining slowly moving waves, such methods can introduce significant distortions of planetary scale waves with periods of 5 days or less [e.g. *Salby* 1982b]. Kalman filtering techniques (such as the sequential estimation method of Rodgers 1976) may be used to generate synoptic grids, but appropriately constructing the needed statistical models can prove troublesome.

Another method is by Chapman *et al*. [1974], in which soundings from ascending and descending orbit sequences at fixed latitudes are arranged in two time series and Fourier transformed. Peaks in the spectra correspond to one of many possible wavenumber-frequency pairs which are Doppler-shifted by the satellite's motion relative to the Earth to the same observed frequency F_0, given by

$$F_0 = m + sf$$

where m is the zonal wavenumber, f the frequency in cycles per day (cpd), and $s = -1$ for the westward-moving waves, $s=+1$ for the eastward-moving waves. This procedure suffers from an inherent ambiguity in ascribing a particular wavenumber and frequency from possible pairs of (m,f) to a spectral feature of F_0. Application of the asynoptic sampling theorem of Salby [1982a] narrows the number of allowed pairs to two, and by comparing the phase difference between the ascending and descending peaks one can usually determine which of the two is".

Fourier transform is most often used as a means of detecting periodic signals in data. A 2D transform isolates the periodicities that exist in two independent dimensions. The discrete zonal space-time Fourier transform of an observed data field $\psi(\lambda, t)$, sampled at regular intervals in λ and t, is given by

$$\Psi(k,\sigma) = \frac{1}{2\pi T} \sum_{m=0}^{M-1} \sum_{n=0}^{N-1} \psi(\lambda_m, t_n) e^{-i(k\lambda_m + \sigma t_n)} \tag{3.1}$$

where λ_m is the mth sampled longitude, t_n is the nth sampled time, k and σ are wavenumber and angular frequency (rad day^{-1}) respectively.

Because the asynoptic data position is a function of time, the above equation cannot be separated into two independent 1D FFTs. Also, all of the approaches for dealing with asynoptic data require an understanding of the limitations posed by the sampling. These limitations and their associated aliasing ambiguities are intrinsic to all discrete data.

Salby [1982a,b] developed a method for computing the exact space-time Fourier transform of asynoptic satellite data, as well as synoptic gridded fields from such transforms. It is shown via a rotation from synoptic to asynoptic coordinates, thus separating Eqn. (3.1) into two independent Fourier transforms, that the sampling pattern uniquely determines the space-time spectrum at all wavenumbers and frequencies within the Nyquist limits. In this procedure, the spectral resolution and aliasing are well defined. Hayashi [1983] offered an alternative formulation of the technique, the "frequency transform method," which has been shown to be equivalent [*Salby and Hayashi*, 1985].

In the following, we will briefly review the theorem of Discrete Fourier Transform and aliasing problems, then present details of Salby's method [*Salby*, 1982ab] for establishing a unique correspondence between alias-free asynoptic data and synoptic maps. From this, a procedure for retrieving synoptic maps is developed. Application of the method to EOS MLS data is then presented.

3.1.2.2 Discrete Fourier transform and aliasing

The Discrete Fourier Transform (DFT) is the most widely used method for determining the frequency spectra of digital signals. This is due to the development of an efficient algorithm for computing DFTs known as the Fast Fourier Transform (FFT). Before we get into Salby's method, we will first review the Discrete Fourier Transform theorem and sampling aliasing.

The discrete Fourier transform, $\psi(k)$, of a one-dimensional function $\varphi(t)$ sampled at interval Δt, is defined as:

$$\Psi(k) = \frac{1}{N\Delta t}\sum_{n=0}^{N-1}\varphi(t_n)e^{-i2\pi f_k t_n} \tag{3.2}$$

where N is the total number of samples, $t_n = n\Delta t$ and $f_k = k / N\Delta t$.

The inverse transform is defined as:

$$\varphi(t) = \sum_{k=0}^{N-1}\Psi(k)e^{i2\pi f_k t} \tag{3.3}$$

Just as the sampled data represents the value of a signal at discrete points in time, the result of a Fast Fourier Transform represents the spectrum of the signal at discrete frequencies. These discrete frequencies are a function of the frequency index k, the number of samples collected N, and the sampling interval Δt:

$$f_k = \frac{k}{N\Delta t} \tag{3.4}$$

where $k = -(N/2-1), -(N/2-2), ..., -1, 0, 1, ..., N/2$. Thus, the frequency spectrum computed above ranges from $-\frac{1}{2\Delta t} + \frac{1}{N\Delta t}$ to $\frac{1}{2\Delta t}$.

Resolution

The frequency resolution is $\frac{1}{N\Delta t}$. In the real world, only a limited range, $T\ (= N\Delta t)$, of data points is considered when doing discrete Fourier transform. The consequence of the limited data range is that a perfectly correct spectrum is impossible to obtain. Instead, convolution of the true spectrum with the finite range represents a certain smoothing of the true spectrum. The degree of smoothing depends on the range T. A shorter T gives stronger smoothing. The spectrum thus calculated is therefore called the *averaged or weighted spectrum*.

The side-lobes of the frequency window can also lead to undesirable effects such as spectral leakage. Much effort has been made to eliminate windowing effects by modifying the weighting function applied to the data before the transform [*Båth*, 1974]. However, it is not possible to completely eliminate the windowing effect.

In summary, the main rules to follow when choosing the window length T are the following:

- A larger T will lead to more detail, i.e., to better resolution in the computed spectrum.
- A smaller T will lead to better stability or better reliability of the computed spectral, because the spectral smoothing then extends over a larger frequency interval.

One extreme, the infinite T, unattainable in practice, will lead to correct spectrum. The other extreme, a very small T approaching zero, will lead to a "*white spectrum*", no resolution at all. A compromise has to be made between various considerations (of resolution, stability, computer time economy, etc.) in the choice of an appropriate range T.

Aliasing

While the range T defines the fundamental period or the lowest frequency in the spectral analysis, the sampling interval Δt defines the highest resolvable frequency. Intuitively, we can understand that at least three points, i.e. two time-intervals ($2\Delta t$), are the minimum information needed to define one period. This means that the shortest period that can be detected is $2\Delta t$, or the highest resolvable frequency is $\frac{1}{2\Delta t}$. This frequency limit f_c for the calculated spectrum is referred to as the *Nyquist frequency* or *Nyquist limit*. Aliasing is a well-known phenomenon in sampled data analysis. It is a consequence of the fact that after sampling, every periodic signal at a frequency greater than the Nyquist limit looks exactly like some other periodic signal at a frequency less than the Nyquist limit (Figure 3-1). It occurs because the time function is not sampled at a sufficiently high rate, i.e., the sample interval Δt is too large. Therefore, if the function $\varphi(t)$ is not band-limited, i.e., $\psi(f) \neq 0$ for some $|f| > f_c$, then sampling will introduce aliasing. To prevent aliasing, frequency components above the Nyquist limit must be removed before sampling.

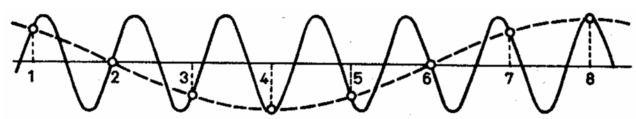

Figure 3-1. A well-known sketch demonstrating the effect of aliasing. By varying the sampling interval and the starting point, it is easily seen that different results will be obtained, regarding both amplitude, frequency and phase (from Båth, p145, Fig.35, 1974).

The rules for the frequency limits as caused by limited record length T and sampling interval Δt, can be summarized in the following rules:

- The record length T defines the lower frequency limit in the spectrum: $f_1 = \dfrac{1}{T}$.
- The sampling interval Δt defines the upper frequency limit in the spectrum: $f_{N/2} = \dfrac{1}{2\Delta t} = \dfrac{N}{2T}$,

  where N is the number of data points. Contamination of computed spectra by frequencies higher than $f_{N/2}$ is termed aliasing and, sometimes, spectrum folding.

Leakage

Leakage is related to having a non-integer multiple of the period in the data set. The effect of this is to create a periodic function with sharp *discontinuities*, as illustrated in Figure 3-2. Intuitively, we expect the introduction of these sharp changes in the time domain to result in additional frequency components in the frequency domain. In discrete Fourier transform, an N point record will produce an N point frequency response. Each of these points in the frequency response is called a frequency bin. Exactly where these frequency bins lie in terms of actual values depends on the number of points in the record, as well as the sampling frequency. The more points, the closer the bins lie together, the higher the sampling frequency the further apart the bins are.

Figure 3-2 shows an example of a sine wave that will suffer from spectral leakage with a range of 1.5 times the period. Since this is a pure sine wave, we would expect to see just one frequency at the frequency of the signal. However, since the discrete Fourier transform assumes the signal to be periodic outside the range T, the discontinuity at both ends of the signal will cause leakage – the actual frequency of the signal won't be at any of the discrete frequencies, it will fall between the adjacent discrete frequencies closest to it. Therefore, the signal leaks to the surrounding frequency bins (Fig. 3-3), and the amplitude for each of the discrete frequencies is less than that of the actual signal.

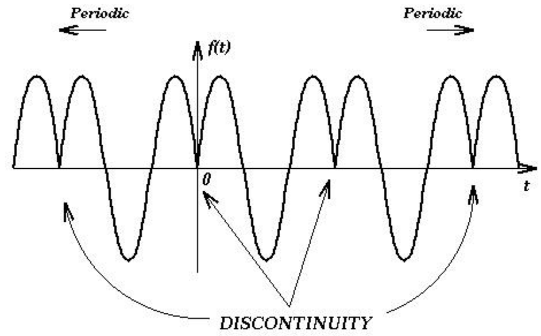

Figure 3-2. Sine wave with the discontinuity at the both ends.

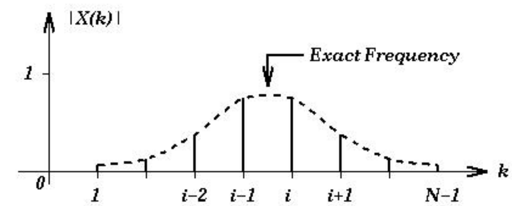

Figure 3-3. Spectra of the sine wave in Figure 3-2.

Increasing the number of samples (with fixed sampling step) to give greater resolution, causes the largest peak to get larger, indicating it is nearer the true frequency. The adjacent frequencies, where the energy has leaked, will also get larger and reduce the accuracy of the spectra.

3.1.2.3 Sampling geometry and coordinate rotation

EOS Aura lies in a retrograde, near polar, orbit, defined by the orbital period τ_0 (98.8 min or 0.0686 day) and the angle of inclination 98.2^o from the equatorial plane. With τ_0 in units of days, a sun-synchronous satellite in such an orbit will complete

$$\nu_0 = \frac{1}{\tau_0}$$

orbits during one complete Earth rotation (2π radians) and the satellite makes $2\nu_0$ ascending and descending measurements in one day on a given latitude circle.

Central to Salby's approach is the separation of measurements into ascending (northgoing) and descending (southgoing) series denoted here by subscripts *a* and *d*. Let c_0 be the angular velocity (radians/day) at which the orbital plane precesses along the latitude circle, so

$$c_0 = 2\pi$$

for sun-synchronous satellites. In the following discussion, we will consider a single latitude. Let λ_d and λ_a represent longitudes of descending and ascending measurements, respectively, for the latitude, with λ_{d0} and λ_{a0} their initial positions. Let t_d and t_a be the times at which the descending and ascending data are taken with t_{d0} and t_{a0} the initial times. Then we have

$$\begin{aligned}
\lambda_{dj} &= \lambda_{d0} - c_0\tau_0 j \\
\lambda_{aj} &= \lambda_{a0} - c_0\tau_0 j \\
t_{dj} &= t_{d0} + \tau_0 j \\
t_{aj} &= t_{a0} + \tau_0 j
\end{aligned} \tag{3.5}$$

where j = 0, 1, 2, ..., N-1, and N is the total number of orbits used in the analysis.

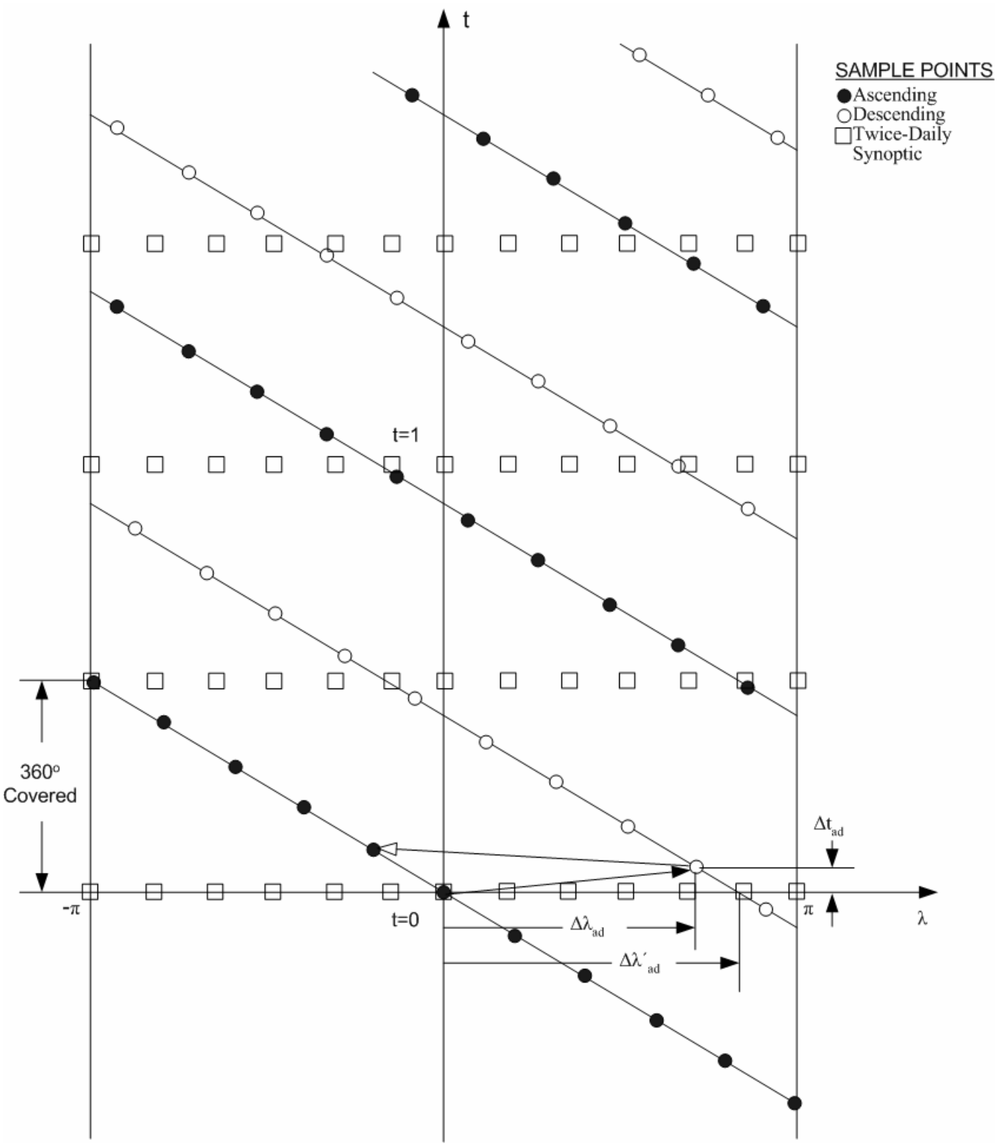

Figure 3-4. Sampling pattern of observations on a latitude circle in the longitude-time plane. The latitude circle is completely sampled by combined (ascending + descending) data in ½ day. Note ascending and descending trajectories are not equidistant. Twice-daily, synoptic sampling pattern also shown (from Salby, 1982a).

The relationships between ascending and descending longitudes and times on any given latitude are the following (Fig. 3-4)

$$\begin{aligned} \lambda_{dj} &= \lambda_{aj} + \Delta\lambda_{ad} \\ t_{dj} &= t_{aj} + \Delta t_{ad} \\ \Delta\lambda'_{ad} &= \Delta\lambda_{ad} + c_0 \Delta t_{ad} \end{aligned} \tag{3.6}$$

where $\Delta\lambda_{ad}$ and Δt_{ad} are the longitudinal and temporal separation between consecutive ascending and descending nodes, $\Delta\lambda'_{ad}$ is the longitude separation between the loci of descending and ascending points along the line of constant time, which is also called the instantaneous separation. It would be the longitude separation as if descending and ascending observations were made simultaneously. Hence, $\Delta\lambda'_{ad} = \pi$ at the equator, but not at other latitudes.

As shown by Salby [1982a], if we rotate the synoptic coordinate system (λ, t) by an angle α to a new asynoptic coordinate system (s, r) (Fig. 3-5b), where

$$\begin{aligned} \tan\alpha &= \frac{1}{c_0} \\ \sin\alpha &= \frac{1}{(1 + c_0^2)^{\frac{1}{2}}} \\ \cos\alpha &= \frac{c_0}{(1 + c_0^2)^{\frac{1}{2}}} \end{aligned} \tag{3.7}$$

Then the relationships between synoptic and asynoptic coordinate systems are

$$\begin{aligned} \lambda &= s\cos\alpha + r\sin\alpha \\ t &= -s\sin\alpha + r\cos\alpha \\ \\ s &= \lambda\cos\alpha - t\sin\alpha \\ r &= \lambda\sin\alpha + t\cos\alpha \end{aligned} \tag{3.8}$$

and

$$\begin{aligned} m &= k_s \cos\alpha + k_r \sin\alpha \\ \sigma &= -k_s \sin\alpha + k_r \cos\alpha \\ \\ k_s &= m\cos\alpha - \sigma\sin\alpha \\ k_r &= m\sin\alpha + \sigma\cos\alpha \end{aligned} \tag{3.9}$$

Here k_s, k_r and m, σ are the wavenumbers and frequencies in asynoptic and synoptic coordinates respectively.

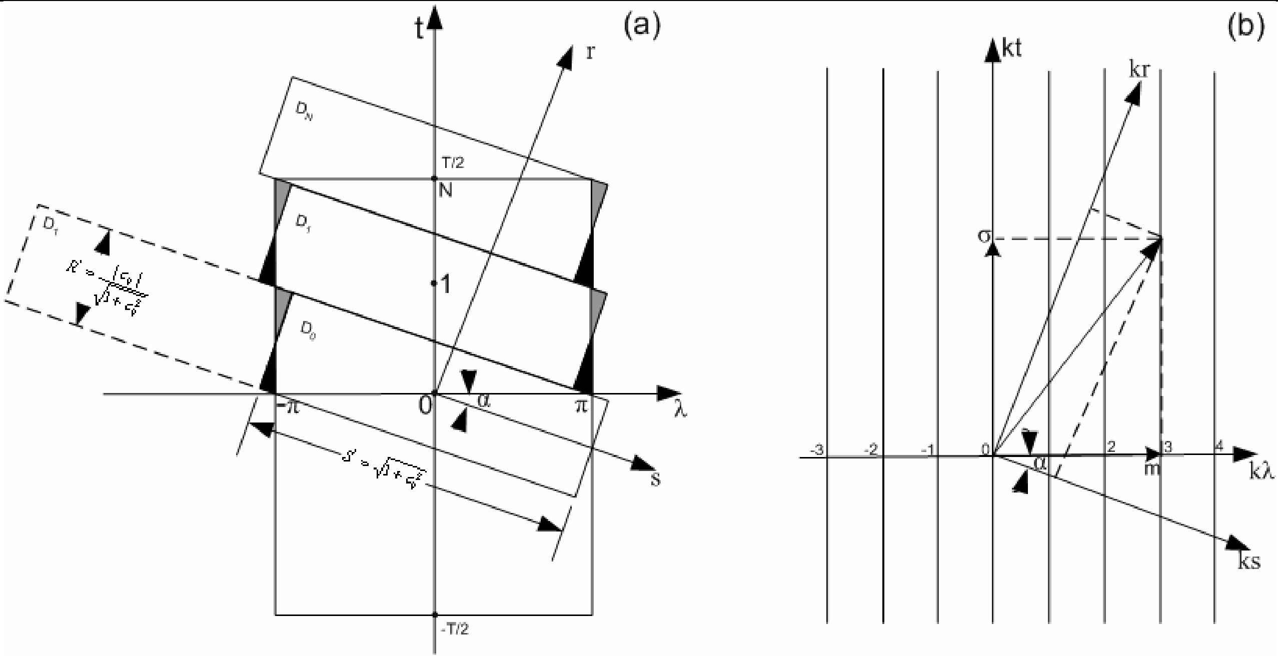

Figure 3-5. Coordinate geometry. (a) Physical plane: (s, r) coordinates are hybrids of longitude and time. Integration elements D_n do not perfectly cover the λ-t rectangle $D = [-\pi, \pi]\times[-T/2, T/2]$, but the miscoverage cancels in adjacent elements, leaving only the hyperextensions at $t = \pm T/2$. Because of zonal periodicity, each element D_n is equivalent to its periodic image; hence the integration may be performed over the strip of elements along the s axis. (b) Transform plane: k_λ, k_t, k_s, k_r are wavenumber components along respective axes (from Salby, 1982a).

It follows that two contiguous nodes of either locus in the asynoptic coordinate system (s, r) (Fig. 3-6) are separated by (See Appendix C for derivation of these formulas)

$$
\begin{aligned}
\Delta s &= \frac{\tau_0}{\sin\alpha} \\
\Delta r_1 &= (2\pi - \Delta\lambda'_{ad})\sin\alpha \\
\Delta r_2 &= \Delta\lambda'_{ad}\sin\alpha \\
r_a &= \tfrac{1}{2}(\Delta r_1 - \Delta r_2) \\
r_d &= -\frac{R}{2} \\
\Delta\lambda'_{ad} &= (r_d - r_a)/\sin\alpha
\end{aligned}
\tag{3.10}
$$

where Δs is the separation between two contiguous nodes of either locus, Δr_1 and Δr_2 are the perpendicular distances between the ascending and descending loci, r_a and r_d are the ascending and descending vertical coordinate values.

3.1.2.4 Fast Fourier synoptic mapping

In reality, the Fourier transform must be calculated discretely. Synoptic sampling results in the choice of rectangles parallel to the (λ, t) axes as the integration elements (Fig 3-5). Therefore, in time region T and round a longitude circle (domain D in Fig 3-6), (3.1) becomes

$$
\Psi(k,\sigma) = \frac{1}{2\pi T}\sum_{m=0}^{M-1}\sum_{n=0}^{N-1}\psi(\lambda_m, t_n)e^{-i(k\lambda_m+\sigma t_n)}\Delta\lambda\Delta t \tag{3.11}
$$

where

$$\Delta\lambda = \frac{2\pi}{M}$$
$$\Delta t = \frac{T}{N}$$

On the other hand, the 1-day integration element is defined in asynoptic coordinates (r, s) as a rectangle with sides of length (Fig 3-3)

$$R' = \cos\alpha$$
$$S' = \frac{1}{\sin\alpha}$$

Therefore, the integration can be performed for time region T over (r, s) strip $D' = [-S/2, S/2]\times[-R/2, R/2]$, where

$$R = R' = \cos\alpha$$
$$S = T \cdot S' = \frac{T}{\sin\alpha}$$

Here, D' is defined by locating the descending sequence at $r_d = -R/2$, and its periodic image at $R/2$. The ascending sequence lies somewhere (depending on the latitude) between these two (Fig. 3-3).

Then the Fourier transform in asynoptic coordinates (r, s) for the continuous case becomes

$$\Psi(k_s, k_r) = \tfrac{1}{RS}\int_{-R/2}^{R/2}\int_{-S/2}^{S/2}\psi(s,r)e^{-i(k_s s + k_r r)}dsdr$$

The discrete case becomes

$$\Psi(k_s, k_r) = \tfrac{1}{RS}\sum_{n=0}^{N-1}[\tfrac{1}{2}(\psi_{dn}e^{-i(k_s s_{dn}+k_r r_d)} + \psi_{an}e^{-i(k_s s_{an}+k_r r_a)})]\Delta r\Delta s + \mathrm{O}(\Delta s^2, \Delta r^2) \tag{3.12}$$

where

$$\begin{aligned} s_{dn} &= -c_0\frac{\Delta r}{2} + n\Delta s \\ s_{an} &= s_{dn} - c_0\Delta r_2 + \frac{\Delta t_{ad}}{\sin\alpha} \\ \psi_{dn} &= \psi(s_{dn}, r_d) \\ \psi_{an} &= \psi(s_{an}, r_a) \\ T &= N\tau_0 \end{aligned} \tag{3.13}$$

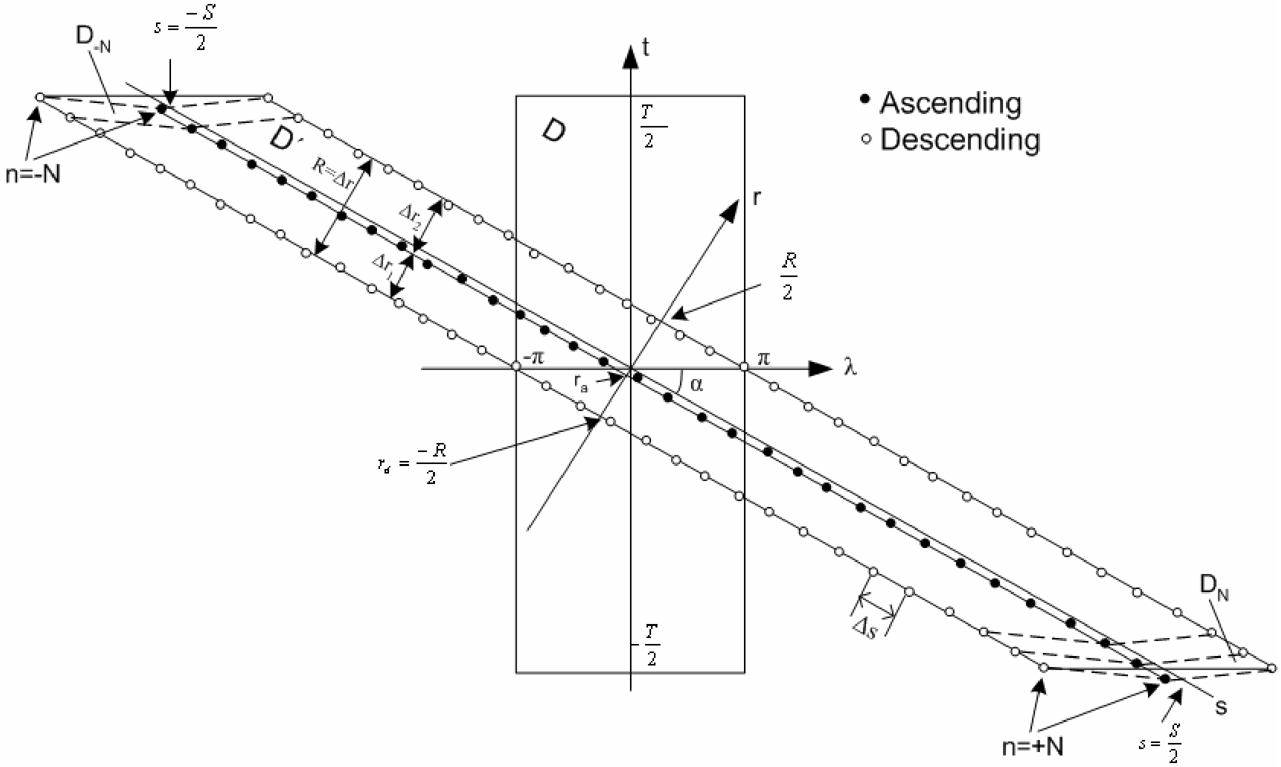

Figure 3-6. Synoptic *D*, and asynoptic *D'*, domains of transformation. The asynoptic strip is defined by the descending nodes located at $r=-R/2$ and their periodic images at $r=R/2$. Ascending nodes lie at $r = r_a$, not in general equidistant, from the descending loci. Integration elements also shown (from Salby, 1982a).

(derivation of (3.13) can be found in the Appendix C)

The spectral resolutions along the k_s and k_r directions will be

$$\begin{aligned} \Delta k_s &= \frac{2\pi}{S} = \frac{2\pi \sin\alpha}{T} \\ \Delta k_r &= \frac{2\pi}{R} = \frac{2\pi}{\cos\alpha} \end{aligned} \tag{3.14}$$

and the Nyquist limits along the k_s and k_r directions are

$$\begin{aligned} k_s^N &= \frac{\pi}{\Delta s} = \frac{\pi \sin\alpha}{\tau_0} \\ k_r^N &= \frac{\pi}{\Delta r} \approx \frac{1}{\sin\alpha} \end{aligned} \tag{3.15}$$

The corresponding spectral resolution and Nyquist wavenumber along the m and σ directions in synoptic coordinates are (Fig. 3-7)

$$\Delta m = \frac{2\pi}{S}$$
$$\Delta \sigma = \frac{2\pi}{T}$$
$$m^N = \frac{\pi}{\Delta \lambda} \tag{3.16}$$
$$\sigma^N = \frac{\pi}{\Delta t}$$

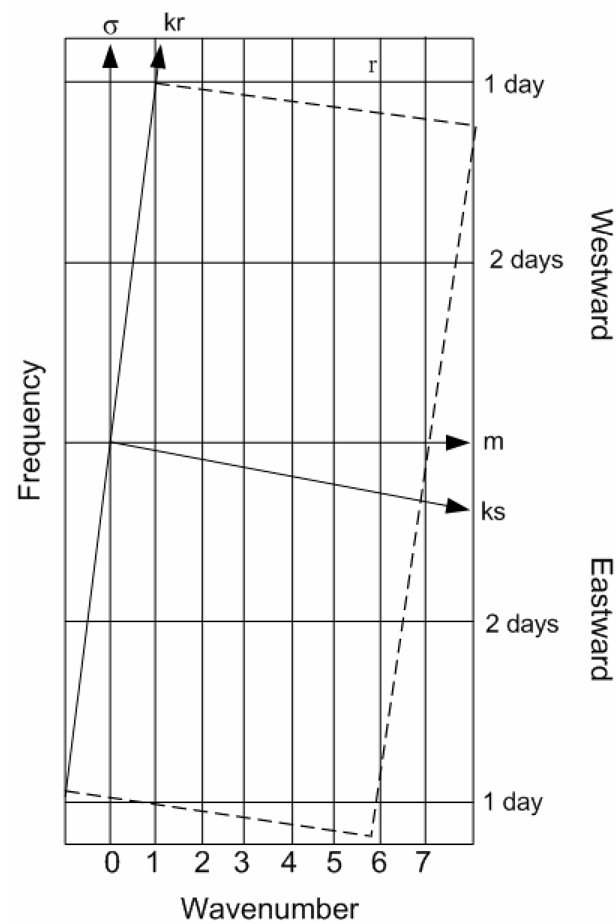

Figure 3-7. Location of points (tick marks) in the zonal space-time Fourier tranform of a 30-day series of asynoptic data. The dash lines mark the Nyquist limits as given by the FFSM technique, while the heavy lines indicate the Nyquist limits of a corresponding transform of synoptic data (from Lait and Stanford, 1988a).

The Nyquist limits in (m,σ) space correspond to a tilted rectangle, due to the rotation of coordinates as shown in Fig. 3-7. If we assume there are no spectral contributions from outside the Nyquist limits, it can be proved (section 3.1.2.4) that the space-time spectra $\Psi(k,\sigma)$ can be uniquely determined via the Fourier transform above. Therefore, the above theory also establishes the uniqueness between alias-free, asynoptic and synoptic sequences.

3.1.2.5 Explicit formulation of FFSM in *combined* mode

In the 2D Fourier Transform as given by Eqn. 3-12 there are only two terms, corresponding to ascending and descending, in the *r* direction in a period. Therefore, there are exactly 2 allowed "*r*" wavenumbers (k_r^- and k_r^+, defined later in Eqn. 3-22) for any given k_s inside the Nyquist rectangle $(-k_s^N, k_s^N) \times (-k_r^N, k_r^N)$ (Fig. 3-8). Thus, only two wave vectors, (k_s, k_r^-) and (k_s, k_r^+) on wavenumbers *m* and *m*+1, correspond to any value of k_s. This means that $\Psi(k_s, r)$ has a Fourier expansion in k_r containing only these two components. Therefore

$$\Psi(k_s,k_r) \;=\; \tfrac{1}{2}[\Psi(k_s,r_d)e^{-ik_r r_d} + \Psi(k_s,r_a)e^{-ik_r r_a}] \tag{3.17}$$

where

$$\Psi(k_s,r) \;=\; \frac{1}{S}\sum_{n=-N}^{N}\gamma_n \psi(s,r)e^{-ik_s s_n}\Delta s \tag{3.18}$$

As shown in Figure 3-8, k_r^- and k_r^+ can be derived to be

$$\begin{aligned} k_r^- &= -k_s c_0 + m\sqrt{1+c_0^2} \\ k_r^+ &= -k_s c_0 + (m+1)\sqrt{1+c_0^2} \end{aligned} \tag{3.19}$$

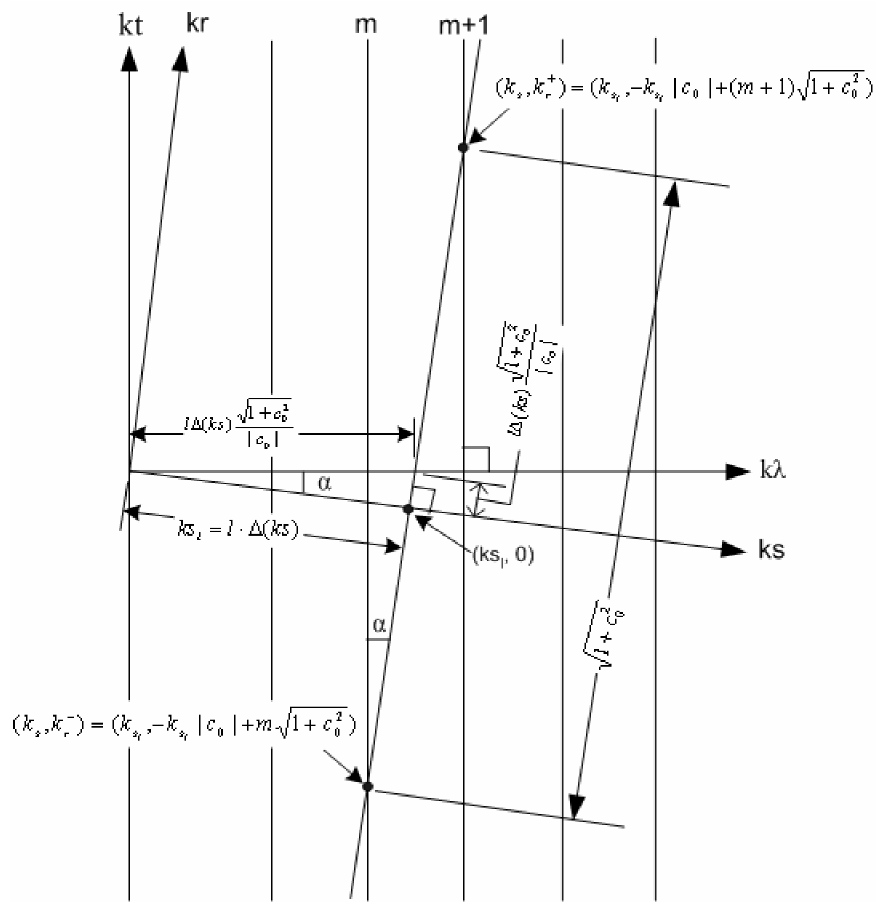

Figure 3-8. Construction of space-time spectra from transforms of asynoptic data. For each ks, there are two allowed spectra, corresponding to the points and on wavenumbers m and m+1, respectively (from Salby, 1982b).

Since we know that $\Psi(k_s, r)$ contains exactly two Fourier components, $\Psi(k_s, k_r^-)$ and $\Psi(k_s, k_r^+)$, they are uniquely derivable from the two entities $\Psi(k_s, r_d)$ and $\Psi(k_s, r_a)$, provided the latter are independent. Then we have

$$\begin{aligned}
\Psi(k_s, r_d) &= \Psi(k_s, k_r^-)e^{ik_r^- r_d} + \Psi(k_s, k_r^+)e^{ik_r^+ r_d} \\
\Psi(k_s, r_a) &= \Psi(k_s, k_r^-)e^{ik_r^- r_a} + \Psi(k_s, k_r^+)e^{ik_r^+ r_a}
\end{aligned} \tag{3.20}$$

The solution is

$$\begin{aligned}
\Psi(k_s, k_r^+) &= \frac{\Psi(k_s, r_d)e^{-ik_r^- r_d} - \Psi(k_s, r_a)e^{-ik_r^- r_a}}{e^{i(k_r^+ - k_r^-)r_d} - e^{i(k_r^+ - k_r^-)r_a}} \\
\Psi(k_s, k_r^-) &= \frac{\Psi(k_s, r_d)e^{-ik_r^+ r_d} - \Psi(k_s, r_a)e^{-ik_r^+ r_a}}{e^{-i(k_r^+ - k_r^-)r_d} - e^{-i(k_r^+ - k_r^-)r_a}}
\end{aligned}$$

This formula can be simplified to

$$\begin{aligned}
\Psi(k_s, k_r^+) &= \frac{\Psi'(k_s, r_d) - \Psi'(k_s, r_a)}{e^{i\lambda_d}[1 - e^{-i\Delta\lambda'_{ad}}]} \\
\Psi(k_s, k_r^-) &= \frac{\Psi'(k_s, r_a) - \Psi'(k_s, r_d)e^{-i\Delta\lambda'_{ad}}}{1 - e^{-i\Delta\lambda'_{ad}}}
\end{aligned} \tag{3.21}$$

where

$$\begin{aligned}
\Psi'(k_s, r) &= \Psi(k_s, r)\, e^{-i(k_s s_0 + k_r^- r)} \\
k_r^- &= -k_s c_0 + \frac{m}{\sin\alpha} \\
k_r^+ &= -k_s c_0 + \frac{m+1}{\sin\alpha}
\end{aligned} \tag{3.22}$$

(The derivation of formula 3.21 is presented in Appendix C)

In order to avoid aliasing, k_r must satisfy $|k_r| \le 1/\sin\alpha$, so we have

$$\begin{aligned}
-k_s c_0 + \frac{m}{\sin\alpha} &\ge -\frac{1}{\sin\alpha} \\
-k_s c_0 + \frac{m+1}{\sin\alpha} &\le \frac{1}{\sin\alpha}
\end{aligned}$$

therefore

$$k_s \cos\alpha - 1 \le m \le k_s \cos\alpha \tag{3.23}$$

Because the transformed coordinate s decreases with time t, it is desirable to reverse the series. When this is done, the $N-1$ term becomes the first term of the series and must be accounted for as an offset when performing the Fourier transform. Therefore we have

$$\begin{aligned} s_{d0} &= \lambda_{d0}\cos\alpha - t_{d0}\sin\alpha - \tau_0\,(N-1)/\sin\alpha \\ s_{a0} &= s_{d0} + (-c_0\Delta\lambda_{ad} + \Delta t_{ad})\sin\alpha \\ r_d &= (\lambda_{d0} + c_0 t_{d0})\sin\alpha \\ r_a &= (\lambda_{d0} - \Delta\lambda_{ad} + c_0 t_{d0} - c_0\Delta t_{ad})\sin\alpha \end{aligned} \tag{3.24}$$

Finally, we can get synoptic data by the following formula

$$\psi(\lambda_l, t_n) = \psi(s_l, r_n) = \sum_{\left|k_{s_j}\right| < k_{sN}} \sum_{k_r = k_r^{\pm}} \Psi(k_{s_j}, k_r) e^{i(k_{s_j} s_l + k_r r_n)} \tag{3.25}$$

The formulas in this section are thus a generalization of the space-time transform for irregular asynoptic data. They constitute the Asynoptic Sampling Theorem [*Salby* 1982b] which uniquely relates combined asynoptic data to their space-time spectrum. Thus, variability which involves only scales within the Nyquist rectangle (Fig. 3-7) can be unambiguously interpreted in asynoptic measurements. The Asynoptic Sampling Theorem ensures that, if only such scales are present in a field being monitored, the variability is adequately sampled and the behavior can be recovered faithfully. However, if the field being monitored involves significant variance beyond the Nyquist limits, the behavior is undersampled. In such case, not only can the rapid variability beyond the sampling limits not be truly recovered, but larger scales within the Nyquist limits (which would otherwise be correctly retrieved) may be "aliased" or misrepresented because of these unresolved scales.

Sampling theory also provides a natural algorithm for synoptically mapping asynoptic measurements. Under the conditions of the Asynoptic Sampling Theorem (i.e., the field is adequately sampled), the full synoptic behavior can be recoved by inverting the space-time spectrum, derivable from the asynoptic measurements [*Salby* 1982b]. Fast Fourier Synoptic Mapping provides the actual sequence of synoptic maps, as if the measurements about the globe were taken simultaneously. Representing a unique transformation between asynoptic and synoptic coordinates, this scheme has been demonstrated as a generally reliable means of synoptically mapping asynoptic data [*Lait and Stanford* 1988ab] and has allowed the identification of several rapidly propagating wave phenomena [*Lait and Stanford* 1988b].

3.1.2.6 Explicit formulation of FFSM in *single* mode

As mentioned before, some geophysical parameters will have diurnal variations. For these we will do the Fourier transform for ascending and descending series separately. There are exactly two terms, ascending and descending, in the *r* direction in a period in Fourier Transform as given by Eqn. 3-12. But for a single mode we only consider one series, ascending or descending. Therefore, the Nyquist limits of single mode along k_r direction become half of the combined mode and are given by

$$k_r^N = \frac{\pi}{2\Delta r} \approx \frac{1}{2\sin\alpha}$$

and the single mode Fourier Transform becomes

$$\Psi(k_s, k_r) = \Psi(k_s, r)e^{-ik_r r} \tag{3.26}$$

where $\Psi(k_s, r)$ is defined in Eqn. (3-18).

As shown in Figure 3-8, k_r will be either $-k_s c_0 + m\sqrt{1+c_0^2}$ or $-k_s c_0 + (m+1)\sqrt{1+c_0^2}$ depending on which is in the Nyquist limits (both cannot be within the limits since their difference is more than the limit).

Finally, we get the synoptic map for separate ascending and descending series by the following formula

$$\begin{aligned}
\psi_a(\lambda_l, t_n) = \psi_a(s_l, r_n) &= \sum_{|k_{s_j}| < k_{sN}} \Psi_a(k_{s_j}, k_r) e^{i(k_{s_j} s_l + k_r r_n)} \\
\psi_d(\lambda_l, t_n) = \psi_d(s_l, r_n) &= \sum_{|k_{s_j}| < k_{sN}} \Psi_d(k_{s_j}, k_r) e^{i(k_{s_j} s_l + k_r r_n)}
\end{aligned} \tag{3.27}$$

Note that the ascending and descending Fourier transform and reconstruction must be treated independently.

3.1.2.7 Uncertainty Estimate

Due to the system and other effects of the instrument measurements, every measurement has an error or uncertainty with it. In this session, we calculate the uncertainties in Level 3 which are propagated from Level 2 data.

Take a general function *f* as an example

$$y = f(\mathbf{x})$$

where $\mathbf{x} = \{x_i\}$. We can make a linear approximation to function *f* over a small change in the measurement $\Delta\mathbf{x}$ in order to access its effects on y. That is

$$\Delta y = \frac{\partial f}{\partial x_i}\Delta x_i$$

For multiple measurements the method often makes use of an assumption of independent errors, which gives

$$(\Delta y)^2 = \sum_i \left(\frac{\partial f}{\partial x_i}\right)^2 (\Delta x_i)^2$$

This is the diagonal form of the more general method for error propagation using covariance matrices

$$\mathbf{C}_y = (\frac{\partial f}{\partial \mathbf{x}})^T \bullet \mathbf{C}_x \bullet (\frac{\partial f}{\partial \mathbf{x}})$$

where $\frac{\partial f}{\partial \mathbf{x}}$ is a matrix of derivatives and $\mathbf{C}_y$ is the covariance of the data which contains information regarding first order correlations between the measurements.

Now we will apply this error propagation method to the Fourier Transform in order to calculate the uncertainty in the Level 3 daily maps. Take 1D Fourier Transform of $\psi(x)$ as an example, we have

$$\Psi_r(\lambda) = \frac{1}{N}\sum_{k=0}^{N-1}\psi_k \cos(\frac{2\pi k}{N}\lambda)$$
$$\Psi_i(\lambda) = -\frac{1}{N}\sum_{k=0}^{N-1}\psi_k \sin(\frac{2\pi k}{N}\lambda)$$

where $\Psi_r(\lambda)$ and $\Psi_i(\lambda)$ are the real and imaginary parts respectively. We can calculate the covariance matrices on the real term in the FT as

$$\mathbf{C}_{r\lambda} = (\frac{\partial \Psi_r}{\partial \psi})^T \bullet \mathbf{C}_\psi \bullet (\frac{\partial \Psi_r}{\partial \psi})$$

where $\mathbf{C}_\psi$ can be written as

$$\mathrm{C}_\psi = \begin{vmatrix} \sigma_0 & & & \\ & \sigma_1 & & \\ & & \ldots & \\ & & & \sigma_{N-1} \end{vmatrix}$$

We see from the definition of $\Psi_r(\lambda)$ that

$$\frac{\partial \Psi_r}{\partial \psi_k} = \frac{1}{N}\cos(\frac{2\pi k}{N}\lambda)$$

where σ_0 , σ_1 , ... σ_{N-1} are the uncertainties of ψ_0 , ψ_1 , ... ψ_{N-1}.

Thus the diagonal form of the error propagation method is applicable and the diagonal component corresponding to wave λ is given by

$$C_{r\lambda} = \frac{1}{N^2}\sum_{k=0}^{N-1}\sigma_k^2\left(\cos\left(\frac{2\pi k}{N}\lambda\right)\right)^2$$

Similarly for the imaginary part

$$\mathbf{C}_i = (\frac{\partial \Psi_i}{\partial \psi})^T \bullet \mathbf{C}_\psi \bullet (\frac{\partial \Psi_i}{\partial \psi})$$

and the diagonal component corresponding to wave λ is given by

$$C_{i\lambda} = \frac{1}{N^2}\sum_{k=0}^{N-1}\sigma_k^2\left(\sin\left(\frac{2\pi k}{N}\lambda\right)\right)^2$$

Therefore, we can derive the uncertainty $\Delta_\sigma \Psi(\lambda)$ of the FT of ψ as

$$\begin{aligned}\Delta_\sigma \Psi(\lambda) &= \frac{1}{N}\left(\sqrt{\sum_{k=0}^{N-1}\sigma_k^2\left(\cos\left(\frac{2\pi k}{N}\lambda\right)\right)^2} + i\sqrt{\sum_{k=0}^{N-1}\sigma_k^2\left(\sin\left(\frac{2\pi k}{N}\lambda\right)\right)^2}\right) \\ &= \Delta_\sigma \Psi_r(\lambda) + i\Delta_\sigma \Psi_i(\lambda)\end{aligned} \tag{3.28}$$

The associated inverse transform is given by

$$\psi(x) = \sum_\lambda (\Psi_r(\lambda) + i\Psi_i(\lambda))(\cos(\lambda x) + i\sin(\lambda x)) = \sum_\lambda (\Phi_r(\lambda) + i\Phi_i(\lambda))$$

where

$$\begin{aligned}\Phi_r &= \Psi_r\cos(\lambda x) - \Psi_i\sin(\lambda x) \\ \Phi_i &= \Psi_i\cos(\lambda x) + \Psi_r\sin(\lambda x)\end{aligned}$$

and the uncertainty of the retrieved field is given by

$$\Delta_\sigma \psi(x) = \sqrt{\sum_\lambda \Delta_\sigma^2 \Psi_r(\lambda)\left(\cos(\lambda x)\right)^2} + \sqrt{\sum_\lambda \Delta_\sigma^2 \Psi_i(\lambda)\left(\sin(\lambda x)\right)^2} \tag{3.29}$$

Similarly, the 2D Fourier Transform of ψ is given

$$\begin{aligned}\Psi_r(\lambda,\omega) &= \frac{1}{MN}\sum_{l=0}^{M-1}\sum_{k=0}^{N-1}\psi_{k,l}\cos\left(\frac{2\pi k}{N}\lambda + \frac{2\pi l}{M}\omega\right) \\ \Psi_i(\lambda,\omega) &= -\frac{1}{MN}\sum_{l=0}^{M-1}\sum_{k=0}^{N-1}\psi_{k,l}\sin\left(\frac{2\pi k}{N}\lambda + \frac{2\pi l}{M}\omega\right)\end{aligned}$$

and the uncertainty $\Delta_\sigma \Psi(\lambda,\omega)$ of the 2D FT of ψ is given by

$$\begin{aligned}\Delta_\sigma \Psi(\lambda,\omega) &= \frac{1}{MN}\left(\sqrt{\sum_{l=0}^{M-1}\sum_{k=0}^{N-1}\sigma_{k,l}^2\left(\cos\left(\frac{2\pi k}{N}\lambda + \frac{2\pi l}{M}\omega\right)\right)^2} + i\sqrt{\sum_{l=0}^{M-1}\sum_{k=0}^{N-1}\sigma_{k,l}^2\left(\sin\left(\frac{2\pi k}{N}\lambda + \frac{2\pi l}{M}\omega\right)\right)^2}\right) \\ &= \Delta_\sigma \Psi_r(\lambda,\omega) + i\Delta_\sigma \Psi_i(\lambda,\omega)\end{aligned} \tag{3.30}$$

The associated inverse transform given by

$$\psi(x,t) = \sum_{\lambda} (\Psi_r(\lambda,\omega) + i\Psi_i(\lambda,\omega))(\cos(\lambda x + \omega t) + i\sin(\lambda x + \omega t))$$

and finally the uncertainty of the retrieved field is given by

$$\Delta_{\sigma}\,\psi(x,t) = \sqrt{\sum_{\omega}\sum_{\lambda}\Delta_{\sigma}^{2}\Psi_r(\lambda,\omega)\big(\cos(\lambda x + \omega t)\big)^{2}} + \sqrt{\sum_{\omega}\sum_{\lambda}\Delta_{\sigma}^{2}\Psi_i(\lambda,\omega)\big(\sin(\lambda x + \omega t)\big)^{2}} \tag{3.31}$$

Now we can calculate the phase uncertainty by using the calculated $\Delta_{\sigma}\Psi(\lambda,\omega)$ which is the uncertainty of the Fourier transform. Phase Θ is defined as follows

$$\Theta(\lambda,\omega) = \tan^{-1}\frac{\Psi_i(\lambda,\omega)}{\Psi_r(\lambda,\omega)}$$

then $\Delta\Theta$ is given by

$$\Delta\Theta(\lambda,\omega) = \frac{\Psi_r(\lambda,\omega)}{\Psi_r^{\,2}(\lambda,\omega) + \Psi_i^{\,2}(\lambda,\omega)}\Delta\Psi_i(\lambda,\omega) - \frac{\Psi_i(\lambda,\omega)}{\Psi_r^{\,2}(\lambda,\omega) + \Psi_i^{\,2}(\lambda,\omega)}\Delta\Psi_r(\lambda,\omega)$$

so the uncertainty of phase Θ is

$$\Delta_{\sigma}\Theta(\lambda,\omega) = \frac{1}{\Psi_r^{\,2}(\lambda,\omega) + \Psi_i^{\,2}(\lambda,\omega)}\Big(\Psi_r^{\,2}(\lambda,\omega)\Delta_{\sigma}^{\ 2}\Psi_i(\lambda,\omega) + \Psi_i^{\,2}(\lambda,\omega)\Delta_{\sigma}^{\ 2}\Psi_r(\lambda,\omega)\Big)^{\frac{1}{2}} \tag{3.32}$$

3.1.2.8 Procedure and data processing

The following summarizes the main algorithm processing steps for producing synoptic maps:

- Sort data into chronological order and into ascending and descending series respectively at each latitude and pressure surface, and interpolate if necessary to cover bad or missing data

- Transform longitude and time in (λ,t) coordinates into (s,r) coordinates. Then perform FFT of ascending and descending nodes respectively

- Combine FFT of ascending and descending nodes for those fields which are not expected to have a significant diurnal signal

- Perform inverse FFT of combined spectra to produce synoptic maps of fields that are not expected to have significant diurnal signal, and also output the corresponding Fourier spectra

- Perform inverse FFT of ascending series, to produce day-side synoptic maps of the fields with diurnal variation, and also output the corresponding Fourier spectra

- Perform inverse FFT of descending series, to produce night-side synoptic maps of the fields with diurnal variation, and also output the corresponding Fourier spectra

- Calculate the uncertainty estimates

These steps are illustrated in Figure 3-9.

Figure 3-10 illustrates the daily synoptic map data processing software flow. The January is taken as an example in the plot. A full month (30 days) of Level 2 daily data must be available for input to the Level 3 software.

- read in 30 days of Level 2 daily data (January 1 to 30), the software will use this 30-day window (January 1 to 30) to calculate the spectra, and the Level 3 daily synoptic data in the middle 10 days (January 11 to January 20)

- wait for another continuous 10 days of Level 2 daily data (January 31 to February 9) to be available

- when the data are available, read in another 10 days of Level 2 daily data (January 31 to February 9), the software will use this 30-day window (January 11 to February 9) to calculate the spectra, and the Level 3 daily synoptic data in the middle 10 days (January 21 to January 30)

- again the software will wait for another continuous 10 days of Level 2 daily data (February 10 to February 19) to be available

- when the data are available, read in another 10 days of Level 2 daily data (February 10 to February 19), the software will use this 30-day window (January 21 to February 19) to calculate the spectra, and the Level 3 daily synoptic data in the middle 10 days (January 31 to February 9)

- the software will continue this processing cycle until the Level 2 data are exhausted

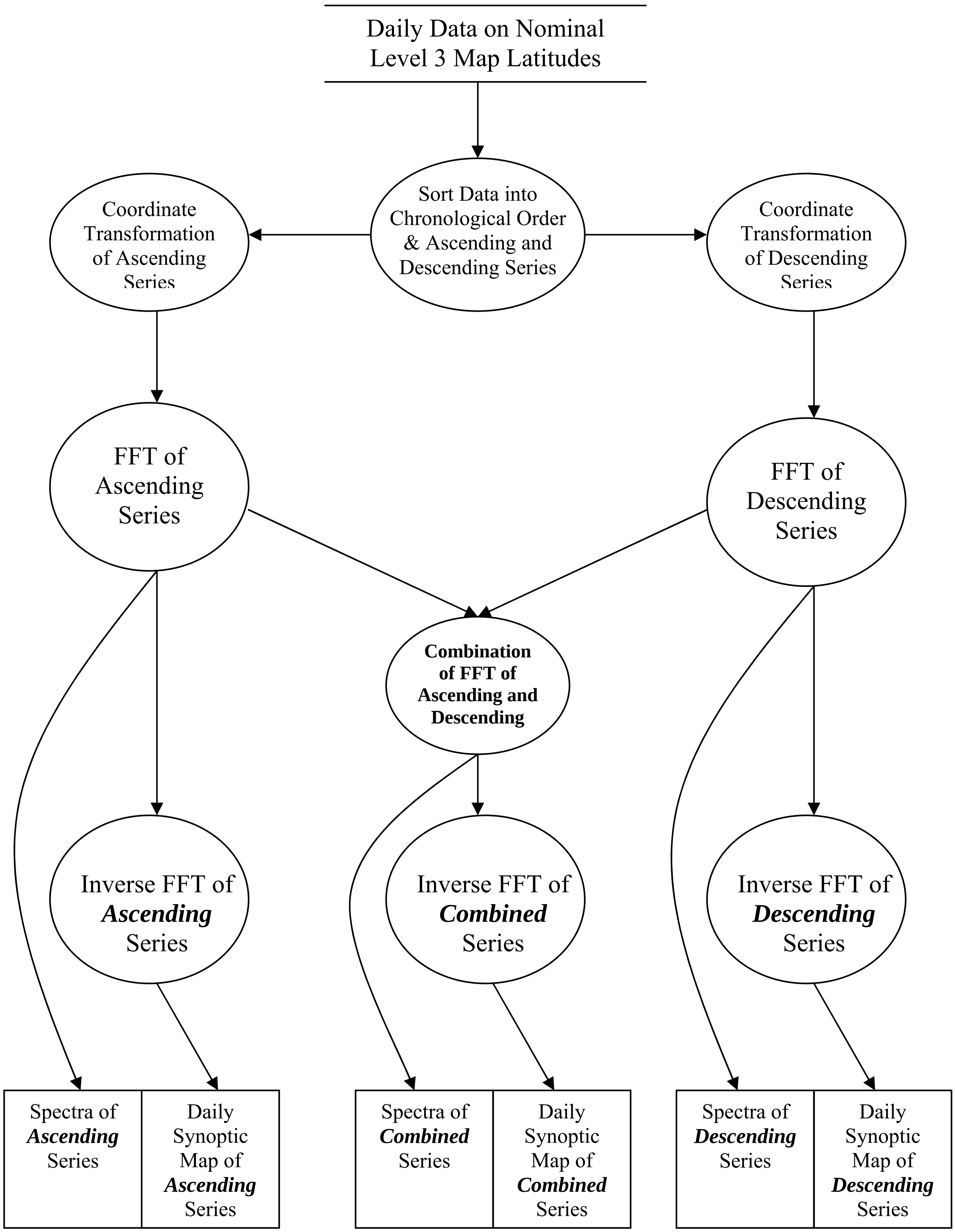

Fig. 3-9. Daily synoptic map data processing algorithm flow.

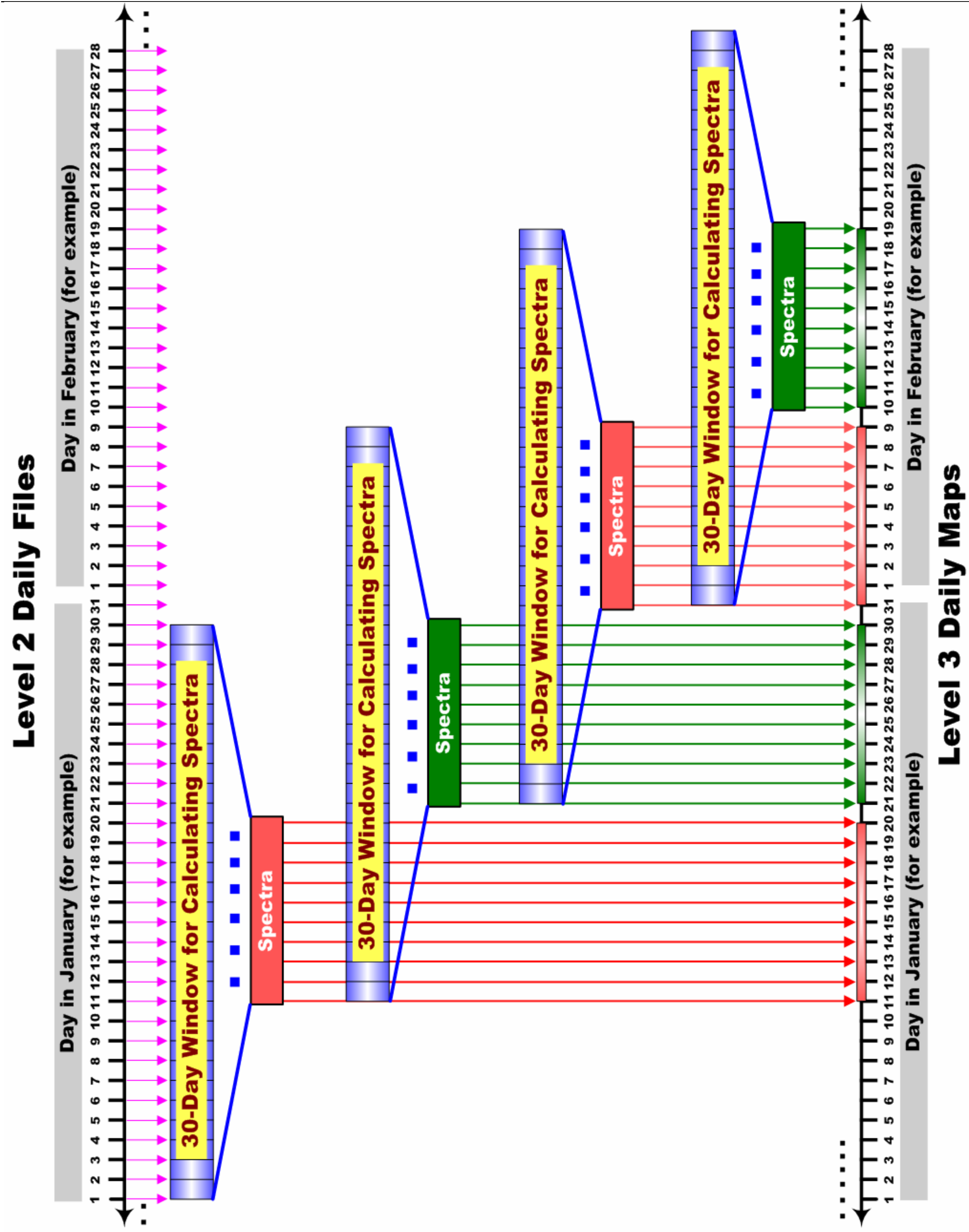

Fig. 3-10. Daily synoptic map data processing software flow.

3.1.2.9 Issues and limitations

As pointed out by Salby [1982a], as the satellite nears the meridional turning point of its orbit, the ascending latitude crossings approach the descending crossings. They coincide at the turning point (the most poleward latitude reached by the satellite). In terms of Figure 3-4, the ascending and descending lines become closer near the poles, thus the data field is greatly undersampled in some regions and oversampled in others along Salby's *r* direction, and the quality of the spectra deteriorates. The spectra obtained by the asynoptic transform thus tend to become noisier towards the poles. In practice, this effect seems to be negligible equatorward of about 70^o-75^o latitude [*Lait and Stanford,* 1988a].

The asynoptic transform method for combining ascending and descending spectra depends crucially upon the phase difference between the Fourier transforms of these two independent data series, each of which may contain irregular sampling, missing data, and nonstationary signals. But as shown by Salby [1982] and Lait and Stanford [1988a], the FFSM technique is robust under both ideal conditions (such as exactly uniform data sampling intervals and no missing data) and typical real world conditions. The limitations of this technique must be kept in mind when interpreting the data. We now address some of the limitations.

a. *Aliasing*

A serious limitation of the FFSM technique is the aliasing that depends on the observing pattern and the signals present in the atmosphere. It is inherent in any analysis of the data, including the Kalman filter technique. One solution to reduce aliasing is to ensure that the signal is composed of frequency components with index less than $N/2$ by prefiltering it with a low-pass filter. The second solution is to see that the number of samples, N, is more than twice the index of the highest frequency component present in the signal, if prior knowledge of the signal is available. Because EOS MLS covers the full longitude range twice (when combining ascending and descending sides of the orbits) in slightly less than 1 day, the Nyquist frequency corresponds to a period of 0.99 days and therefore variations with a period less than 0.99 days cannot be fully resolved. Variations with a period less than ~2 days cannot be fully resolved when using data separately from the ascending and descending portions of the orbits.

b. *Effects of satellite parameters and sampling errors*

The FFSM technique requires equal sampling intervals in both longitude and time, which is how the MLS Level 2 data will normally be produced. Sampling variations in both space and time may impair the accuracy of the spectra. Any changes in the orbital period of satellite must be accounted for as pointed out by Elson and Froidevaux [1993] for UARS, and still interpolate to regular sampling points and then apply FFSM technique.

c. *Leakage, filtering and weighting*

The "smearing" or "leakage" effect of the Fourier Transform is a direct result of the definition of the Discrete Fourier Transform and is not due to any inaccuracy in the FFT. Leakage occurs when some of the actual frequency values do not lie in the chosen *frequency bins*. Therefore the energy of the actual spectrum leaks out to the surrounding frequency bins. Leakage can be reduced by increasing the length of the record, or by choosing a sample size that includes an integral number of cycles of the frequency component of interest, or by employing a windowing algorithm.

In the study of climate system, such as the small-scale and high-frequency convective systems in the tropics, undersampled small-scale variability will aliase large-scale variability which describes the organization of climate properties on space and time scales that would otherwise be correctly represented. Much of that undersampled variance in water vapor, cloud, and related distributions follow from small-scale convective structure, which comprises the convective pattern at any instant. Such structure involves space and time scales too short to be determined on a global basis from asynoptic data. However, the variance on those scales is largely random [*Salby and Sassi*, 2001]. Accordingly, the asynoptic power spectrum is dominated by broadband variance in a background spectrum that is (statistically) almost flat.

Salby and Sassi [1999] developed a scheme that utilizes the random nature of convective fluctuations to identify small-scale undersampled variance in asynoptic data and then eliminate it. Since random small-scale variations of a field are manifested in that field's complex amplitude spectrum by random phases of neighboring spectral components, processing the asynoptic spectrum with a convolution leads to a cancellation among incoherent spectral components. The scheme rejects a major component of undersampled convective variance, leaving a more accurate representation of large-scale variance. The prerequisite of this scheme is that the small-scale variability is random, therefore their phases are random. The scheme distinguishes itself when the power of broadband or background variance is comparable to the large-scale variations (low signal/noise ratio), such as in the tropical convective climate system. In the reconstruction of physical parameters from EOS Aura satellite data, this scheme is useful to the retrieval of water vapor in the tropical region. Its application to our reconstruction of synoptic map will reduce the noise, and its usefulness to the EOS MLS will be addressed in a later version of this document.

3.1.2.10 Algorithm testing

There are several ways to test the FFSM scheme. Simple tests using analytic functions are done to verify that the signals inside the Nyquist limits are accurately represented. Tests involving the CTM (Chemical Transport Model driven with winds from the UK Met Office analyses) simulations of the atmosphere are done to obtain a realistic assessment of the algorithm performance.

Results of tests done to date are in Appendix D and E.

3.1.2.11 Diagnostics

Diagnostics and goodness-of-fit assessment will be produced as part of the retrieval of daily synoptic maps. The goodness-of-fit assessment summarizes the overall difference between the retrieved daily maps and the Level 2 data input to the algorithm. As shown in Figure 3-11, the Fourier spectra are used to reconstruct the Level 2 fields ϕ_i^r at the Level 2 measurement locations and times, and differences between the fields (residuals) determined. Then an overall (global) 'Level 3 residual' for each pressure surface can be calculated as a root sum square (rss) difference

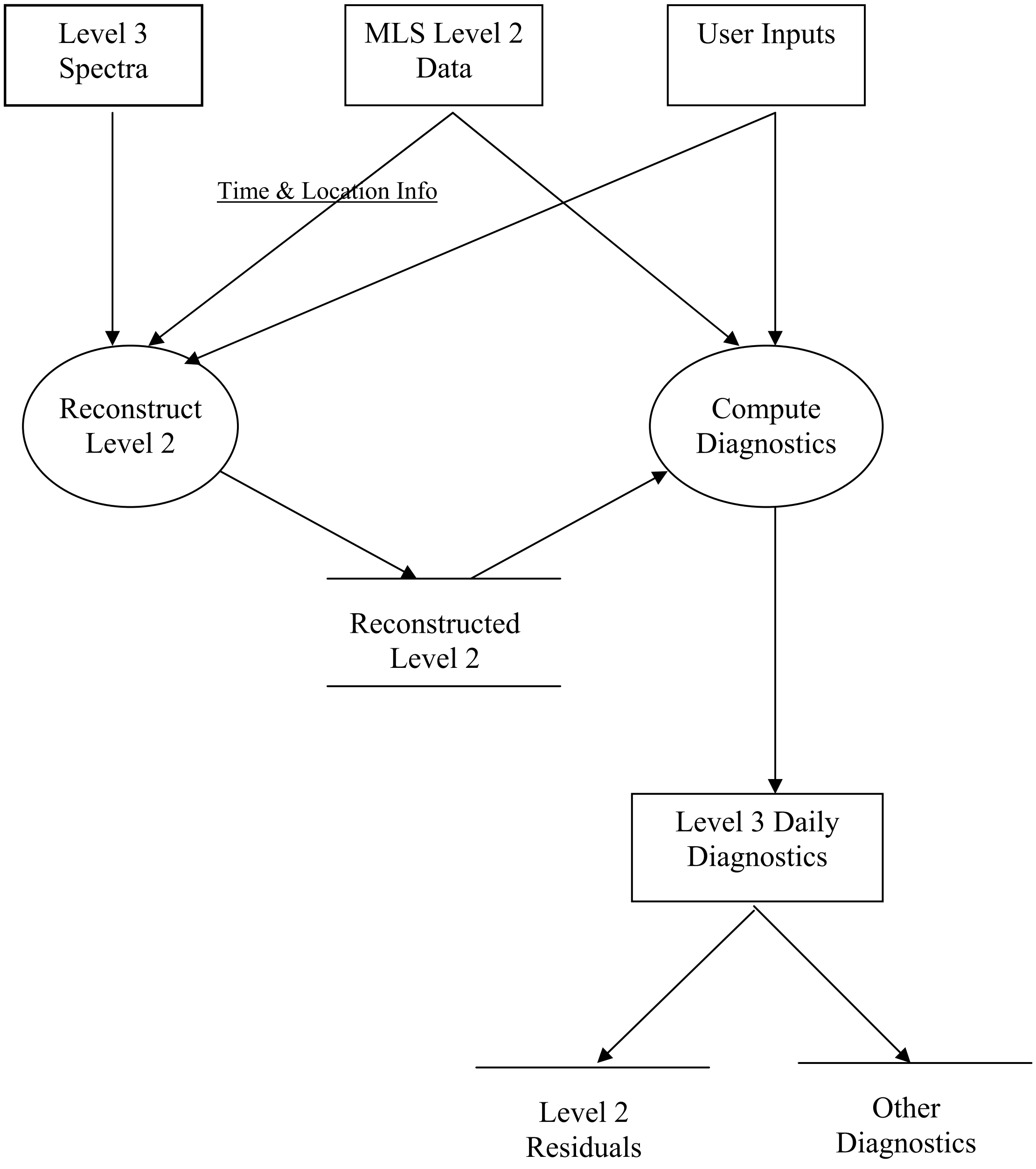

Figure 3-11. Generation of the EOS MLS Level 3 daily diagnostics.

$$\sigma_{L3g} = \sqrt{\frac{1}{N}\sum_{i=1}^{N}(\phi_i^{\ r} - \phi_i^{\ m})^2} \tag{3.33}$$

where ϕ_i^m is the measured field at $(\theta_i, \lambda_i, t_i)$.

In addition to σ_{L3g} as an overall evaluation of the retrieval, other diagnostics will be produced, such as:

Routine Diagnostics

- Maximum differences (maybe the first 10 or so largest) between the measured and reconstructed field points, and the location and time at which each occurred. This process will be separated between ascending and descending orbits (no overlapped points).
- The number or percentage of the missing points or the so-called "bad" data points from Level 2 analysis.
- Root sum square (rss) $\sigma_{L3DMP}(\varphi,p,\theta)$ between measured and reconstructed fields for each latitude θ (separately for ascending and descending) for all geophysical parameters φ on selected pressure level p. The $\sigma_{L3DMP}(\varphi,p,\theta)$ is defined as:

$$\sigma_{L3DMP}(\varphi, p, \theta) = \sqrt{\frac{1}{N}\sum_{i=1}^{N}(\phi_i^{\ r}(p,\theta) - \phi_i^{\ m}(p,\theta))^2} \tag{3.34}$$

where N is the number of valid points on pressure level p and latitude θ, $\phi_i^r(p,\theta)$ and $\phi_i^m(p,\theta)$ are the reconstructed and measured field values on pressure level p and latitude θ.

The plots of $\sigma_{L3DMP}(\varphi,p,\theta)$ versus latitude on one page will be produced. The rss $\sigma_{L3DMP}(\varphi,p,\theta)$ is a good measure of high frequencies and wavenumbers that are outside the Nyquist limits. Sample plot from Level 3 software is shown in Figure 3-12. This plot indicates that the higher variability throughout the atmosphere in the middle latitude of the northern hemisphere, while the higher variability can be found in both tropopause and upper stratosphere in middle latitude of the southern hemisphere. This phenomenon may be related to the northern winter polar vortex which was very dynamically active and had various spatial and temporal scale waves on February 15, 1996. Furthermore, the comparison of $\sigma_{L3DMP}(\varphi,p,\theta)$ among some other geophysical parameters will provide rich information on the chemistry and dynamics of the atmosphere which will not be covered in this document.

Special Diagnostics

- Daily anomaly map between constructed and measured fields. These maps will not be synoptic maps, but will be for the asynoptic measurement times in a day.
- Latitude variation of $\sigma_{L3Lat}(\varphi,p,\theta,\Delta\theta)$ in each latitude bin $\Delta\theta$ at latitude θ on selected pressure level p. User controls the latitude bin width $\Delta\theta$. The $\sigma_{L3Lat}(\varphi,p,\theta,\Delta\theta)$ is defined as:

$$\sigma_{L3Lat}(\varphi, p, \theta, \Delta\theta) = \sqrt{\frac{1}{N}\sum_{i=1}^{N}(\phi_i^{\ r}(p,\theta,\Delta\theta) - \phi_i^{\ m}(p,\theta,\Delta\theta))^2} \tag{3.35}$$

where N is the number of valid points in latitude bin $\Delta\theta$ at latitude θ on pressure level p, $\phi_i^r(p,\theta,\Delta\theta)$ and $\phi_i^m(p,\theta,\Delta\theta)$ are the reconstructed and measured field values in latitude bin $\Delta\theta$ at latitude θ on pressure level p.

- Confidence level of the retrieval

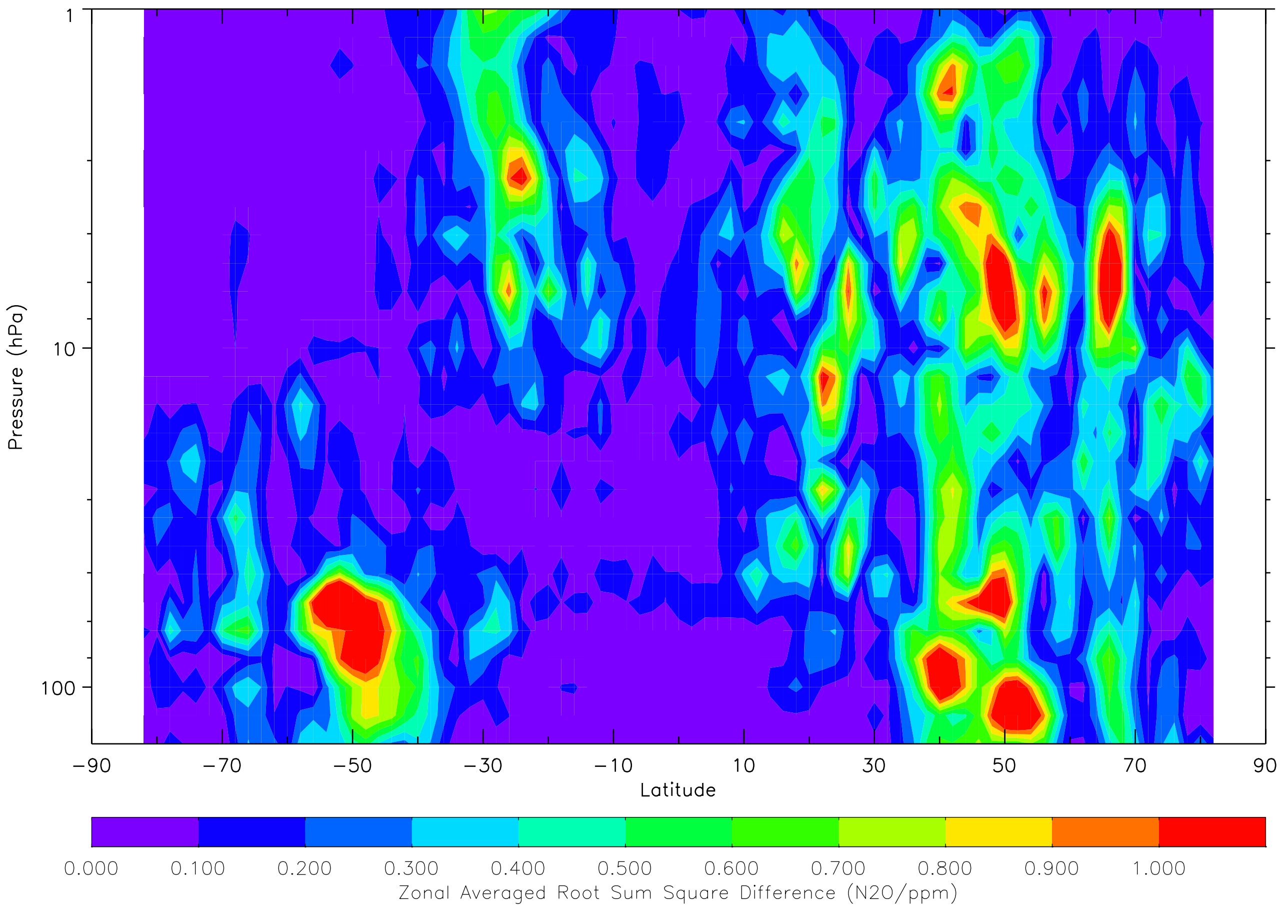

Fig. 3-12. Zonal averaged root sum square difference of N_2O between the reconstructed data and CTM model results on February 15, 1996.

3.2 Daily zonal mean products

3.2.1 Algorithms

Daily zonal mean products will be produced from the daily data on the nominal Level 2 latitude grid. The daily zonal mean at each latitude is obtained simply by averaging all the measurements in a day at that latitude. The software will have the capability, under the control of the user input file, to produce separate 'ascending-only', 'descending-only', and 'combined' zonal means.

3.2.2 Diagnostics

Daily zonal mean diagnostics being considered include:

- Standard deviation of points about the zonal mean σ_{L3DZM}.
- Flags for the latitudes where daily zonal mean cannot be obtained due to the lack of data.

3.3 Monthly map products

3.3.1 Algorithms

Monthly map products on the nominal Level 3 grid will be produced from the asynoptic daily data on the nominal Level 3 latitude-longitude grid. After interpolating MLS Level 2 data to the nominal Level 3 Map grid as shown in Figure 2-1, the monthly maps will be obtained simply by averaging all the asynoptic daily data on nominal Level 3 grid in a month at each grid point.

3.3.2 Diagnostics

Monthly map diagnostics being considered include:

- Maps of the rss scatter of daily values about the monthly mean.
- Maps of the maximum and minimum daily difference from the monthly mean.

3.4 Monthly zonal mean products

3.4.1 Algorithms

Monthly zonal mean products on nominal Level 2 latitudes will be produced from the daily zonal means on nominal Level 2 latitudes. The monthly zonal means are obtained simply by averaging the daily zonal means for that month.

3.4.2 Diagnostics

Monthly zonal mean diagnostics being considered include:

- Standard deviation of points about the monthly zonal mean σ_{L3MZM}.
- Flags for the latitudes where monthly zonal mean can not be obtained due to the lack of data.
- Flags for the days when there are no data available.

4. Additional Topics

This section considers additional issues with MLS Level 3 data processing algorithms, including topics that, while not strictly part of the theoretical basis for the algorithms, are worthy of discussion here.

4.1 Tuning of algorithms and strategy for post-launch operations

Tuning of the algorithms includes the following:

- Choice of record range T (see Section D. 1.3)
- Change of interpolation method to be applied to the data before doing FFT (see Section 3.1.1)
- Change of weighting function to be applied to the data before doing FFT (see Section 3.1.2.9)
- Maximum size of data gaps before Level 3 processing is halted (see Section 3.1.1)
- Others

4.2 Quality control, exception handling and related issues

4.2.1 Quality of products

In addition to producing synoptic maps for each physical parameter, the MLS data processing algorithms as described in Section 3.1.2.7 will compute an estimated uncertainty for each datum in the synoptic maps generated.

As described in section 3.1.2, the uncertainty on the generated result should always be compared with the uncertainty given in the input data. This comparison, along with the uncertainty information itself will form a major part of quality control. In the UARS MLS case, the uncertainty in Level 2 is set negative if it is greater than half of the *a priori* uncertainty. This serves as a useful flag to the users of the data, to indicate where and when data should be approached with caution. Similar flags may be implemented for EOS MLS Level 3, but these issues remain to be decided.

Another source of quality control information will be the σ_{L3g} information (see section 3.1.2). Cases where the retrieval of synoptic map is poor for some reason will be clearly indicated by a high value of σ_{L3g}. A complete set of σ_{L3g} statistics will be produced by the synoptic mapping algorithms routinely, giving the values of σ_{L3g} for each map generated. This σ_{L3g} information will also form the basis of a simple quality flag for each product, indicating the validity of the data, as was done for UARS MLS.

4.2.2 Bad or missing data

If the number of missing data does not exceed the limits that the algorithm can handle, the process of reconstruction of synoptic maps will continue. But the percentage of the missing points will be calculated and put in diagnostics as pointed out in section 3.1.3.

4.2.3 Numerical exceptions

The synoptic mapping algorithm described here is sufficiently well posed and numerically stable that occurrences such as division by zero, or requesting the square root of a negative number should never occur. For this reason, no special handling is needed for such events; any attempt to perform such calculation will be indicative of a “bug” in the program, and so should simply bring the processing to an immediate halt with an appropriate error message.

4.3 Validation of Level 3 algorithms and data products

The approach to the validation of the EOS MLS data follows the procedure used successfully for the UARS MLS, and is summarized in the overview document [*Waters* 2004]. Some validation of the Level 3 algorithm itself will also be required. A vital tool for this validation is the use of CTM simulated atmosphere. The algorithm has been tested (see Appendix E) by sampling, with the MLS measurement pattern, a known field from a CTM output. Comparison of synoptic maps with the original CTM output both in the presence and absence of instrumental noise and systematic errors yields valuable insight into the performance of the synoptic mapping algorithm. The primary validation of the Level 3 data will be the comparison of how well the reconstructed Level 2 field fits the actual Level 2 data.

4.4 Data volumes

Table 4.6-1 summarizes the estimated EOS MLS Level 3 routine daily data volumes. Values are given in terms of ‘equivalent daily volume’ (e.g., volumes for monthly files are divided by 30). Appendix B gives details on which these estimates are based.

Table 4.6-1. Level 3 Estimated Equivalent Daily Data Volumes.

Product name	**equivalent volume for one day / Megabytes**
Daily Map	36
Daily Map Diagnostics	20
Spectra	44
Monthly Map	4
Daily Zonal Means	2.1
Monthly Zonal Means	0.07
total	~106

Appendix A. User Input File Information

Information that has currently been identified for the Level 3 User Input File is itemized here. Many additional pieces of information are expected to be added as our concept for the Level 3 processing, and diagnostics, matures. It is also possible that, as part of the overall software design, it may be desirable to break the single "user input parameter file" implied in Figure 2-1 into several files (for example separate ones for daily and monthly maps, and daily and monthly zonal means).

1. Related to Level 2 Input Data

   - Which Level 2 data products are to be read
   - Which Level 2 data version to read
   - For what range of days to input Level 2 data

2. Related to Output Data Products and Algorithm Control

   a. For interpolating to latitude grids:
      - Latitude grid for maps
      - Latitude grid for zonal means
      - What method(s) to use for interpolating Level 2 data to fill in missing or bad data
      - Maximum size of Level 2 data gap before Level 3 processing is halted
      - Whether 'along-track' spectra are to be computed and, if so, the parameters needed for controlling this computation

   b. For daily maps (following information to be provided separately for 'ascending-only', 'descending-only' and 'combined ascending/descending' maps):
      - The data products and pressure levels for which maps are to be produced
      - The range of wavenumbers and frequencies to be fit for each product
      - The range(s) of days to be used for fitting Fourier components for each product
      - The longitude grid for which mapped values are to be output for each product
      - The synoptic time for which mapped values are to be output for each product
      - The method(s) of low-pass filtering that are to be used before the Fourier transformation
      - The method(s) of weighting that are to be used after the Fourier transformation to reconstruct the synoptic maps
      - Information on diagnostic information to be produced, such as the following
        - For which, if any, data products, pressure levels, latitude ranges, and days to produce an anomaly file (difference between Level 2 data and values from Level 3 Fourier coefficients evaluated at time and location of each Level 2 measurement) and time-series.
        - The number N for the N largest differences between the Level 2 measurements and the Level 3 'reconstruction' of these measurements to output (the output file produced for this will include the values, differences, time, location, pressure, etc., for each – listed in decreasing absolute value of the difference)
        - What data products, pressure levels, and days, for which a file is to be made of the latitude variation in zonal mean rss difference between Level 2 measurements and Level 3 reconstruction

c. For monthly maps (following information to be provided separately for 'ascending-only', 'descending-only' and 'combined ascending/descending' maps):
   - The data products and pressure levels for the maps that are to be produced
   - The method(s) of averaging to produce the 'monthly' map
   - The range(s) of days to be averaged together to produce the 'monthly' map
   - The version of Level 3 data to be used for producing these maps
   - Information on diagnostic information to be produced, such as the following
     - What products, if any, for producing a map of standard deviations of the daily data about the monthly mean
     - What products, if any, for producing a map of maximum deviations of the daily data about the monthly mean
     - What products, if any, for producing a map of data quality flags
     - ? What products, if any, for producing a map of number of data points that went into grid point for monthly map

d. For daily zonal means (following information to be provided separately for 'ascending-only', 'descending-only' and 'combined ascending/descending' zonal means):
   - The data products and pressure levels for the zonal means that are to be produced
   - Information on diagnostic information to be produced, such as the following:
     - What products, if any, for producing standard deviations of the individual points about the zonal mean
     - What products, if any, for producing maximum deviations of the individual points about the zonal mean
     - Whether to produce zonal mean and standard deviations of (1) the local solar time, (2) the local solar zenith angle, and (3) the line-of-sight angle at each latitude grid point

e. For monthly zonal means (following information to be provided separately for 'ascending-only', 'descending-only' and 'combined ascending/descending' maps):
   - The data products and pressure levels for the monthly zonal means that are to be produced
   - The range(s) of days to be averaged together to produce the 'monthly' zonal means
   - The version of Level 3 data to be used for producing these maps
   - Information on diagnostic information to be produced, such as the following:
     - What products, if any, for producing standard deviations of the daily data about the monthly mean
     - What products, if any, for producing maximum deviations of the daily data about the monthly mean
     - What products, if any, for producing a map of data quality flags
     - Whether to produce 'monthly' zonal mean and standard deviations of (1) the local solar time, (2) the local solar zenith angle, and (3) the line-of-sight angle at each latitude grid point

Appendix B. Data Volume Estimates

B.1 Output files of daily maps, diagnostics, and their FFSM spectra

Each file will contain one standard geophysical data product and its diagnostics. These files will be used to examine the temporal evolution over many days of the maps for single parameters, and keeping the size of these files down to a few MB is worthwhile. The separate ascending and descending maps for the diurnally-varying parameters will be grouped together into the file for that data product. The daily map volume estimate is summarized in Table B.1-1.

Diagnostic information on the maps produced by Level 3 data processing will be put in the same files as the data. Some information planned for the daily map diagnostics is discussed in 3.1 and 3.2. The daily map diagnostic volume estimate is summarized in Table B.1-2.

FFSM spectra are produced separately for each standard geophysical data product. The spectra are produced from ~30 days of Level 2 data and used to reconstruct 10 days of daily maps in the center of the ~30-day period. The ~30 days window used for producing the spectra will be moved forward 10 days for the next 10 days synoptic map reconstruction and so forth. Table B.1-3 gives the volume estimate for Level 3 FFSM spectra.

B.2 Output files of monthly maps

There will be one file (~39 MB) for each month which groups together monthly maps of all standard data products. The primary reason for grouping them together is to reduce the number of file names we have to keep up with. The monthly map volume estimate is summarized in Table B.2-1.

B.3 Output files of daily zonal means and monthly zonal means

Separate zonal means will be produced for the ascending and descending side of the orbits for all products, and will have the varying latitude resolution of Level 2 data. Files will contain both estimated value and precision for each datum that is produced.

A single file (~2 MB) will contain all zonal means of standard geophysical data products, one file for each day (daily zonal means), and one file for each month (monthly zonal means). These files will also contain zonal mean diagnostic information produced by Level 3 data processing. Some of the diagnostic information to be produced – for each latitude bin and each geophysical parameter – are discussed in 3.1 and 3.2. The volume estimates are shown in Table B.3-1 and Table B.3-2.

Table B.1-1. Level 3 Daily Map Products and Their Estimated Volumes. The number of pressure surfaces, and volumes, assume the maximum 12 retrieval points per decade pressure, and 4-byte words for the value and precision at each grid point.

Product name	Units	vertical range pressure / hPa max	vertical range pressure / hPa min	vertical range ~ height / km min	vertical range ~ height / km max	number of pressure surfaces	volume for one day / Megabytes
TEMPERATURE	K	464	0.01	0	80	56	3.28
CO	Vmr	464	0.01	0	80	56	3.28
H2O	Vmr	464	0.01	0	80	56	3.28
HNO3	Vmr	100	1	15	50	24	1.49
O3	Vmr	316	.316	9	55	36	2.15
O3_ascending	Vmr	3.16	0.01	40	80	30	2.15
O3_descending	Vmr	3.16	0.01	40	80	30	2.15
HCl	Vmr	100	0.1	15	65	36	2.15
N2O	Vmr	215	1	9	50	28	1.67
ClO_ascending	Vmr	100	1	15	50	24	1.49
ClO_descending	Vmr	100	1	15	50	24	1.49
OH_ascending	Vmr	10	0.1	15	65	24	1.49
OH_descending	Vmr	10	0.1	15	65	24	1.49
HCN	Vmr	215	22	9	25	12	0.66
GPH	Vmr	464	0.01	0	80	56	3.28
IWC	Vmr	464	0.01	0	80	56	3.28
RHI	Vmr	464	0.01	0	80	56	3.28
						Estimated total daily volume	36.39

Table B.1-2. Level 3 Daily Map Products Diagnostics and Their Estimated Volumes. The number of pressure surfaces, and volumes, assume the maximum 12 retrieval points per decade pressure, and 4-byte words for the value and precision at each grid point.

Product name	units	vertical range pressure / hPa max	vertical range pressure / hPa min	vertical range ~ height / km min	vertical range ~ height / km max	number of pressure surfaces	volume for one day / Megabytes Diagnostic	volume for one day / Megabytes Residual
TEMPERATURE	K	464	0.01	0	80	56	0.024	1.553
CO	vmr	464	0.01	0	80	56	0.024	1.553
H2O	vmr	464	0.01	0	80	56	0.024	1.553
HNO3	vmr	100	1	15	50	24	0.011	0.839
O3	vmr	316	.316	9	55	36	0.016	1.147
O3_ascending	vmr	3.16	0.01	40	80	30	0.016	1.147
O3_descending	vmr	3.16	0.01	40	80	30	0.016	1.147
HCl	vmr	100	0.1	15	65	36	0.016	1.175
N2O	vmr	215	1	9	50	28	0.013	0.923
ClO_ascending	vmr	100	1	15	50	24	0.011	0.839
ClO_descending	vmr	100	1	15	50	24	0.011	0.839
OH_ascending	vmr	10	0.1	15	65	24	0.011	0.839
OH_descending	vmr	10	0.1	15	65	24	0.011	0.839
HCN	vmr	215	22	9	25	12	0.005	0.448
GPH	vmr	464	0.01	0	80	56	0.024	1.553
IWC	vmr	464	0.01	0	80	56	0.024	1.553
RHI	vmr	464	0.01	0	80	56	0.024	1.553
						Estimated total daily volume	19.777	

Table B.1-3. Level 3 Spectra Products and Their Estimated Volumes. The number of pressure surfaces, and volumes, assume the indicated number of spectral output points per decade pressure, and 4-byte words for the value and precision at each grid point. Note that the spectra are not saved to the full vertical resolution of the maps or Level 2 data.

Product name	units	Vertical range pressure / hPa max	min	~ height / km min	max	number of pressure surfaces per decade	volume for ~10 days period / Megabytes
TEMPERATURE	K	464	0.01	0	80	6	36.2
CO	vmr	464	0.01	0	80	6	36.2
H2O	vmr	464	0.01	0	80	6	36.2
HNO3	vmr	100	1	15	50	3	16.5
O3	vmr	316	.316	9	55	6	23.3
O3_ascending	vmr	3.16	0.01	40	80	3	23.3
O3_descending	vmr	3.16	0.01	40	80	3	23.3
HCl	vmr	100	0.1	15	65	3	25.0
N2O	vmr	215	1	9	50	6	18.9
ClO	vmr	100	1	15	50	3	16.5
ClO_ascending	vmr	100	1	15	50	3	16.5
ClO_descending	vmr	100	1	15	50	3	16.5
OH	vmr	10	0.1	15	65	3	16.5
OH_ascending	vmr	10	0.1	15	65	3	16.5
OH_descending	vmr	10	0.1	15	65	3	16.5
HCN	vmr	215	22	9	25	3	7.5
GPH	vmr	464	0.01	0	80	6	36.2
IWC	vmr	464	0.01	0	80	6	36.2
RHI	vmr	464	0.01	0	80	6	36.2
						Estimated total monthly volume	435.1
						Estimated equivalent total daily volume	43.5

Table B.2-1. Level 3 Monthly Map Products and Their Estimated Volumes. The number of pressure surfaces, and volumes, assume the maximum 12 retrieval points per decade pressure, and 4-byte words for the value and precision at each grid point.

product name	units	vertical range pressure / hPa max	min	~ height / km min	max	number of pressure surfaces	volume for one month / Megabytes
TEMPERATURE	K	464	0.01	0	80	56	3.28
CO	vmr	464	0.01	0	80	56	3.28
H2O	vmr	464	0.01	0	80	56	3.28
HNO3	vmr	100	1	15	50	24	1.50
O3	vmr	316	.316	9	55	36	2.10
O3_ascending	vmr	3.16	0.01	40	80	30	2.10
O3_descending	vmr	3.16	0.01	40	80	30	2.10
HCl	vmr	100	0.1	15	65	36	2.21
N2O	vmr	215	1	9	50	28	1.67
ClO	vmr	100	1	15	50	24	1.50
ClO_ascending	vmr	100	1	15	50	24	1.50
ClO_descending	vmr	100	1	15	50	24	1.50
OH_ascending	vmr	10	0.1	15	65	24	1.50
OH_descending	vmr	10	0.1	15	65	24	1.50
HCN	vmr	215	22	9	25	12	0.66
GPH	vmr	464	0.01	0	80	56	3.28
IWC	vmr	464	0.01	0	80	56	3.28
RHI	vmr	464	0.01	0	80	56	3.28
						Estimated total monthly volume	38.71
						Estimated equivalent total daily volume	3.87

Table B.3-1. Level 3 Daily Zonal Means Products and Their Estimated Volumes. The number of pressure surfaces, and volumes, assume the maximum 12 retrieval points per decade pressure, and 4-byte words for the value and precision at each grid point.

product name	units	vertical range				number of pressure surfaces	volume for one day / Megabytes
		pressure / hPa		~ height / km			
		max	min	min	max		
TEMPERATURE	K	464	0.01	0	80	56	0.216
CO	vmr	464	0.01	0	80	56	0.216
H2O	vmr	464	0.01	0	80	56	0.216
HNO3	vmr	100	1	15	50	24	0.102
O3	vmr	316	.316	9	55	36	0.145
RHI	vmr	464	0.01	0	80	55	0.216
HCl	vmr	100	0.1	15	65	36	0.148
N2O	vmr	215	1	9	50	28	0.113
ClO	vmr	100	1	15	50	24	0.102
GPH	vmr	464	0.01	0	80	55	0.216
OH	vmr	10	0.1	15	65	24	0.102
IWC	vmr	464	0.01	0	80	55	0.216
HCN	vmr	215	22	9	25	12	0.047
Estimated total daily volume							2.1

Table B.3-2. Level 3 Monthly Zonal Means Products and Their Estimated Volumes. The number of pressure surfaces, and volumes, assume the maximum 12 retrieval points per decade pressure, and 4-byte words for the value and precision at each grid point.

product name	units	vertical range				number of pressure surfaces	volume for one month / Megabytes
		pressure / hPa		~ height / km			
		max	min	min	max		
TEMPERATURE	K	464	0.01	0	80	56	0.216
CO	vmr	464	0.01	0	80	56	0.216
H2O	vmr	464	0.01	0	80	56	0.216
HNO3	vmr	100	1	15	50	24	0.102
O3	vmr	316	.316	9	55	36	0.145
RHI	vmr	464	0.01	0	80	55	0.216
HCl	vmr	100	0.1	15	65	36	0.148
N2O	vmr	215	1	9	50	28	0.113
ClO	vmr	100	1	15	50	24	0.102
GPH	vmr	464	0.01	0	80	55	0.216
OH	vmr	10	0.1	15	65	24	0.102
IWC	vmr	464	0.01	0	80	55	0.216
HCN	vmr	215	22	9	25	12	0.047
Estimated total monthly volume							2.1
Estimated equivalent total daily volume							0.07

Appendix C. Derivation of Certain Formulae

C.1 Derivation of Eqn. (3-10)

From Fig.3-4, due to the rotation of asynoptic coordinates (r, s) relative to synoptic coordinates (λ, t), the separation Δs of two contiguous nodes of either locus is

$$\Delta s = \frac{\tau_0}{\sin\alpha}$$

Also we can immediately derive that

$$\Delta r_2 = \Delta\lambda'_{ad} \sin\alpha = \frac{\Delta\lambda'_{ad}}{(1+c_0^2)^{\frac{1}{2}}}$$

$$\Delta r_1 = (2\pi - \Delta\lambda'_{ad})\sin\alpha = \frac{2\pi - \Delta\lambda'_{ad}}{(1+c_0^2)^{\frac{1}{2}}}$$

C.2 Derivation of Eqn. (3-13)

To derive equation

$$s_{dn} = -c_0 \frac{\Delta r}{2} + n\Delta s$$

$$s_{an} = s_{dn} - c_0\Delta r_2 + \Delta t_{ad}(1+c_0^2)^{\frac{1}{2}}$$

In Fig. 3-6 assuming the first descending point is at longitude $\lambda = 0$, then the corresponding coordinate in (r, s) is (from top descending loci in Fig 3-6)

$$s_{d0} = -c_0 \frac{\Delta r}{2}$$

therefore

$$s_{dn} = -c_0 \frac{\Delta r}{2} + n\Delta s$$

Now from

$$\Delta r_2 = \frac{\Delta\lambda'_{ad}}{(1+c_0^2)^{\frac{1}{2}}}$$

we have

$$\begin{aligned}\Delta\lambda'_{ad} &= \Delta r_2(1+c_0^2)^{\frac{1}{2}} \\ \Delta\lambda_{ad} &= \Delta\lambda'_{ad} - c_0\Delta t_{ad} \\ &= \Delta r_2(1+c_0^2)^{\frac{1}{2}} - c_0\Delta t_{ad}\end{aligned}$$

But from

$$s = \lambda\cos\alpha - t\sin\alpha$$

we have

$$\begin{aligned}s_a &= \lambda_a\cos\alpha - t_a\sin\alpha \\ &= (\lambda_d - \Delta\lambda_{ad})\cos\alpha - (t_d - \Delta t_{ad})\sin\alpha \\ &= s_d - \Delta\lambda_{ad}\cos\alpha + \Delta t_{ad}\sin\alpha \\ &= s_d - [\Delta r_2(1+c_0^2)^{\frac{1}{2}} - c_0\Delta t_{ad}]\cos\alpha + \Delta t_{ad}\sin\alpha \\ &= s_d - c_0\Delta r_2 + \Delta t_{ad}(1+c_0^2)^{\frac{1}{2}}\end{aligned}$$

C.3 Derivation of Eqn. (3-21)

From (3.20)

$$\begin{aligned}\Psi(k_s, r_d) &= \Psi(k_s, k_r^-)e^{ik_r^- r_d} + \Psi(k_s, k_r^+)e^{ik_r^+ r_d} \\ \Psi(k_s, r_a) &= \Psi(k_s, k_r^-)e^{ik_r^- r_a} + \Psi(k_s, k_r^+)e^{ik_r^+ r_a}\end{aligned}$$

we can get

$$\begin{aligned}\Psi(k_s, k_r^+) &= \frac{\Psi(k_s, r_d)e^{-ik_r^- r_d} - \Psi(k_s, r_a)e^{-ik_r^- r_a}}{e^{i(k_r^+ - k_r^-)r_d} - e^{i(k_r^+ - k_r^-)r_a}} \\ \Psi(k_s, k_r^-) &= \frac{\Psi(k_s, r_d)e^{-ik_r^+ r_d} - \Psi(k_s, r_a)e^{-ik_r^+ r_a}}{e^{-i(k_r^+ - k_r^-)r_d} - e^{-i(k_r^+ - k_r^-)r_a}}\end{aligned}$$

Let's first simplify $\Psi(k_s, k_r^-)$:

$$\begin{aligned}\Psi(k_s, k_r^-) &= \frac{\Psi(k_s, r_a)e^{-ik_r^+ r_a} - \Psi(k_s, r_d)e^{-ik_r^+ r_d}}{e^{-i(k_r^+ - k_r^-)r_a} - e^{-i(k_r^+ - k_r^-)r_d}} \\ &= \frac{\Psi(k_s, r_a)e^{-ik_r^+ r_a}e^{-ik_r^- r_a}e^{ik_r^+ r_a} - \Psi(k_s, r_d)e^{-ik_r^+ r_d}e^{-ik_r^- r_a}e^{ik_r^+ r_a}}{e^{-i(k_r^+ - k_r^-)r_a}e^{-ik_r^- r_a}e^{ik_r^+ r_a} - e^{-i(k_r^+ - k_r^-)r_d}e^{-ik_r^- r_a}e^{ik_r^+ r_a}} \\ &= \frac{\Psi(k_s, r_a)e^{-ik_r^- r_a} - \Psi(k_s, r_d)e^{-ik_r^- r_d}e^{ik_r^- r_d}e^{-ik_r^+ r_d}e^{-ik_r^- r_a}e^{ik_r^+ r_a}}{e^{-i(k_r^+ - k_r^-)r_a}e^{-ik_r^- r_a}e^{ik_r^+ r_a} - e^{-i(k_r^+ - k_r^-)r_d}e^{-ik_r^- r_a}e^{ik_r^+ r_a}}\end{aligned}$$

By using $\Psi'(k_s, r) = \Psi(k_s, r)e^{-i(k_s s_0 + k_r r)}$, the above formula can be simplified to

$$\Psi(k_s,k_r^-) = \frac{\Psi'(k_s,r_a) - \Psi'(k_s,r_d)e^{-i(k_r^+ - k_r^-)(r_d - r_a)}}{1 - e^{-i(k_r^+ - k_r^-)(r_d - r_a)}}$$

From (3.10) and (3.22), we get

$$k_r^+ - k_r^- = 1/\sin\alpha$$
$$\Delta\lambda'_{ad} = (r_d - r_a)/\sin\alpha$$

Finally the derived equation becomes

$$\Psi(k_s,k_r^-) = \frac{\Psi'(k_s,r_a) - \Psi'(k_s,r_d)e^{-i(r_d - r_a)/\sin\alpha}}{1 - e^{-i(r_d - r_a)/\sin\alpha}}$$
$$= \frac{\Psi'(k_s,r_a) - \Psi'(k_s,r_d)e^{-i\Delta\lambda'_{ad}}}{1 - e^{-i\Delta\lambda'_{ad}}}$$

Now let's simplify $\Psi(k_s,k_r^+)$:

$$\Psi(k_s,k_r^+) = \frac{\Psi(k_s,r_d)e^{-ik_r^- r_d} - \Psi(k_s,r_a)e^{-ik_r^- r_a}}{e^{i(k_r^+ - k_r^-)r_d} - e^{i(k_r^+ - k_r^-)r_a}}$$
$$= \frac{\Psi'(k_s,r_d) - \Psi'(k_s,r_a)}{e^{i(k_r^+ - k_r^-)r_d}\left[1 - e^{-i(k_r^+ - k_r^-)(r_d - r_a)}\right]}$$
$$= \frac{\Psi'(k_s,r_d) - \Psi'(k_s,r_a)}{e^{ir_d/\sin\alpha}\left[1 - e^{-i\Delta\lambda'_{ad}\sin\alpha/\sin\alpha}\right]}$$
$$= \frac{\Psi'(k_s,r_d) - \Psi'(k_s,r_a)}{e^{i\lambda_d}\left[1 - e^{-i\Delta\lambda'_{ad}}\right]}$$

C.4 Derivation of Eqn. (3-22)

In (k_s,k_r) space, for each k_s, there are two allowed spectra, corresponding to the points (k_s,k_r^-) and (k_s,k_r^+) on wavenumbers *m* and *m*+1, respectively. From (3.9), we can get

$$\sigma = \frac{m\cos\alpha - k_s}{\sin\alpha}$$

Substitute into (3.9) again, we have

$$k_r^- = m\sin\alpha + \frac{m\cos\alpha - k_s}{\sin\alpha}\cos\alpha$$
$$= -k_s\frac{\cos\alpha}{\sin\alpha} + \frac{m}{\sin\alpha}$$
$$= -k_s c_0 + \frac{m}{\sin\alpha}$$

We can get

$$k_r^+ = -k_s c_0 + \frac{m+1}{\sin\alpha}$$

by the same procedure.

Appendix D. Examples of Results from Level 3 Software

This section discusses the test results from Level 3 v1.0 software. It will show the agreement between synthetic and simulated results, and CTM model results and reconstructed Daily Maps. Finally it will show some limitations of the Level 3 software and planned improvements.

D.1 Daily Maps

The main results from the Level 3 software are the Daily Maps.

D.1.1 Daily Maps from Synthetic Wave Patterns

The input data for the first round test of the Level 3 V1.0 software is the synthetic wave patterns with waves that could not be resolved by the algorithm. Figure D-1a, b show the comparisons of the reconstructed Daily Map and the synthetic data in selected latitudes for the combined mode. The results from the model are in agreement with the synthetic data within 5% (Figure D-1a) through all latitudes without noise added and within 10-20% (Figure D-1b) with 10% random noise added. The results also show the good agreement even in the higher latitudes (±80°).

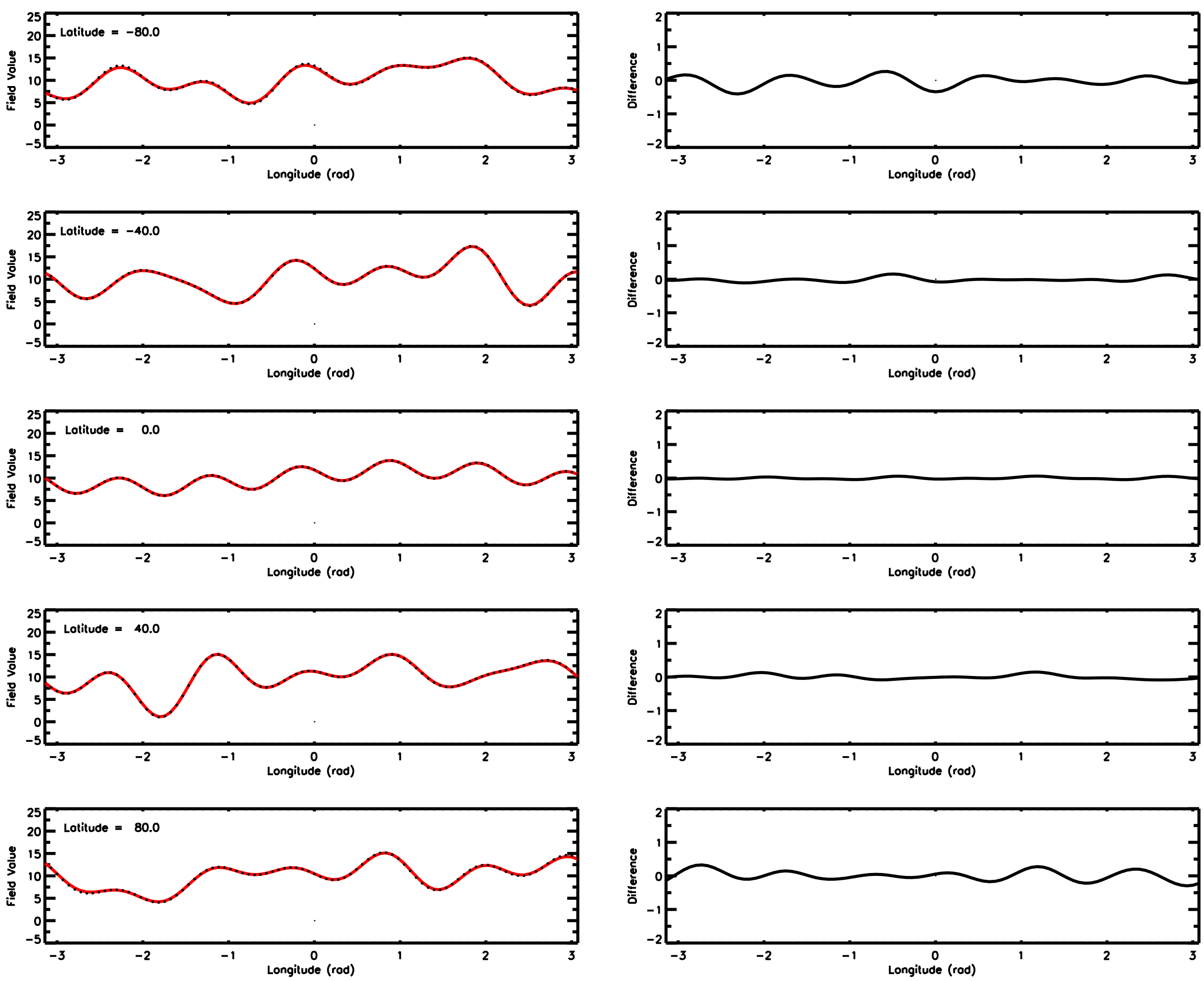

Figure D-1a. Comparisons of the reconstructed Daily Map at five latitudes (-80 °, -40 °, 0 °, 40 °, 80°) as compared to the synthetic wave pattern (no noise). The left panel gives the synthetic waves (solid lines) and reconstructed waves (dotted lines). The right panel shows the differences at these latitudes.

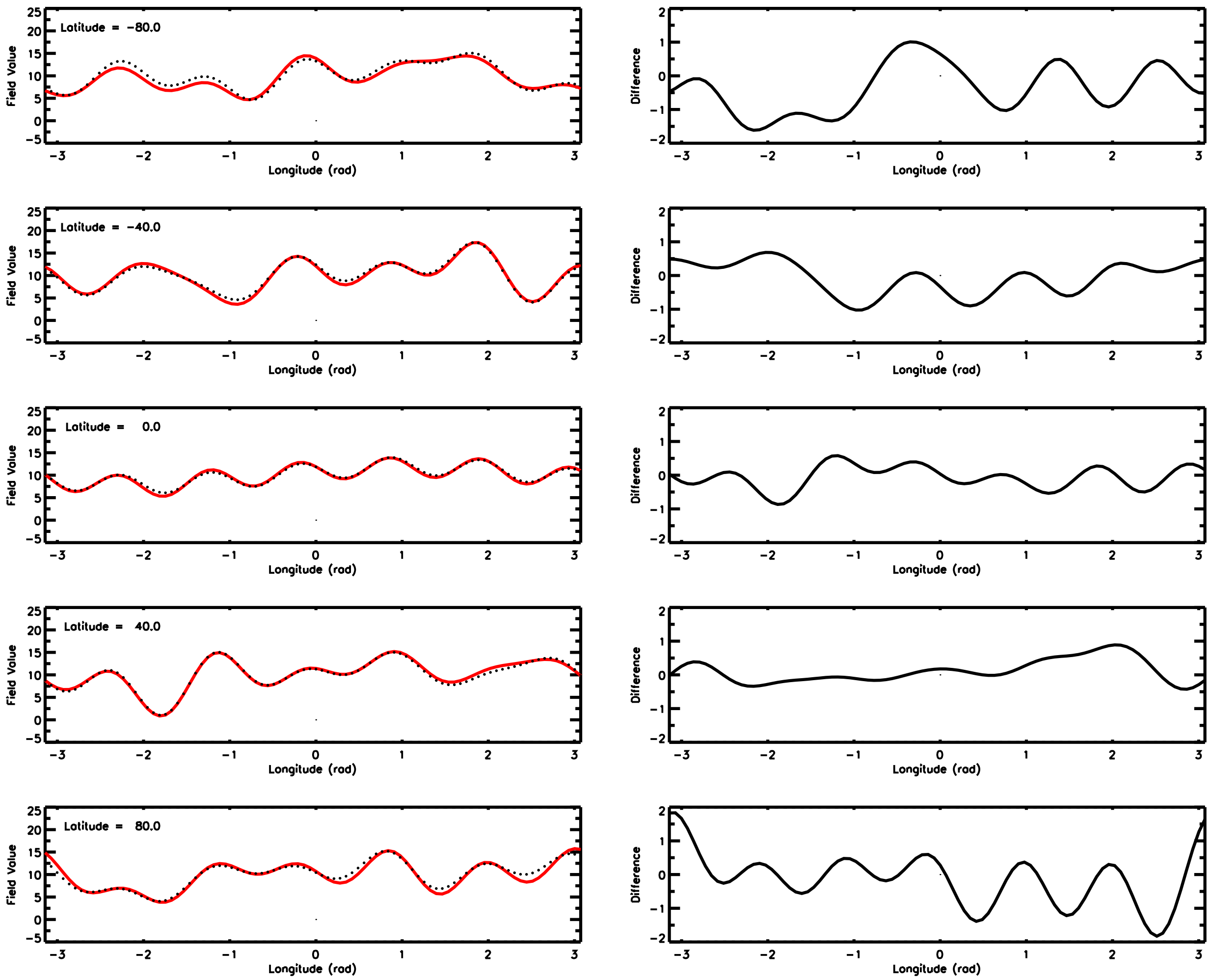

Figure D-1b. Comparison of the reconstructed Daily Map at five latitudes (-80°, -40°, 0°, 40°, 80°) as compared to the synthetic wave pattern with 10% random noise added. The left panel gives the synthetic waves (solid lines) and reconstructed waves (dotted lines). The right panel shows the differences in these latitudes.

Figure D-2 shows the residuals between the synthetic wave pattern and the reconstructed field value at the same location and time with that of synthetic wave pattern without noise added. As can be seen, the residuals are within 10% as compared with the true wave pattern.

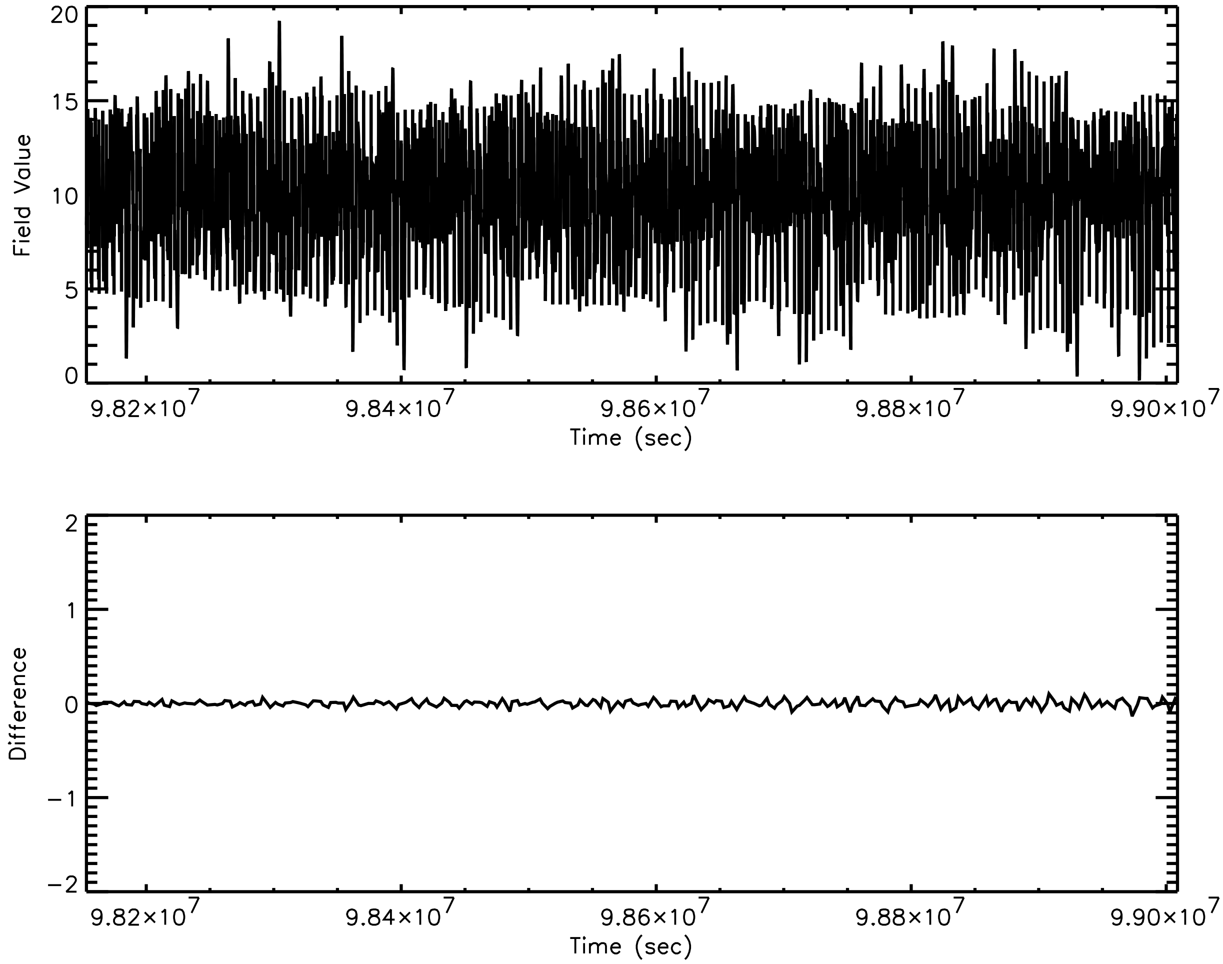

Figure D-2. Residual between the synthetic and reconstructed wave pattern along the satellite track. The top panel gives the synthetic wave and the bottom panel shows the residuals.

D.1.2 Daily Maps from Edinburgh University SLIMCAT Chemical Transport Model

The Level 3 algorithms were tested more realistically by using a simulated one-month (February 1, 1996 to February 29, 1996) of atmospheric data produced by the University of Edinburgh MLS team (using the SLIMCAT CTM driven with winds/temperatures from the Met Office stratosphere-troposphere data assimilation system, with vertical velocities from a middle atmosphere radiation code) and sampled in space and time according to the MLS measurement pattern.

Figure D-3 (northern polar view) and D-4 (southern polar view) show the constructed synoptic daily maps, and the model true synoptic maps of N_2O on February 11, 1996 from the one-month SLIMCAT CTM results. The CTM results and constructed daily maps of N_2O are compared at six pressure levels (147 hPa, 100 hPa, 32 hPa, 10 hPa, 3.2 hPa, and 1.0 hPa). The constructed maps match the true fields well within 10% of differences and are smoother due to the low-pass filtering effects of Level 3 algorithm. Since we reconstruct the fields at locations and times that no measurements are taken, there maybe some discrepancies between the truth and reconstructed fields. The comparison shows that the Level 3 software is producing the products as expected.

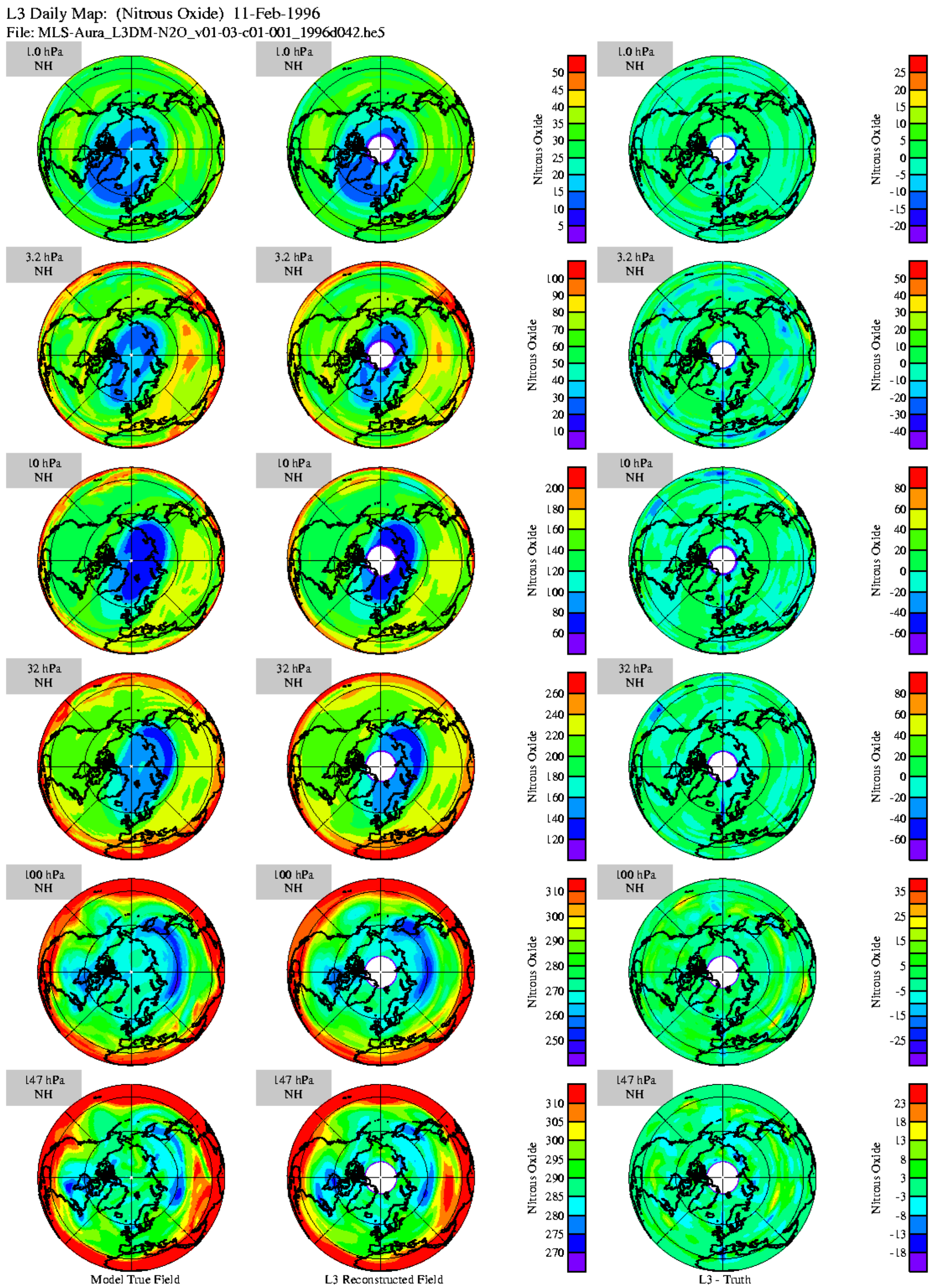

Figure D-3. Comparison between the CTM results and constructed daily maps of N_2O at six pressure levels (147 hPa, 100 hPa, 32 hPa, 10 hPa, 3.2 hPa, and 1.0 hPa) on February 11, 1996. The left two columns are the CTM synoptic maps and reconstructed synoptic maps. The right column shows the difference between the reconstructed and modeled fields. These plots show the view from North Pole.

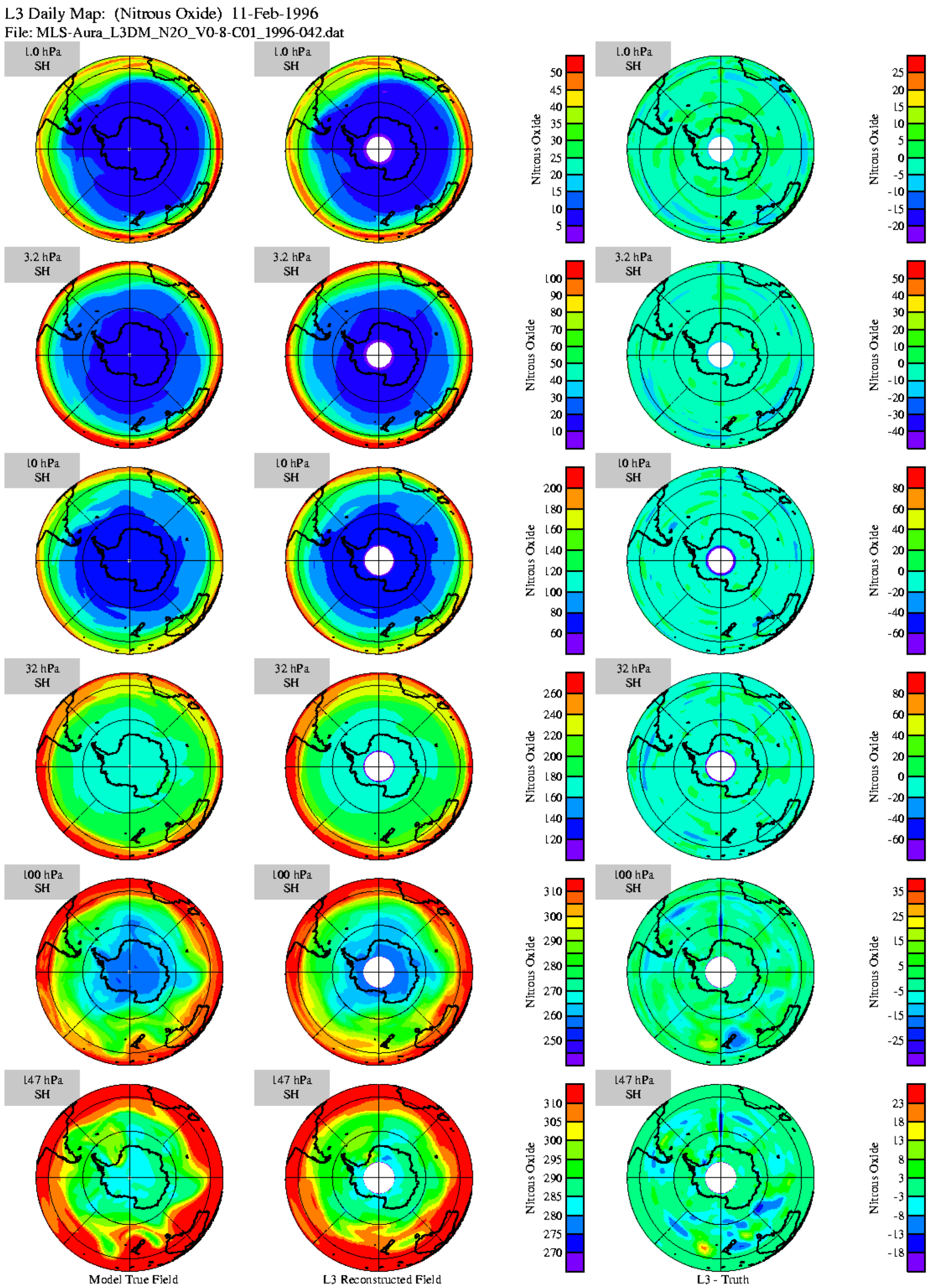

Figure D-4. Comparison between the CTM results and constructed daily maps of N_2O at six pressure levels (147 hPa, 100 hPa, 32 hPa, 10 hPa, 3.2 hPa, and 1.0 hPa) on February 11, 1996. The left two columns are the CTM synoptic maps and reconstructed synoptic maps. The right column shows the difference between the reconstructed and modeled fields. These plots show the view from South Pole.

D.1.3 Daily Maps vs. Input Window Size

A series of runs of N_2O by using a simulated one-month (February 1, 1996 to February 29, 1996) of atmospheric data produced by SLIMCAT CTM have been carried out by changing the input window size (number of days) in order to decide on the window size of input data for the Level 3 software. As was pointed out previously, only the middle ten days of Level 3 Daily Maps are constructed.

Here we choose the global averaged square root residuals of each pressure level between the constructed and synthetic data as criteria for evaluating the reconstructed daily map accuracy. Due to the dynamical and chemical properties of N_2O, there is not much change of wave pattern in the middle ten days of constructed maps. So we choose February 11, 1996 as an example in order to illustrate the conclusion we are going to make. Figure D-5 left plot shows the profile of global averaged mixing ratios at all pressure levels reconstructed as a reference, the middle plot shows the profile of global averaged square root residuals at all pressure levels reconstructed, the right plot shows global averaged square root of residuals at different pressure levels for different input window size ranging from 11 to 29 days. In this plot, different color represents different pressure level as shown in the color bar. The higher residuals around tropopause are expected as more higher frequencies and wavenumbers waves exist in that region. As it can be seen clearly in the right plot, although there are variations, but the residuals have a decreasing trend in each pressure level, the larger the window size the smaller the residuals.

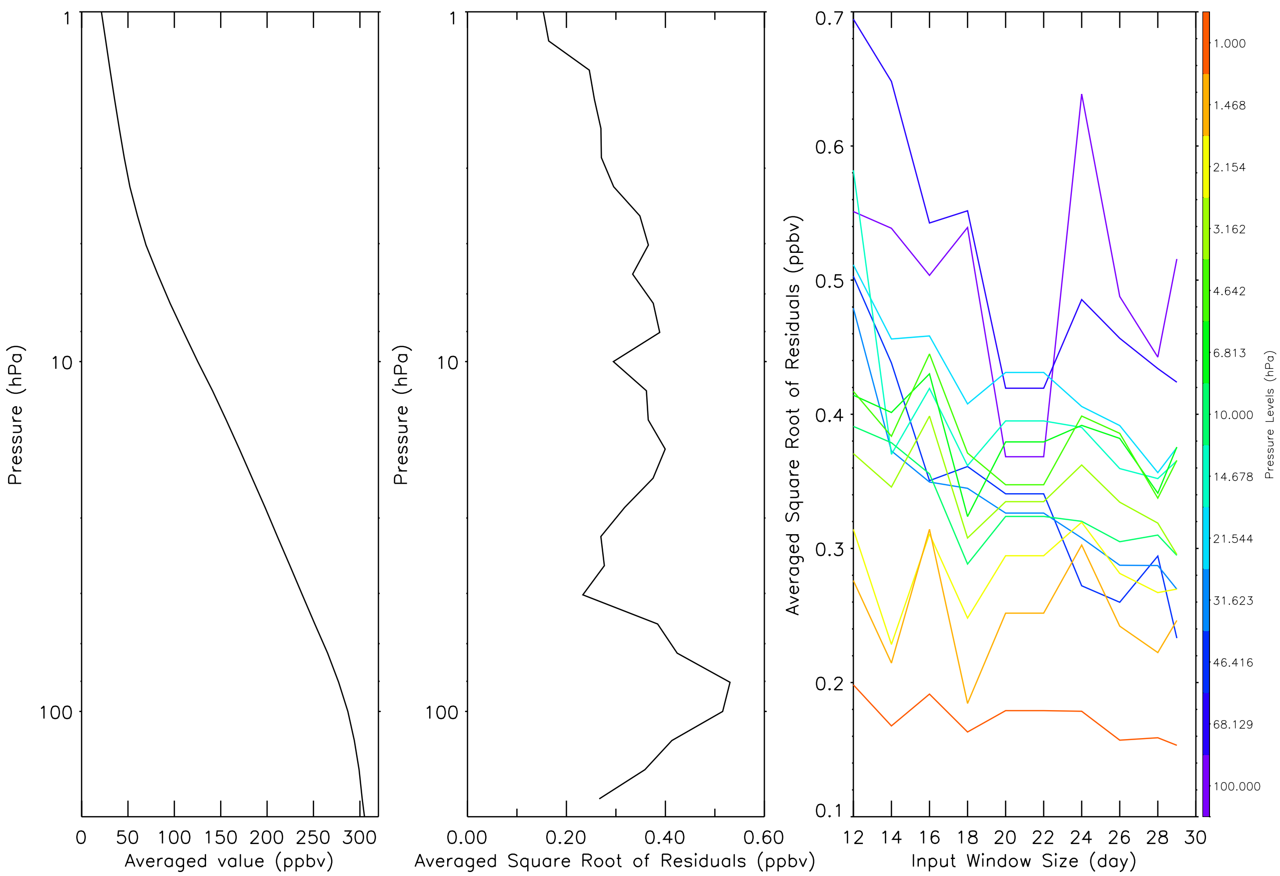

Figure D-5. Left and center plots show the global averaged mixing ratio and square root of residuals (ppbv) respectively at different pressure levels when the input window size is set to be 29 days. The right plot shows global averaged square root of residuals (ppbv) at different pressure levels for different input window size ranging from 12 to 28 days. Both plots are taken February 15, 1996 as an example.

Figure D-6 shows the global averaged square root of residuals (ppbv) on different MLS days (February 11, 1996 – February 20, 1996) at pressure 147 hPa. Its results show that the reconstructed fields in the center of 10 days (Day 46 are better than those at the edges (Day 42 and 51).

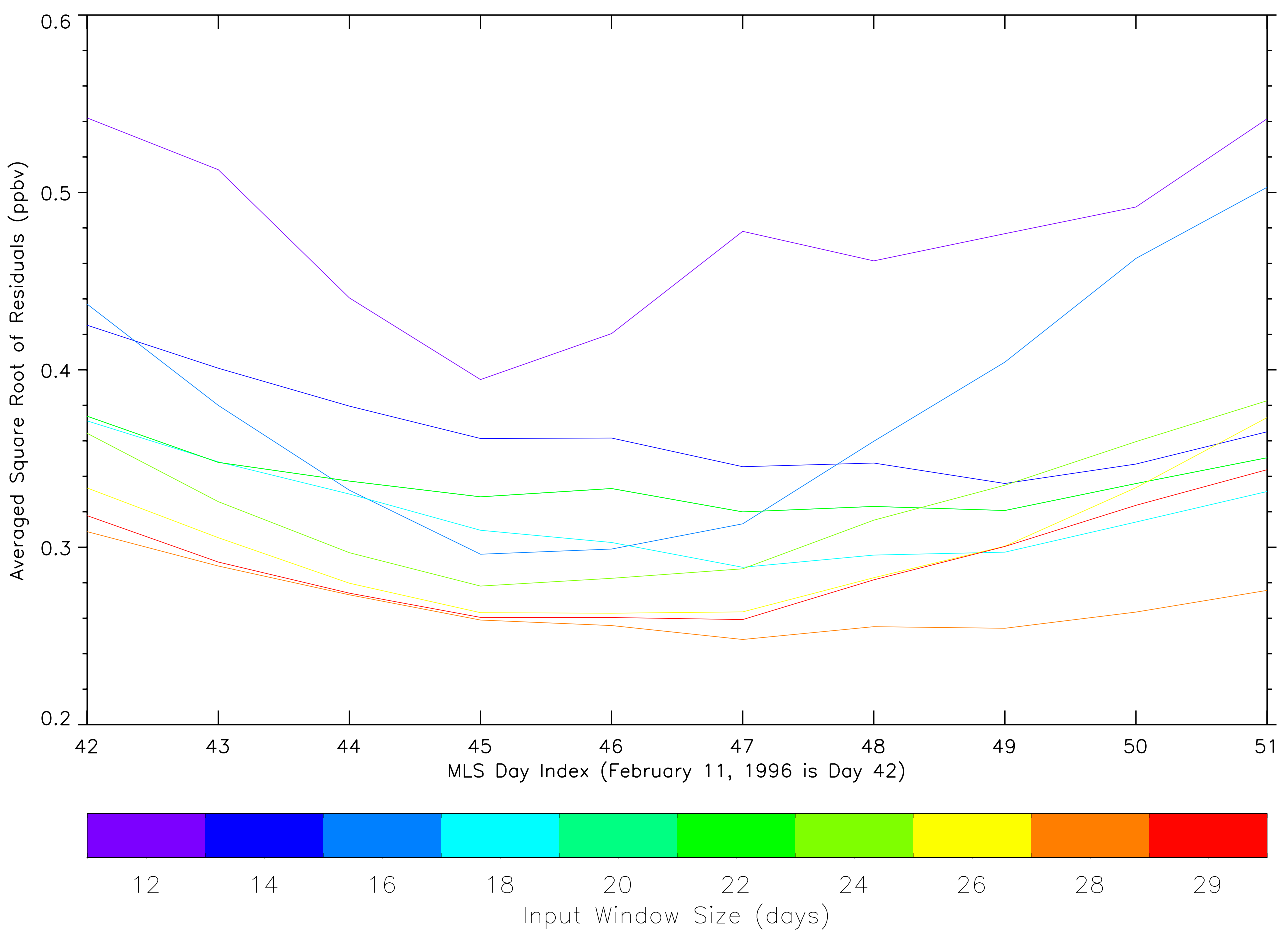

Figure D-6. Global averaged square root of residuals (ppbv) on different MLS days (February 11, 1996 – February 20, 1996) at pressure 147 hPa. The color lines show the values at different input window size.

Appendix E. Examples of Level 3 Data Inspection Plots

This appendix shows samples of the plots to be used for routine inspection of the Level 3 data. The examples given here were generated by running the Level 3 software on simulated Level 2 data provided by SLIMCAT CTM. N_2O is the data field used for the examples shown here, but similar plots will be routinely produced for all other appropriate fields.

E.1 Daily Maps

The main results from the Level 3 software are the daily maps and the residuals between Level 2 and reconstructed Level 2 from Level 3.

E.1.1 Polar Projections (1 page) and Cylindrical Projections (1 page) of Level 2 Residuals and Reconstructed Fields

Figure E1: Polar projection showing comparison between the input and reconstructed daily maps of N_2O at six pressure levels (147 hPa, 100 hPa, 31.6 hPa, 10 hPa, 3.16 hPa, and 1.0 hPa) (we select every other two pressure levels in the six pressure levels per decade scale in order to cover the atmosphere from upper troposphere to upper stratosphere) for February 15, 1996. The left two columns show the reconstructed N_2O fields for synoptic time. The right two columns are the residuals between the input and reconstructed fields. The first and third columns give the view from North Pole and the second and fourth give the view from South Pole.

Figure E2: As in Figure 1, but for cylindrical projection; Level 2 residuals are shown in the left column, and reconstructed fields in right column.

E.1.2 Longitude-Height Cross Sections (1 page)

Figure E3: Longitude-height cross section plots of N_2O at all latitudes (80^oN - 80^oS) produced on February 15, 1996.

E.1.3 Curtain Plots of Residual between Level 2 and Reconstructed Level 2 (1 pages)

Figure E4: Curtain plots of Level 2 residuals on linear contour scale on February 15, 1996.

E.1.4 Polar Projections (1 page) and Cylindrical Projections (1 page) of Level 3 Precision Estimates

Figure E5: Polar projection showing the Level 3 precision estimates of N_2O at 12 pressure levels on February 15, 1996. The first and third columns give the view from North Pole and the second and fourth give the view from South Pole.

Figure E6: As in Figure 5, but for cylindrical projection.

E.1.5 Spectra Plots

1. Amplitude vs. Period and Wavenumber for Different Pressures (7 pages)

   Figure E7: Amplitude in wave number and period coordinates in all latitudes (80^{o}N - 80^{o}S) at seven pressure levels (147 hPa, 100 hPa, 31.6 hPa, 10 hPa, 3.16 hPa, and 1.0 hPa). Each page represents one pressure level.

2. Phase vs. Period and Wavenumber for Different Pressures (7 pages)

   Figure E8: Phase in wave number and period coordinates in all latitudes (80^{o}N - 80^{o}S) at seven pressure levels (147 hPa, 100 hPa, 31.6 hPa, 10 hPa, 3.16 hPa, and 1.0 hPa). Each page represents one pressure level.

3. Amplitude vs. Period and Pressure for Different Wavenumbers (7 pages)

   Figure E9: Amplitude in period and pressure level coordinates in all latitudes (80^{o}N - 80^{o}S) at seven wave numbers (0, 1, 2, 3, 4, 5, 6). Each page represents one wave number.

4. Phase vs. Period and Pressure for Different Wavenumbers (7 pages)

   Figure E10: Phase in period and pressure level coordinates in all latitudes (80^{o}N - 80^{o}S) at seven wave numbers (0, 1, 2, 3, 4, 5, 6). Each page represents one wave number.

E.1.6 Spectra Plots of Precision Estimates

1. Amplitude vs. Period and Wavenumber for Different Pressures (7 pages)

   Figure E11: Amplitude in wave number and period coordinates in all latitudes (80^{o}N - 80^{o}S) at seven pressure levels (147 hPa, 100 hPa, 31.6 hPa, 10 hPa, 3.16 hPa, and 1.0 hPa). Each page represents one pressure level.

2. Phase vs. Period and Wavenumber for Different Pressures (7 pages)

   Figure E12: Phase in wave number and period coordinates in all latitudes (80^{o}N - 80^{o}S) at seven pressure levels (147 hPa, 100 hPa, 31.6 hPa, 10 hPa, 3.16 hPa, and 1.0 hPa). Each page represents one pressure level.

3. Amplitude vs. Period and Pressure for Different Wavenumbers (7 pages)

   Figure E13: Amplitude in period and pressure level coordinates in all latitudes (80^{o}N - 80^{o}S) at seven wave numbers (0, 1, 2, 3, 4, 5, 6). Each page represents one wave number.

4. Phase vs. Period and Pressure for Different Wavenumbers (7 pages)

   Figure E14: Phase in period and pressure level coordinates in all latitudes (80^{o}N - 80^{o}S) at seven wave numbers (0, 1, 2, 3, 4, 5, 6). Each page represents one wave number.

E.2 Monthly Maps

E.2.1 Polar Projections (1 page) and Cylindrical Projections (1 page)

Figure E15: The polar projection plots of N_2O at selected pressure levels in February, 1996.

Figure E16: The cylindrical projection plots of N_2O at selected pressure levels in February, 1996.

E.2.2 Longitude-Height Cross Sections (1 page)

Figure E17: Longitude-Height cross sections of N_2O at all latitudes (80^oN - 80^oS) produced in February, 1996.

E.3 Daily Zonal Means

E.3.1 Longitude-Height Cross Sections (1 page)

Figure E18: Daily zonal means of N_2O in February, 1996.

E.4 Monthly Zonal Means

E.4.1 Longitude-Height Cross Sections (1 page)

Figure E19: Monthly zonal means of all standard products produced for February, 1996.

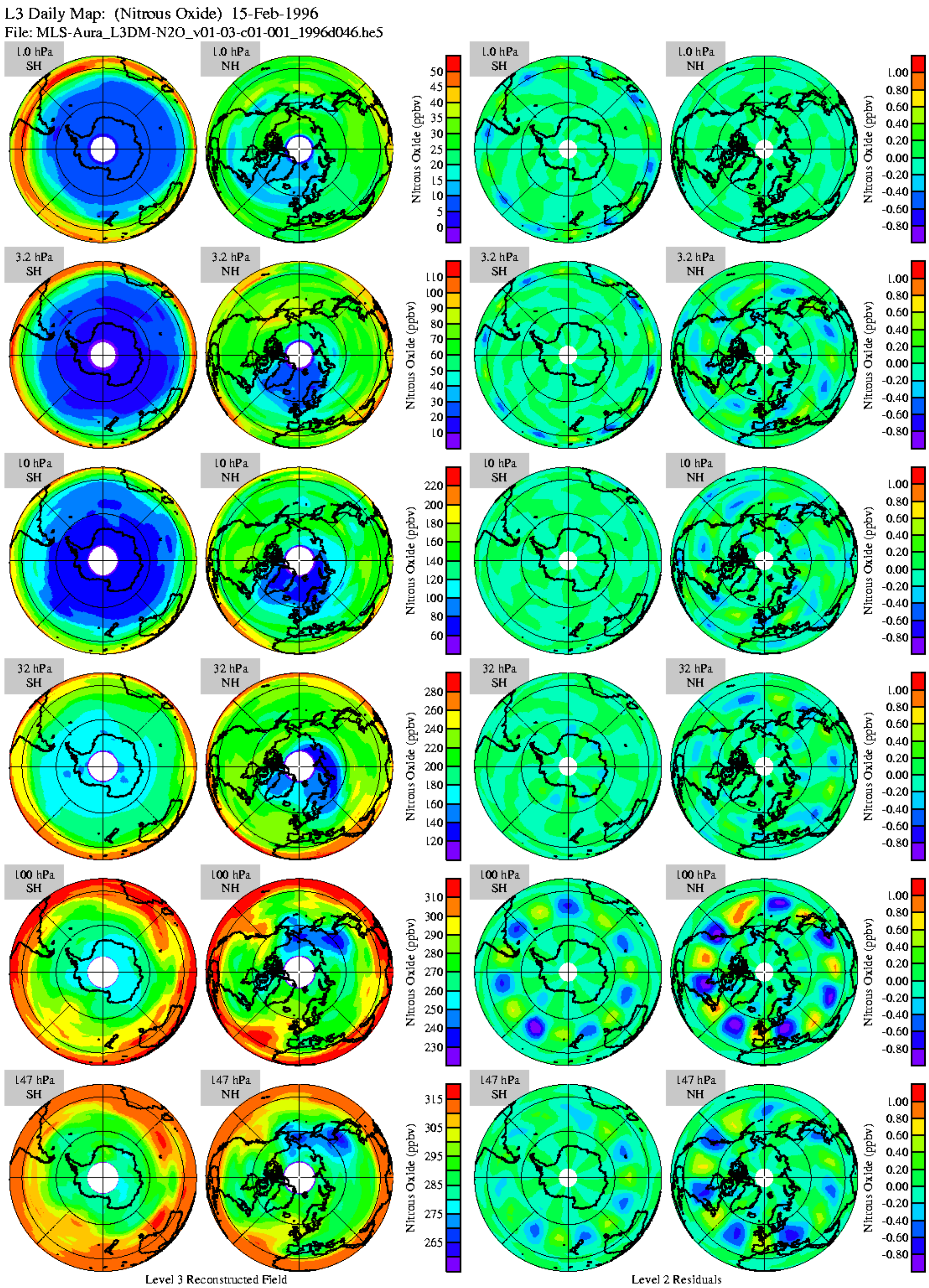
L3 Daily Map: (Nitrous Oxide) 15-Feb-1996
File: MLS-Aura_L3DM-N2O_v01-03-c01-001_1996d046.he5
1.0 hPa SH
1.0 hPa NH
3.2 hPa SH
3.2 hPa NH
10 hPa SH
10 hPa NH
32 hPa SH
32 hPa NH
100 hPa SH
100 hPa NH
147 hPa SH
147 hPa NH
Nitrous Oxide (ppbv)
Level 3 Reconstructed Field
Level 2 Residuals

Figure E1

L3 Daily Map: (Nitrous Oxide) 15-Feb-1996
File: MLS-Aura_L3DM-N2O_v01-03-c01-001_1996d046.he5

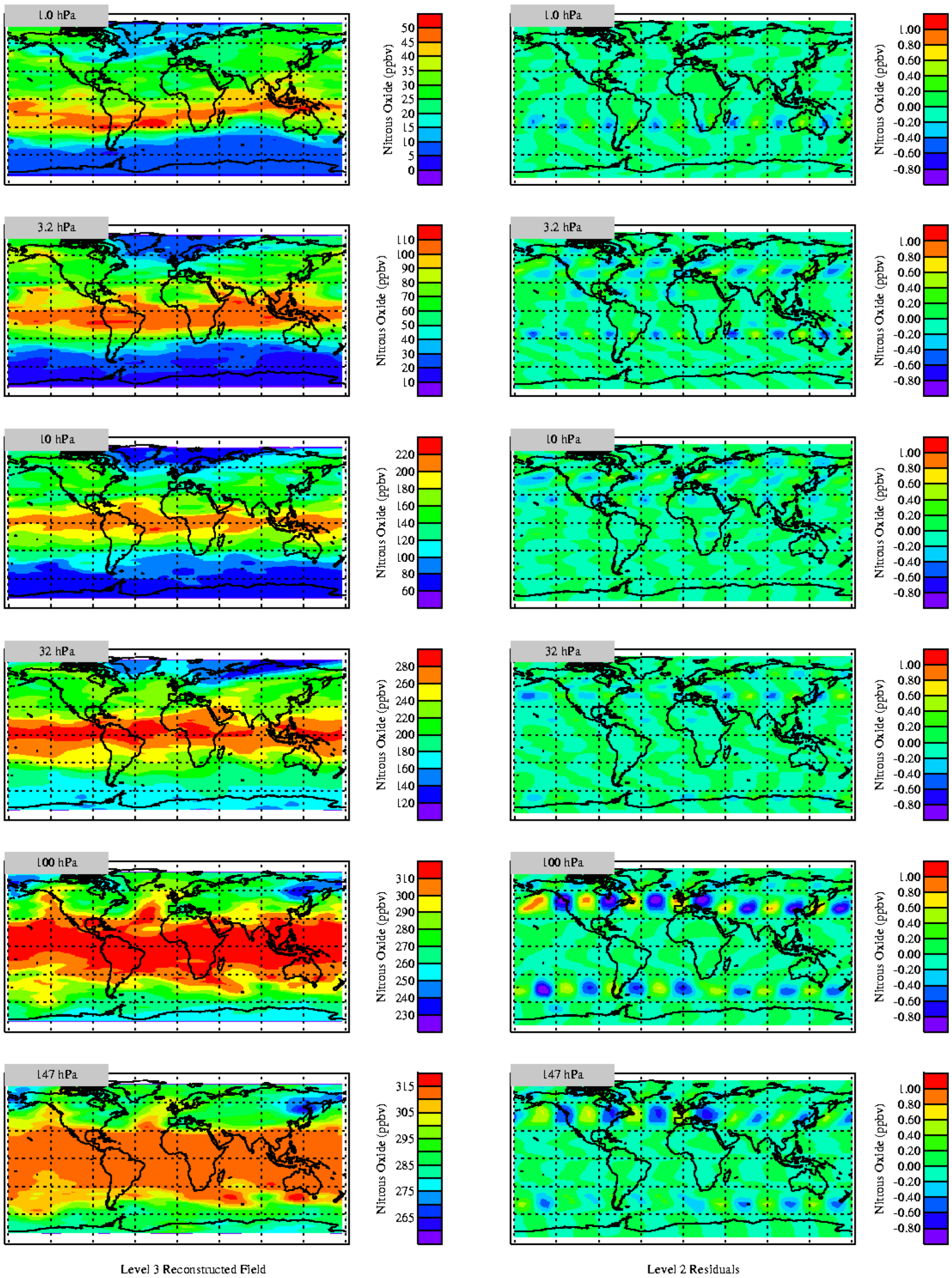

Figure E2

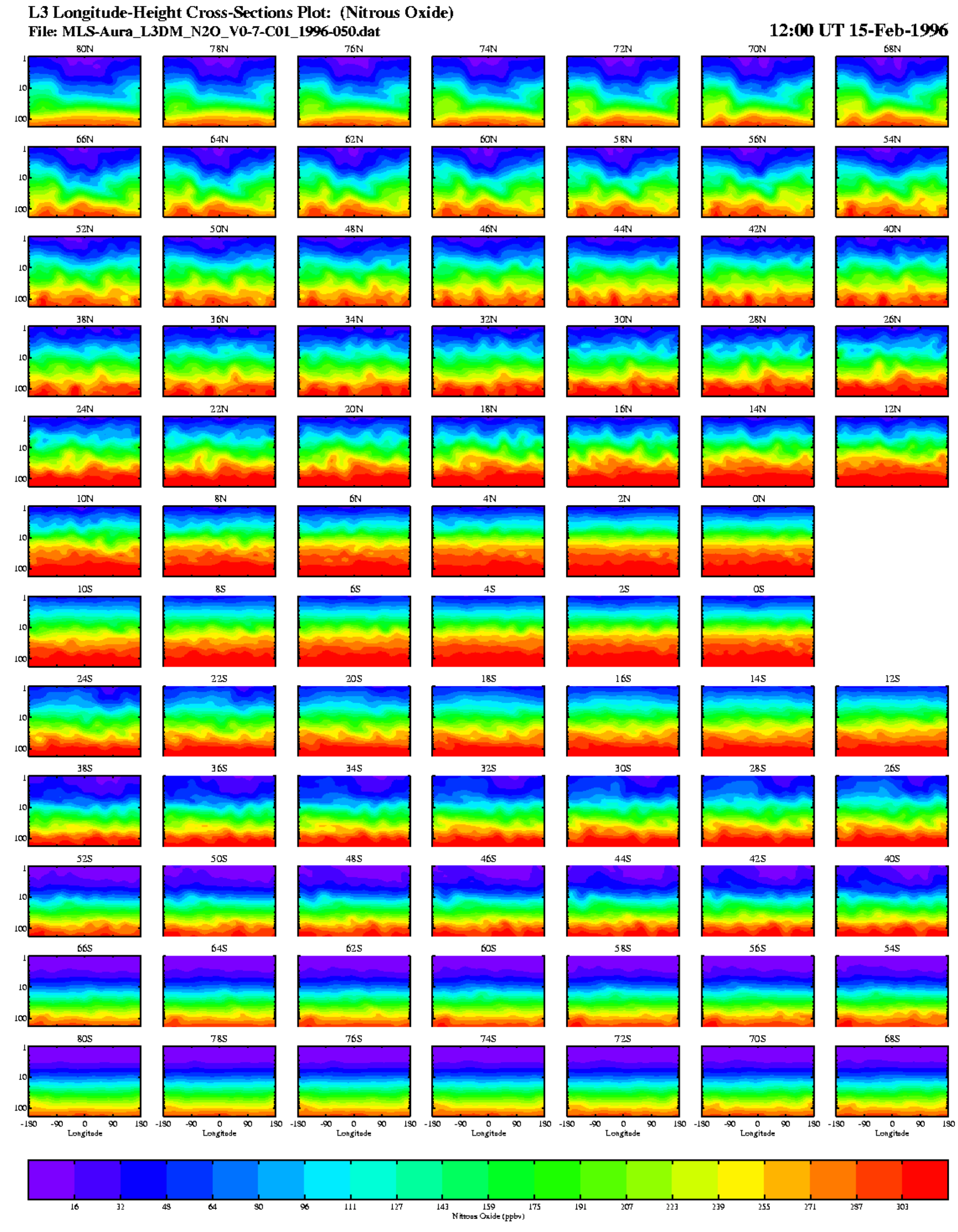
L3 Longitude-Height Cross-Sections Plot: (Nitrous Oxide)
File: MLS-Aura_L3DM_N2O_V0-7-C01_1996-050.dat
12:00 UT 15-Feb-1996
Longitude
Nitrous Oxide (ppbv)
16 32 48 64 80 96 111 127 143 159 175 191 207 223 239 255 271 287 303
Produced on 8-Jan-2004, v1.0

Figure E3

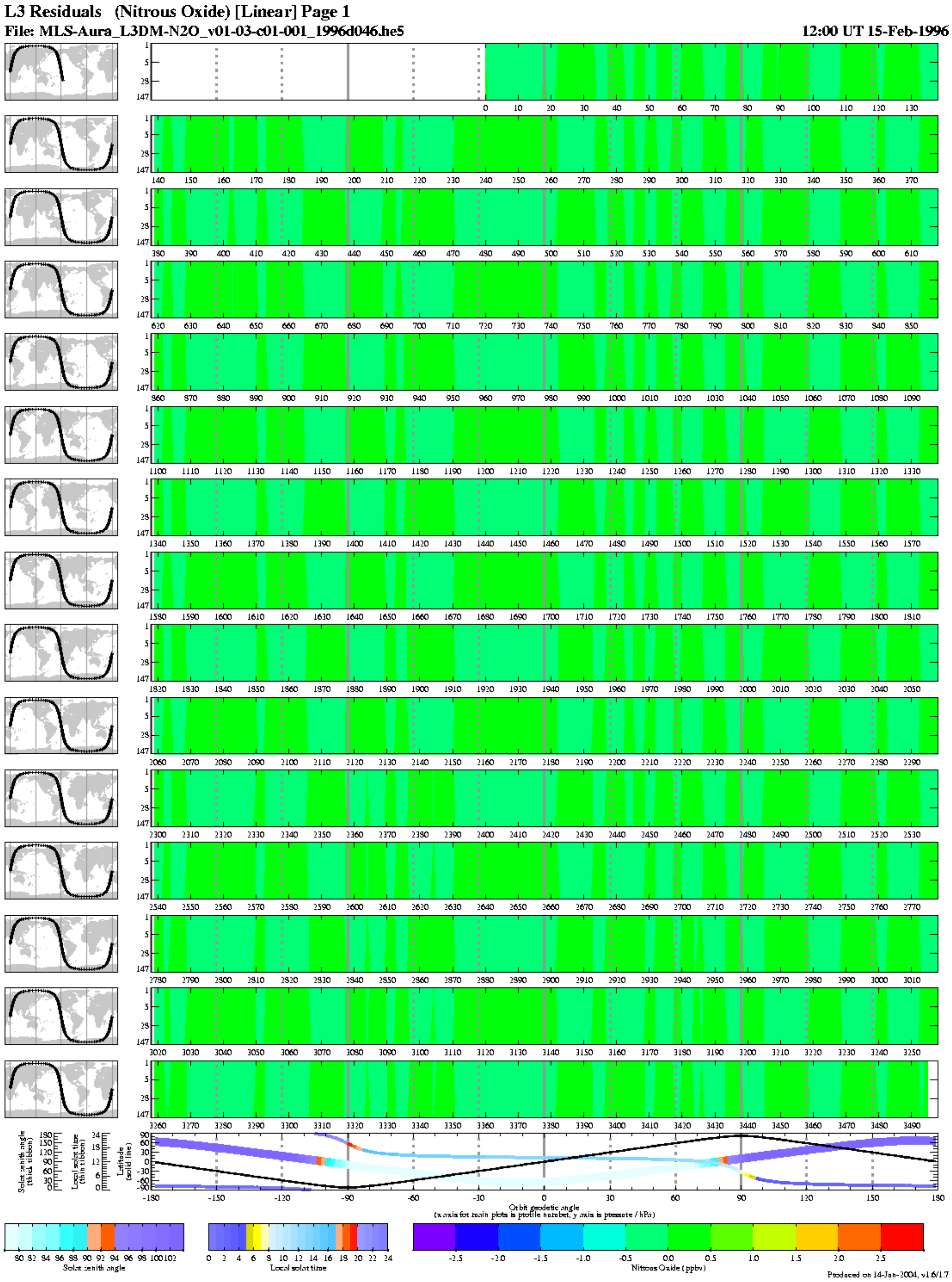
L3 Residuals (Nitrous Oxide) [Linear] Page 1
File: MLS-Aura_L3DM-N2O_v01-03-c01-001_1996d046.he5
12:00 UT 15-Feb-1996
Orbit geodetic angle
(x axis for main plots is profile number, y axis is pressure / hPa)
Solar zenith angle
Local solar time
Nitrous Oxide (ppbv)
Produced on 14-Jan-2004, v1.6/1.7

Figure E4

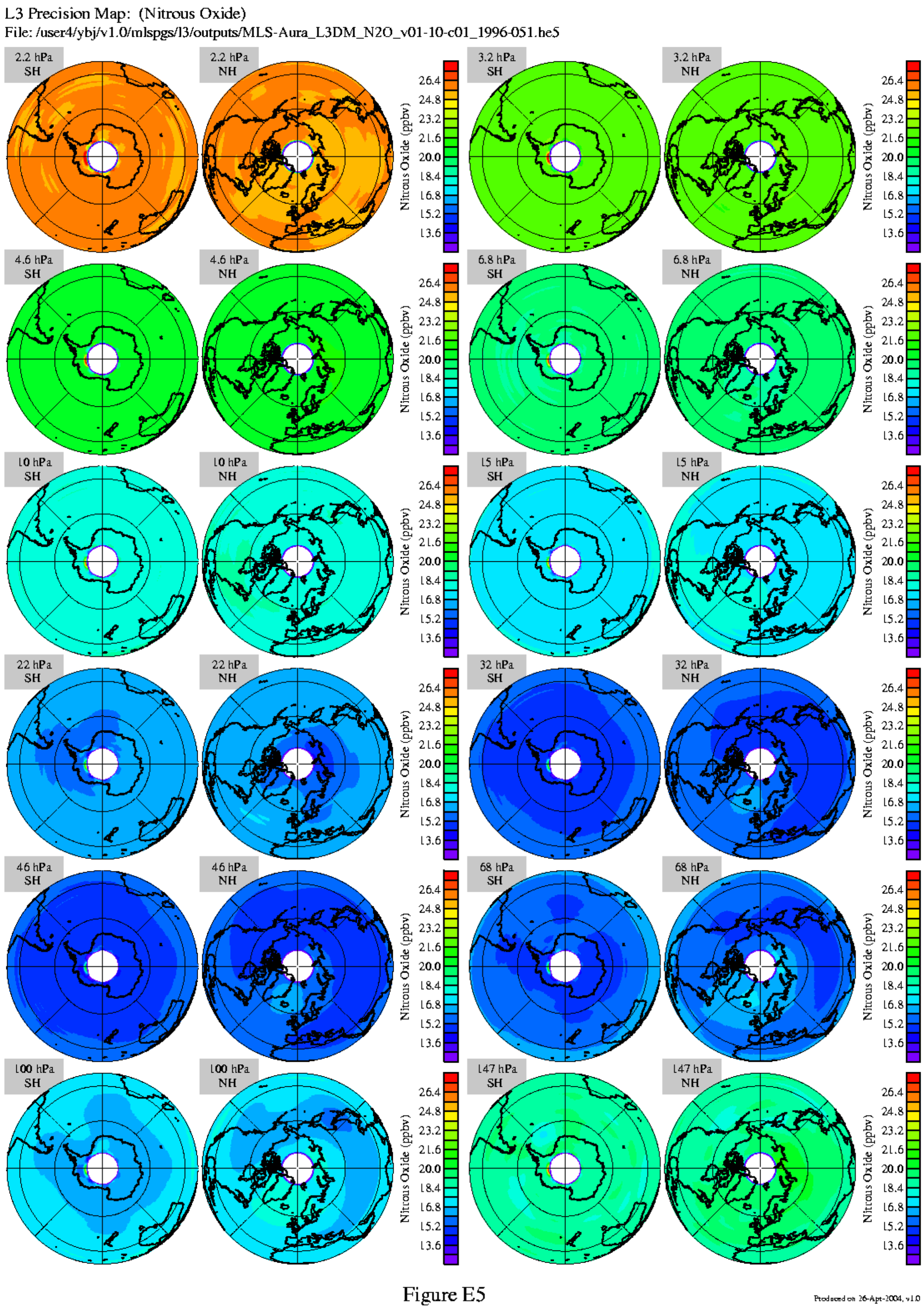
L3 Precision Map: (Nitrous Oxide)
File: /user4/ybj/v1.0/mlspgs/l3/outputs/MLS-Aura_L3DM_N2O_v01-10-c01_1996-051.he5
2.2 hPa SH
2.2 hPa NH
3.2 hPa SH
3.2 hPa NH
4.6 hPa SH
4.6 hPa NH
6.8 hPa SH
6.8 hPa NH
10 hPa SH
10 hPa NH
15 hPa SH
15 hPa NH
22 hPa SH
22 hPa NH
32 hPa SH
32 hPa NH
46 hPa SH
46 hPa NH
68 hPa SH
68 hPa NH
100 hPa SH
100 hPa NH
147 hPa SH
147 hPa NH
Nitrous Oxide (ppbv)
26.4
24.8
23.2
21.6
20.0
18.4
16.8
15.2
13.6
Produced on 26-Apr-2004, v1.0

Figure E5

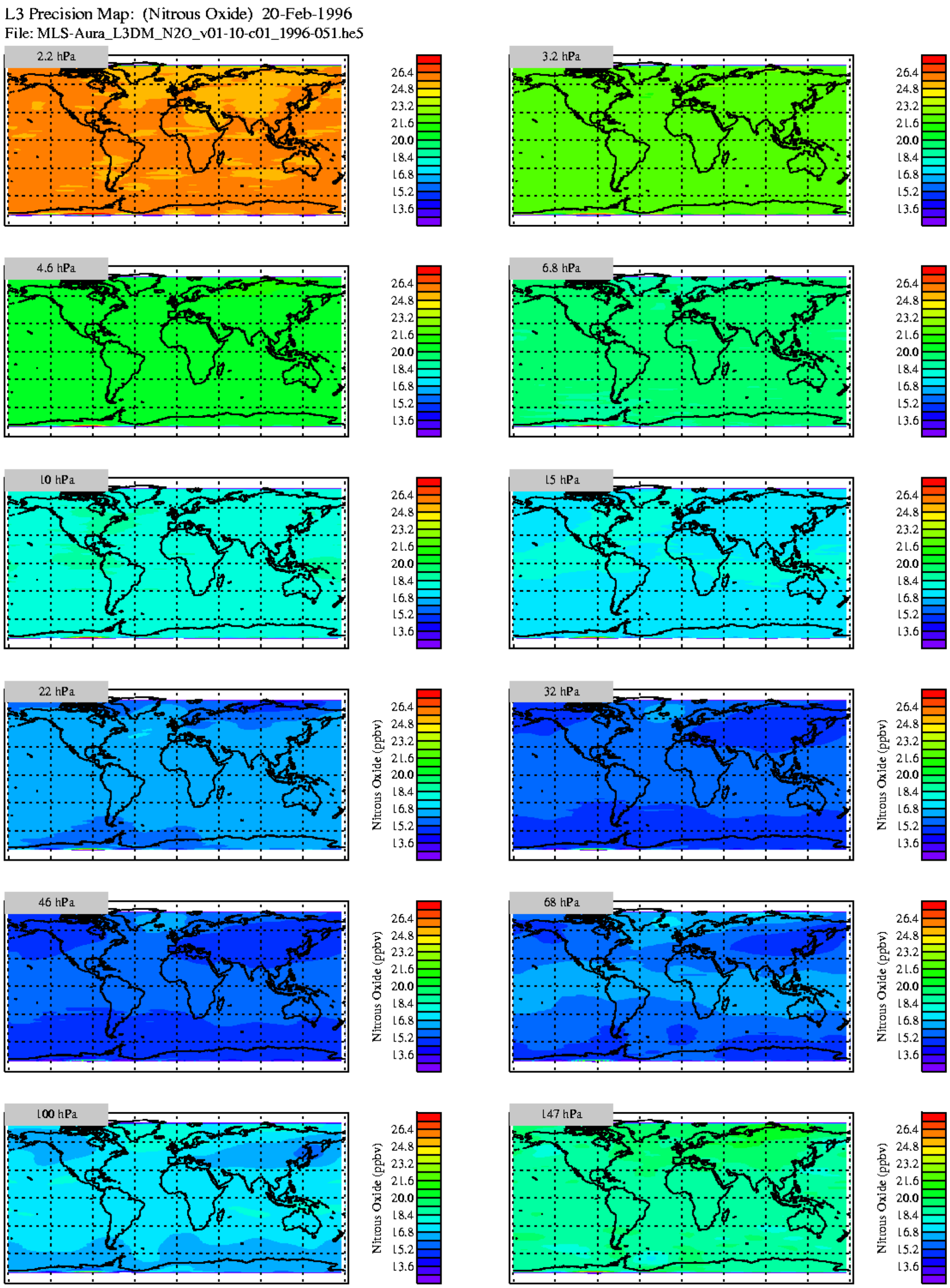
L3 Precision Map: (Nitrous Oxide) 20-Feb-1996
File: MLS-Aura_L3DM_N2O_v01-10-c01_1996-051.he5
2.2 hPa
3.2 hPa
4.6 hPa
6.8 hPa
10 hPa
15 hPa
22 hPa
32 hPa
46 hPa
68 hPa
100 hPa
147 hPa
26.4
24.8
23.2
21.6
20.0
18.4
16.8
15.2
13.6
Nitrous Oxide (ppbv)

Figure E6

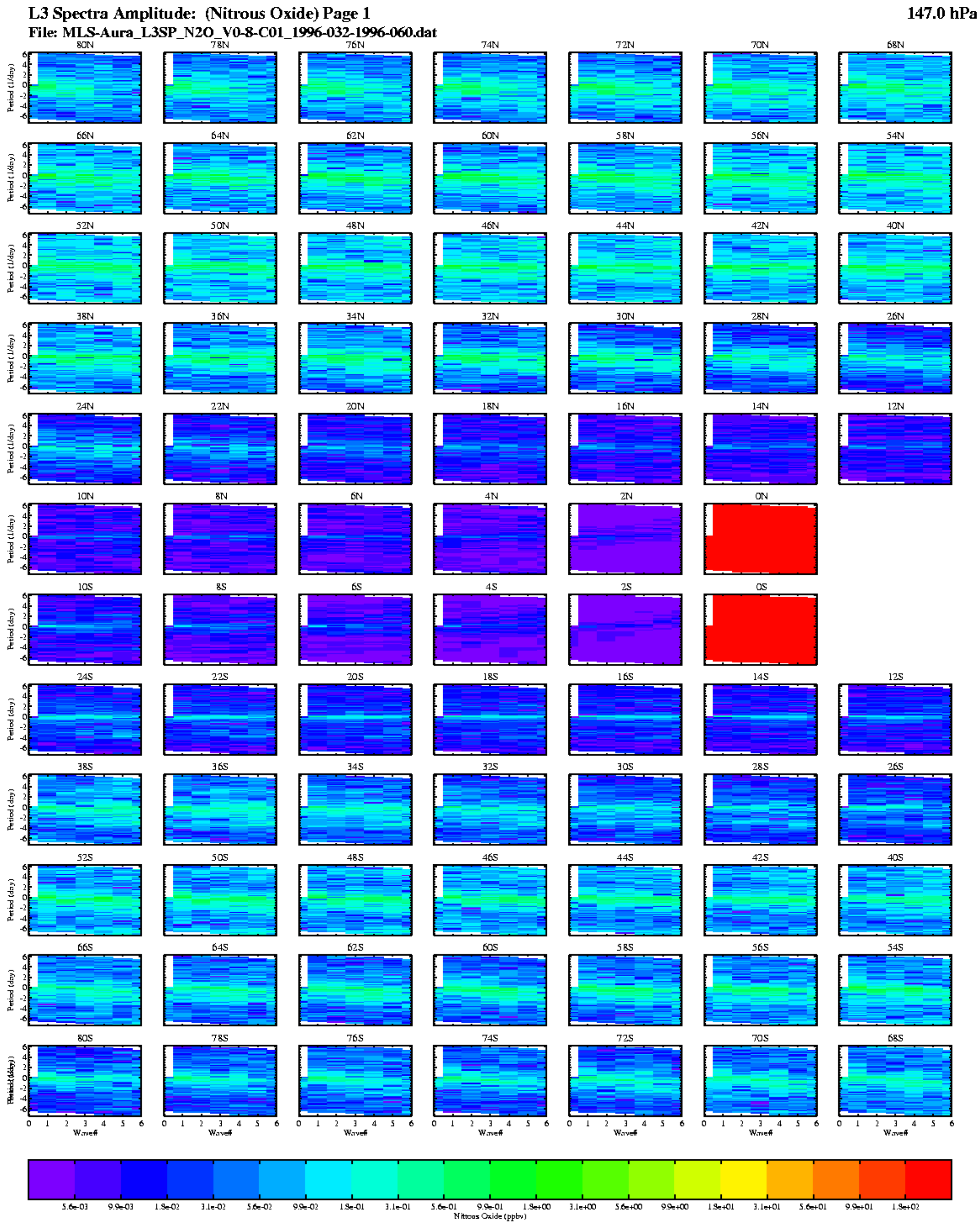

L3 Spectra Amplitude: (Nitrous Oxide) Page 1
147.0 hPa
File: MLS-Aura_L3SP_N2O_V0-8-C01_1996-032-1996-060.dat
Nitrous Oxide (ppbv)
Produced on 7-May-2004, v1.0

Figure E7-1

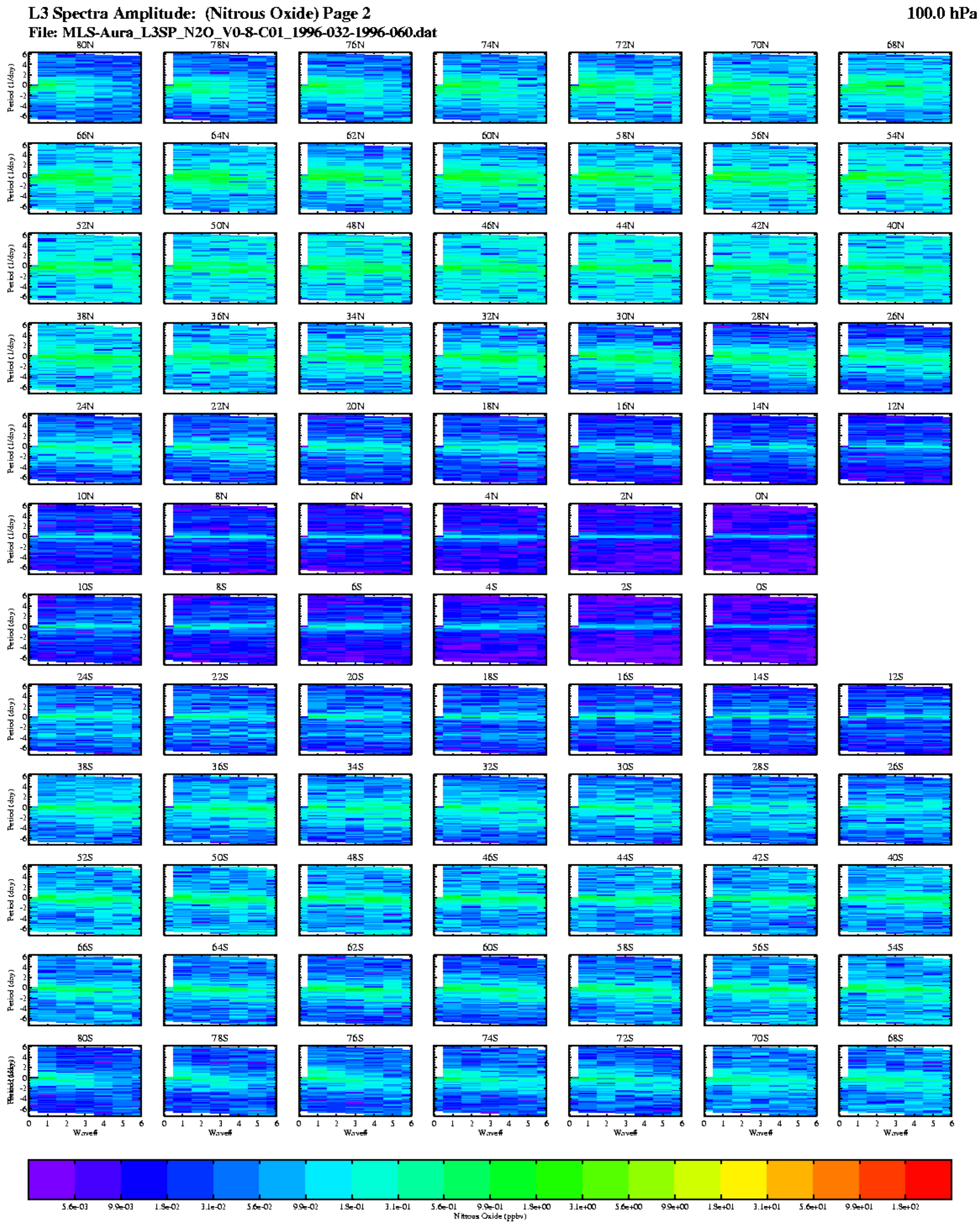
L3 Spectra Amplitude: (Nitrous Oxide) Page 2
100.0 hPa
File: MLS-Aura_L3SP_N2O_V0-8-C01_1996-032-1996-060.dat
Period (1/day)
Wave#
Nitrous Oxide (ppbv)
Produced on 7-May-2004, v1.0

Figure E7-2

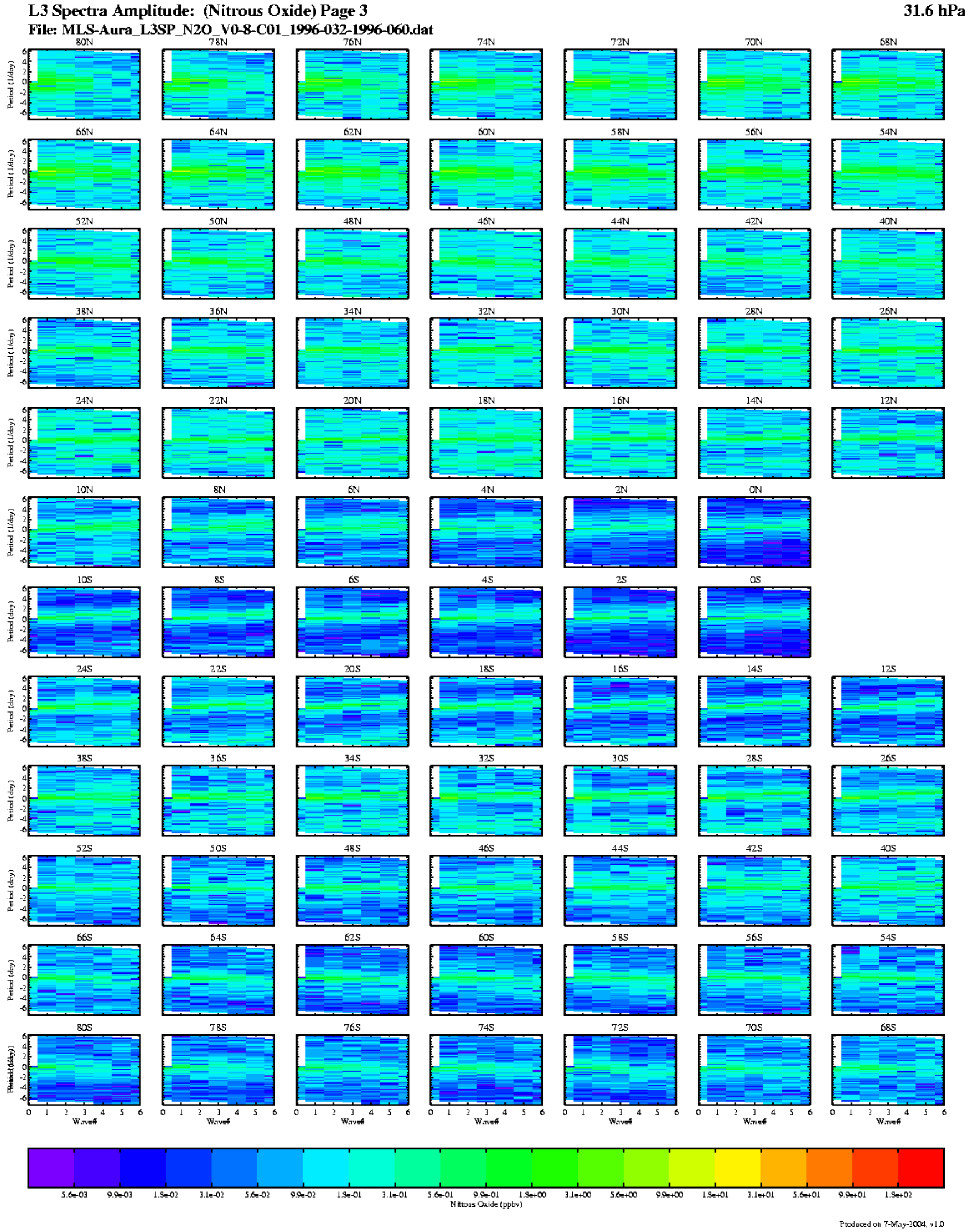
L3 Spectra Amplitude: (Nitrous Oxide) Page 3
31.6 hPa
File: MLS-Aura_L3SP_N2O_V0-8-C01_1996-032-1996-060.dat
80N
78N
76N
74N
72N
70N
68N
66N
64N
62N
60N
58N
56N
54N
52N
50N
48N
46N
44N
42N
40N
38N
36N
34N
32N
30N
28N
26N
24N
22N
20N
18N
16N
14N
12N
10N
8N
6N
4N
2N
0N
10S
8S
6S
4S
2S
0S
24S
22S
20S
18S
16S
14S
12S
38S
36S
34S
32S
30S
28S
26S
52S
50S
48S
46S
44S
42S
40S
66S
64S
62S
60S
58S
56S
54S
80S
78S
76S
74S
72S
70S
68S
Period (1/day)
Period (day)
Wave#
5.6e-03
9.9e-03
1.8e-02
3.1e-02
5.6e-02
9.9e-02
1.8e-01
3.1e-01
5.6e-01
9.9e-01
1.8e+00
3.1e+00
5.6e+00
9.9e+00
1.8e+01
3.1e+01
5.6e+01
9.9e+01
1.8e+02
Nitrous Oxide (ppbv)
Produced on 7-May-2004, v1.0

Figure E7-3

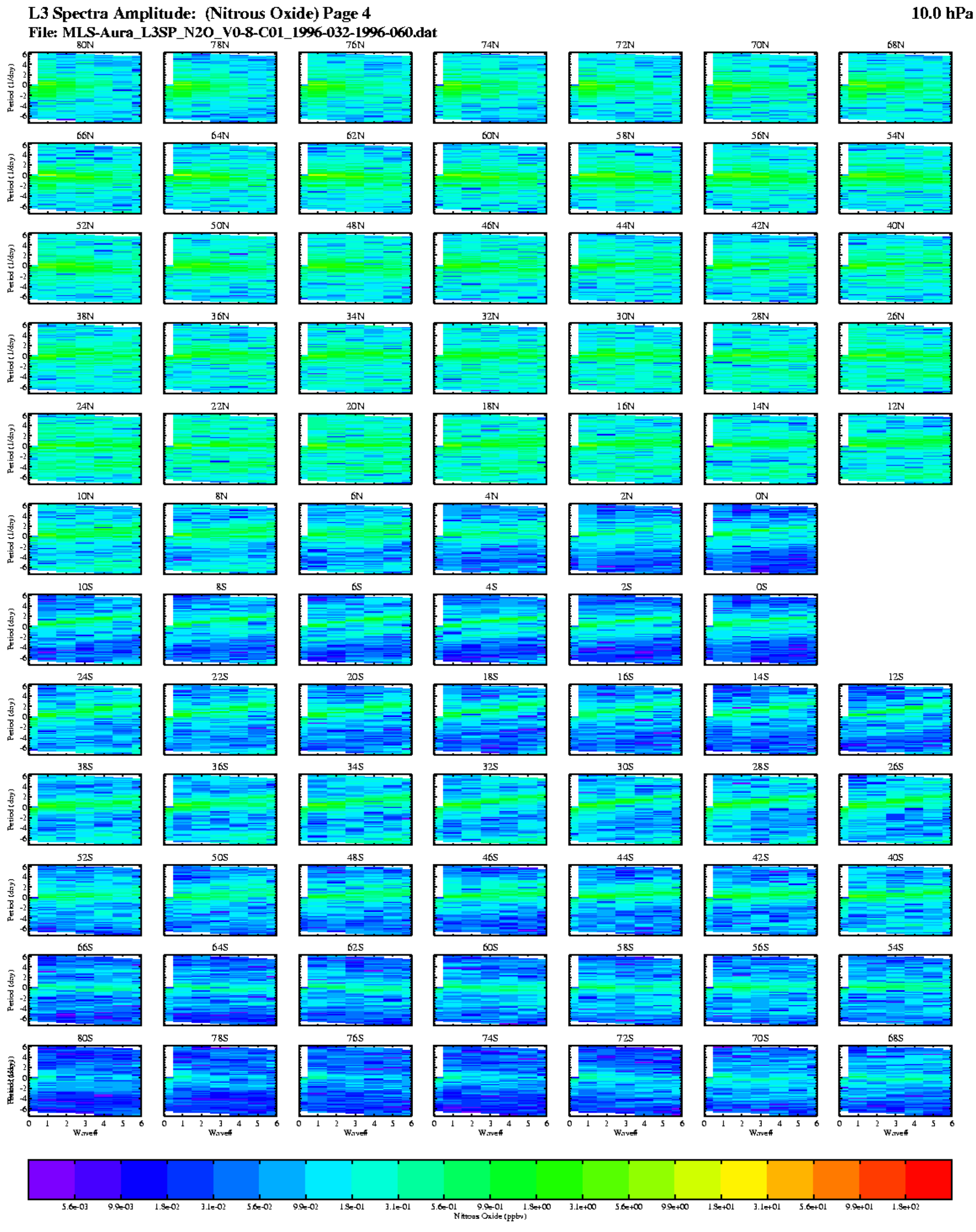

L3 Spectra Amplitude: (Nitrous Oxide) Page 4
10.0 hPa
File: MLS-Aura_L3SP_N2O_V0-8-C01_1996-032-1996-060.dat
Period (1/day)
Wave#
Nitrous Oxide (ppbv)
Produced on 7-May-2004, v1.0

Figure E7-4

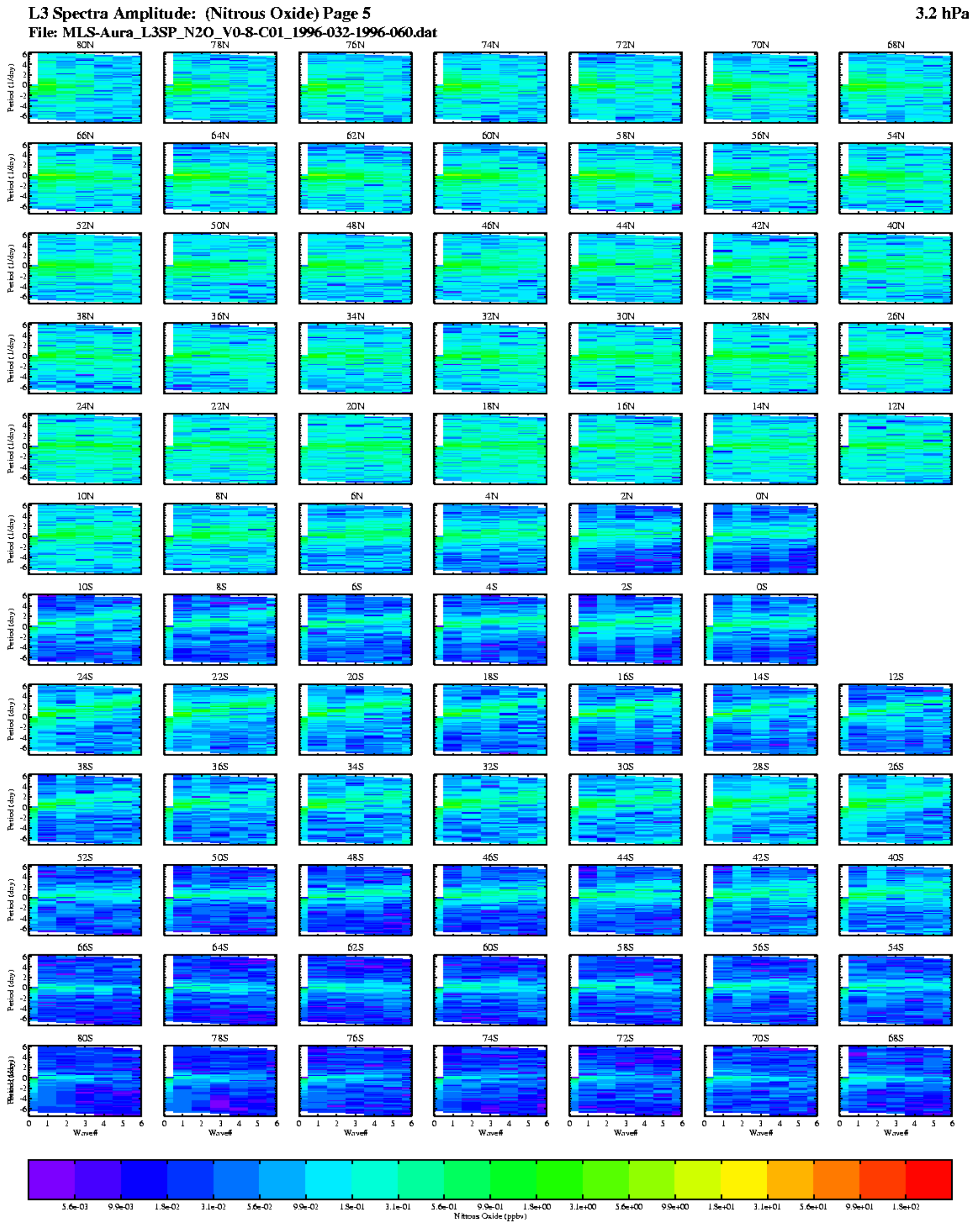
L3 Spectra Amplitude: (Nitrous Oxide) Page 5
3.2 hPa
File: MLS-Aura_L3SP_N2O_V0-8-C01_1996-032-1996-060.dat
Period (1/day)
Period (day)
Wave#
Nitrous Oxide (ppbv)
Produced on 7-May-2004, v1.0

Figure E7-5

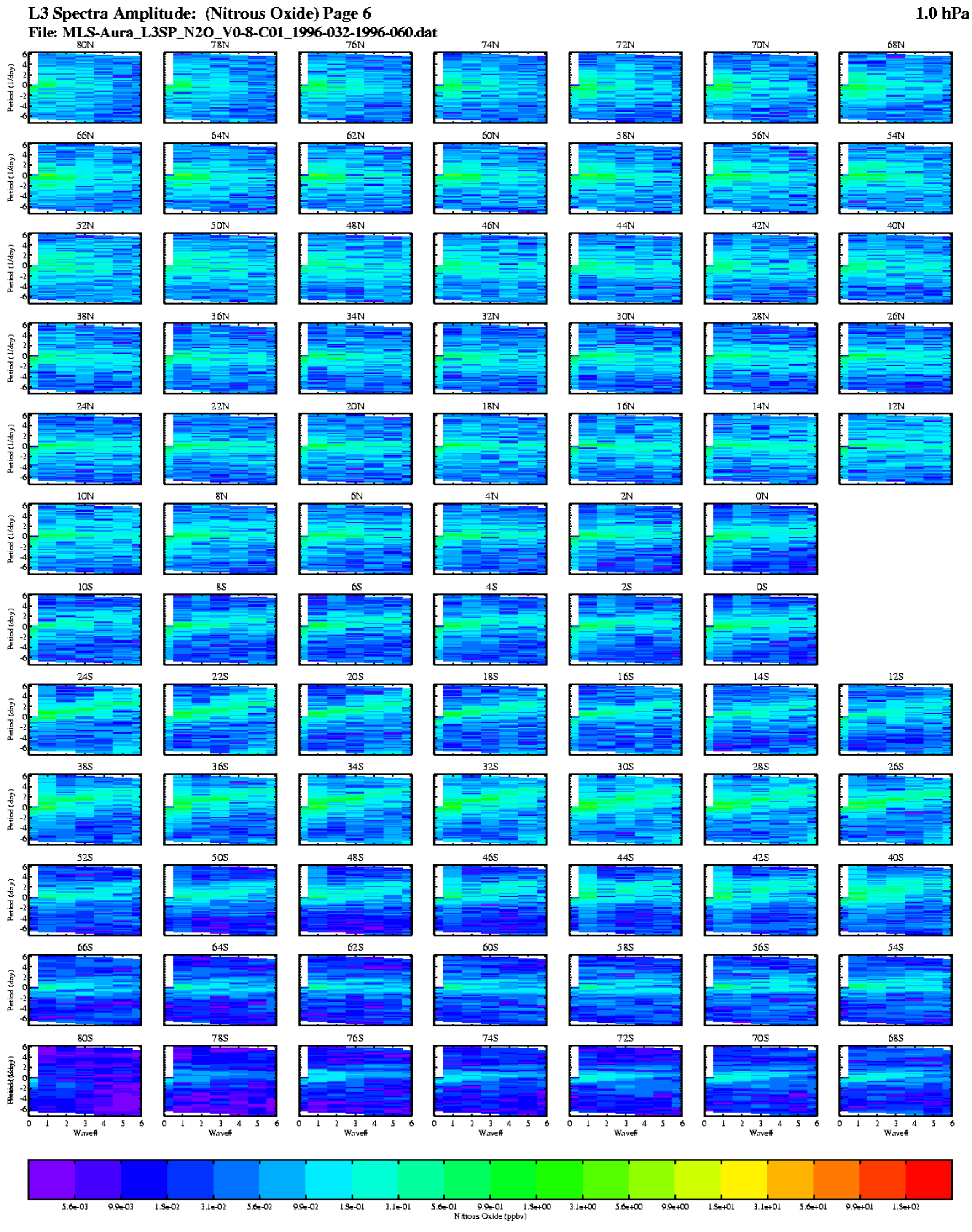
L3 Spectra Amplitude: (Nitrous Oxide) Page 6
1.0 hPa
File: MLS-Aura_L3SP_N2O_V0-8-C01_1996-032-1996-060.dat
Period (1/day)
Period (day)
Wave#
Nitrous Oxide (ppbv)
Produced on 7-May-2004, v1.0

Figure E7-6

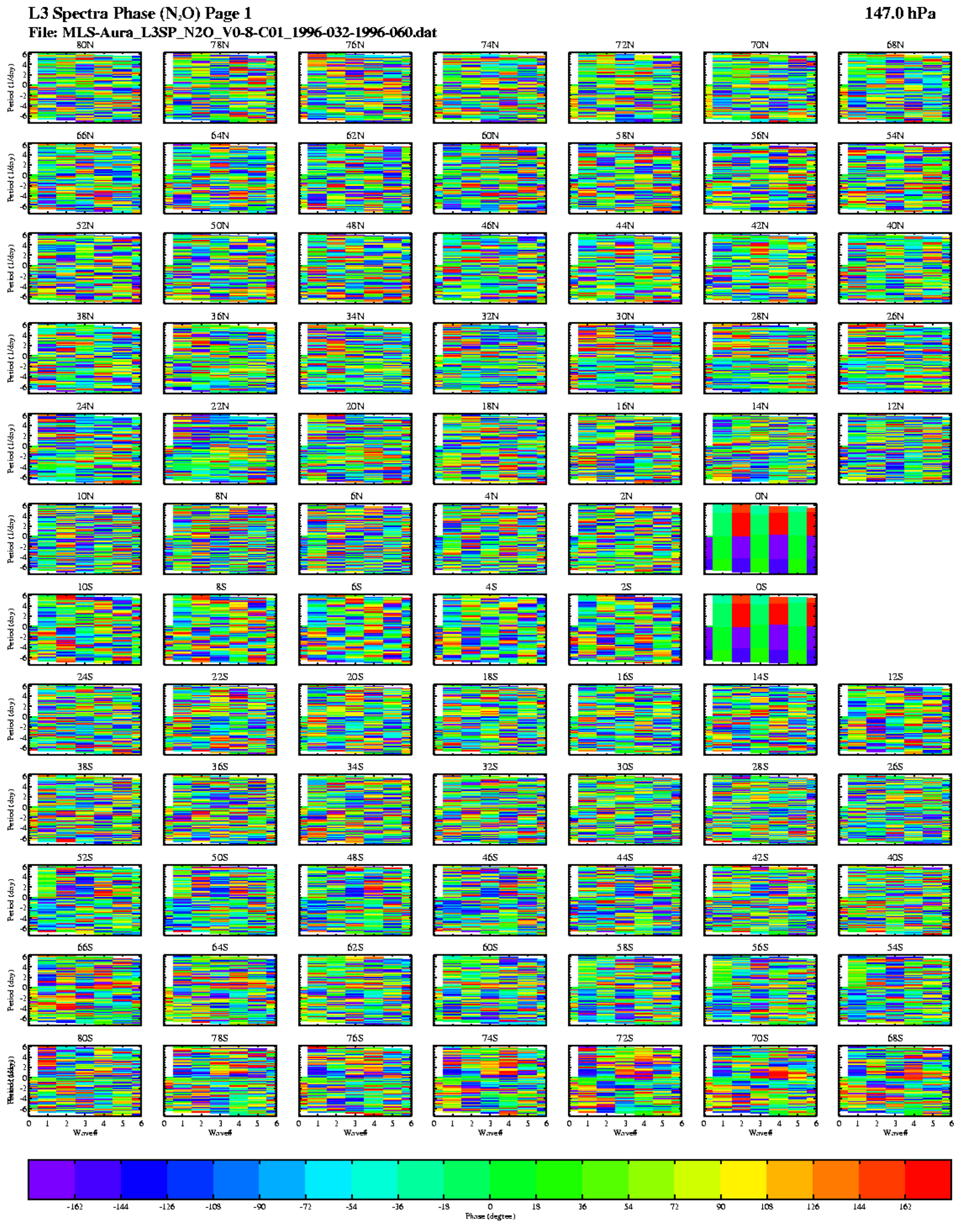
L3 Spectra Phase (N2O) Page 1
147.0 hPa
File: MLS-Aura_L3SP_N2O_V0-8-C01_1996-032-1996-060.dat
Period (1/day)
Period (day)
Wave#
Phase (degree)
Produced on 7-May-2004, v1.0

Figure E8-1

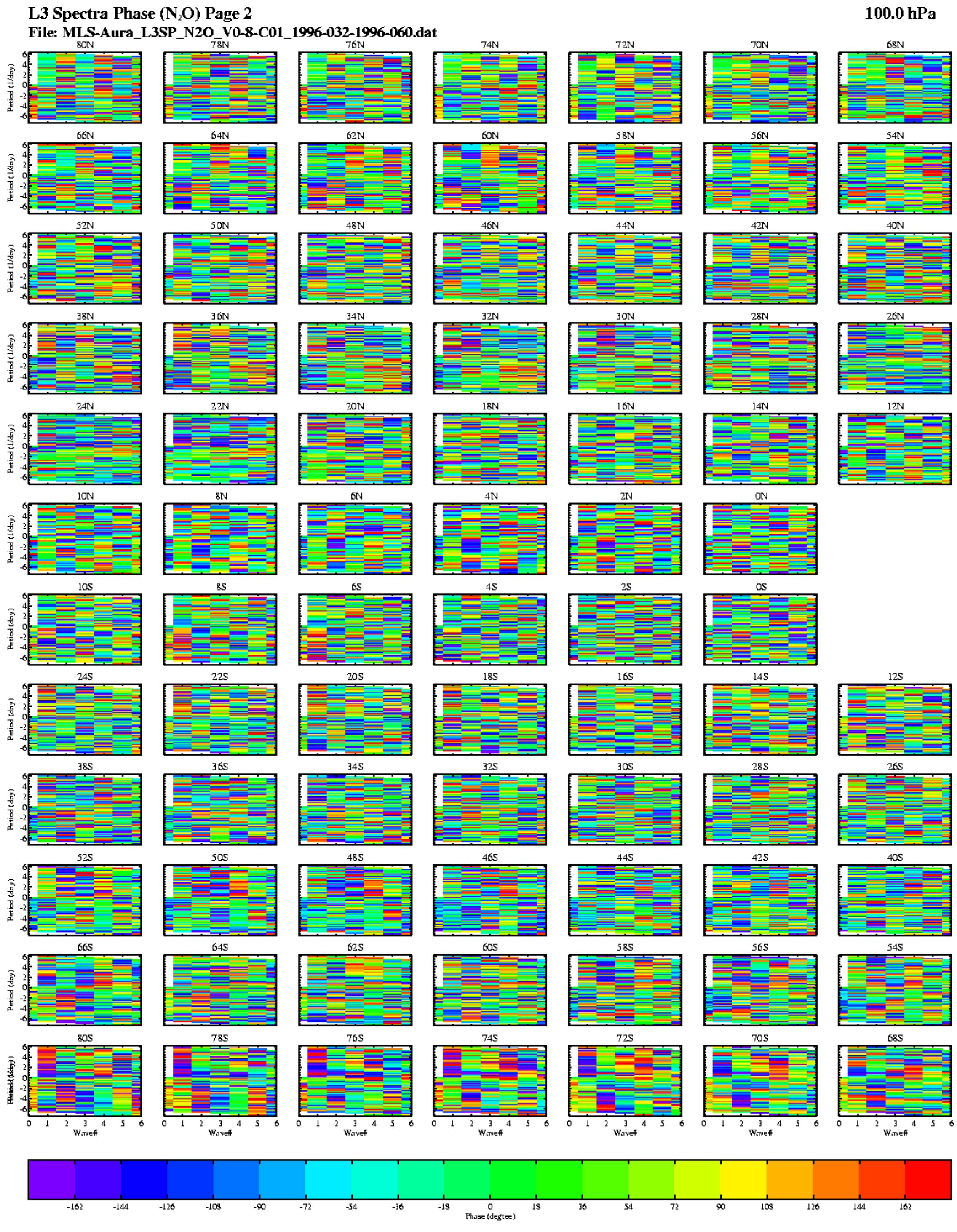

L3 Spectra Phase (N_2O) Page 2
100.0 hPa
File: MLS-Aura_L3SP_N2O_V0-8-C01_1996-032-1996-060.dat
Period (1/day)
Period (day)
Wave#
Phase (degree)
Produced on 7-May-2004, v1.0

Figure E8-2

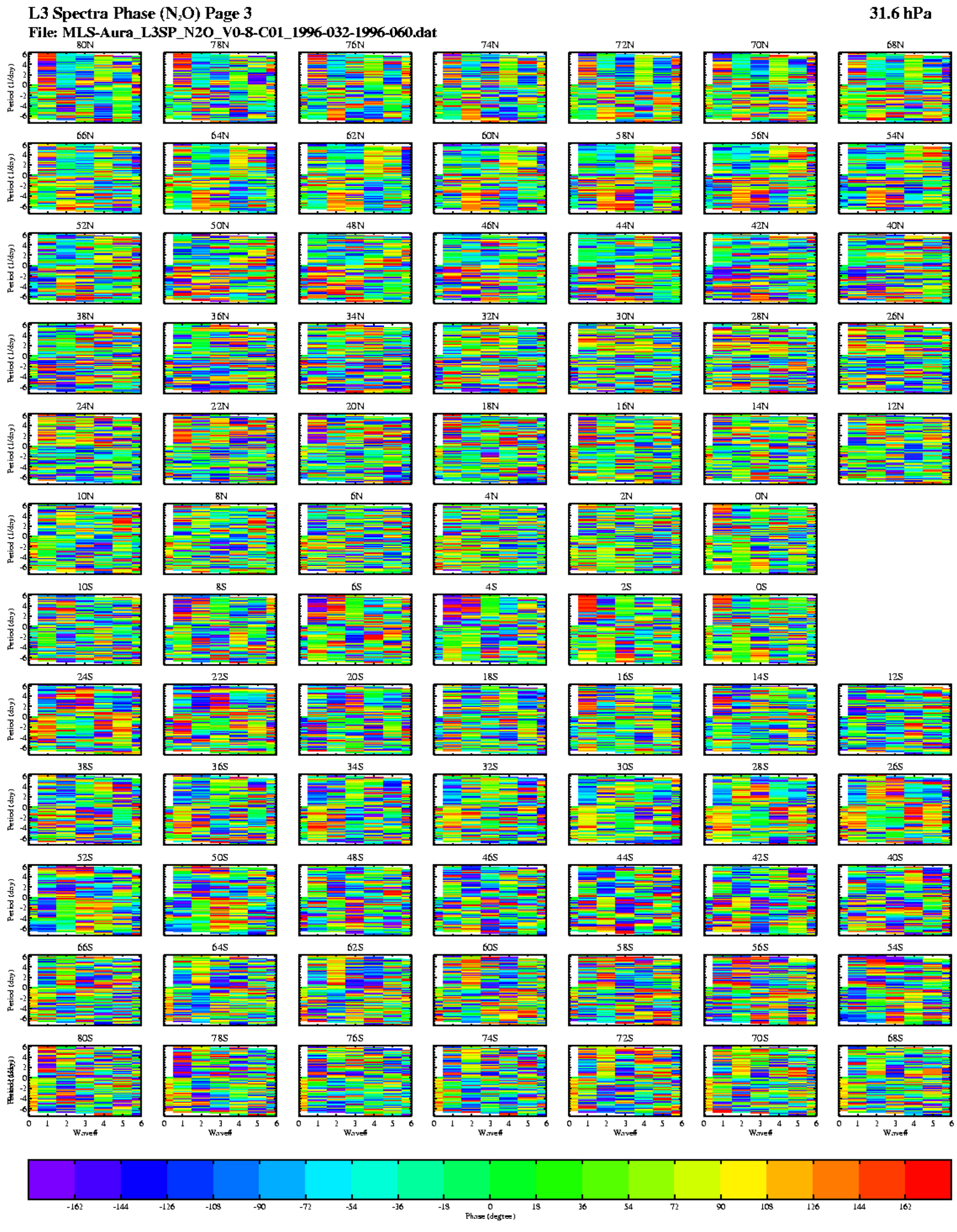
L3 Spectra Phase (N_2O) Page 3
31.6 hPa
File: MLS-Aura_L3SP_N2O_V0-8-C01_1996-032-1996-060.dat
Period (1/day)
Period (day)
Wave#
Phase (degree)
Produced on 7-May-2004, v1.0

Figure E8-3

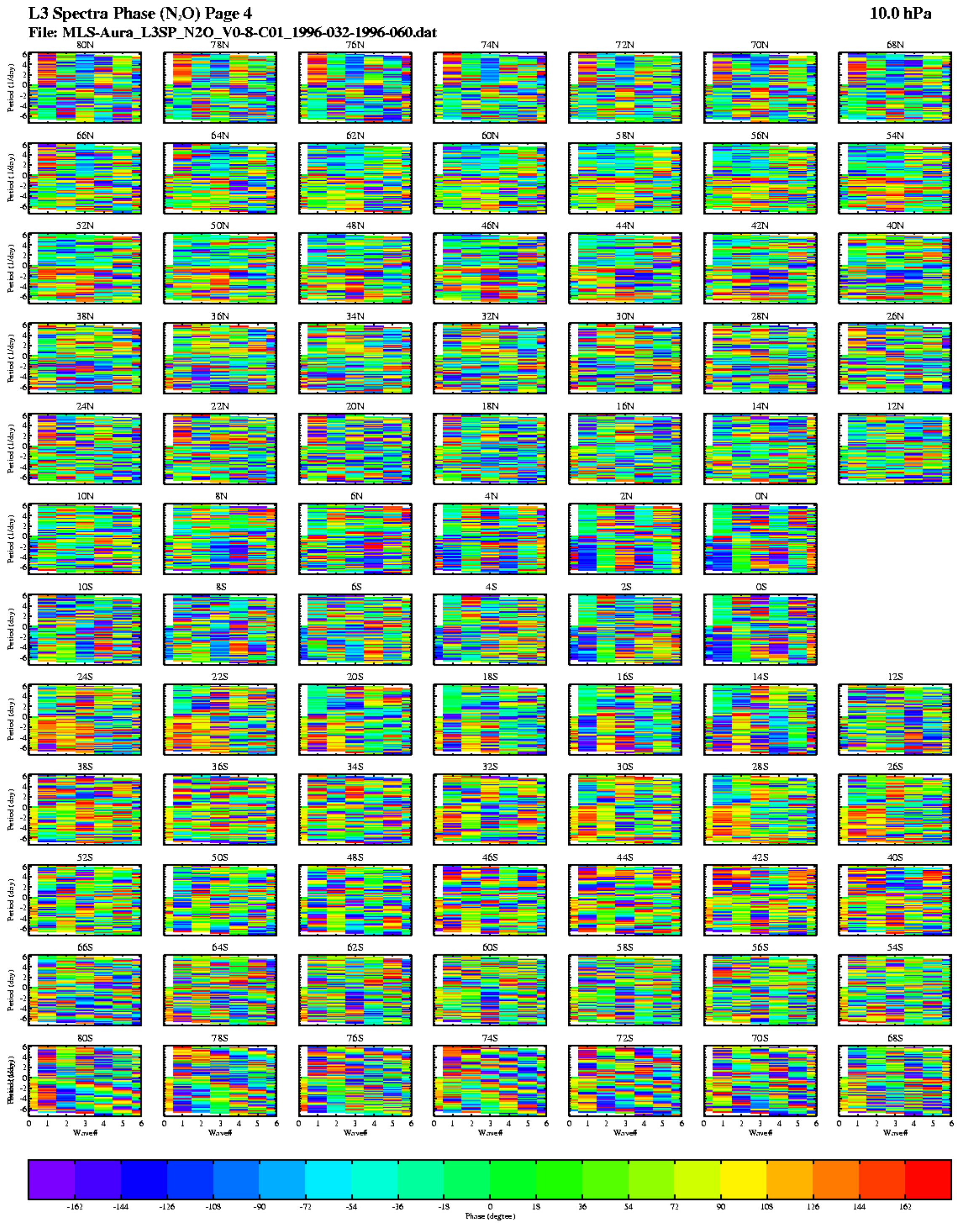

L3 Spectra Phase (N_2O) Page 4
10.0 hPa
File: MLS-Aura_L3SP_N2O_V0-8-C01_1996-032-1996-060.dat
Wave#
Phase (degree)
Produced on 7-May-2004, v1.0

Figure E8-4

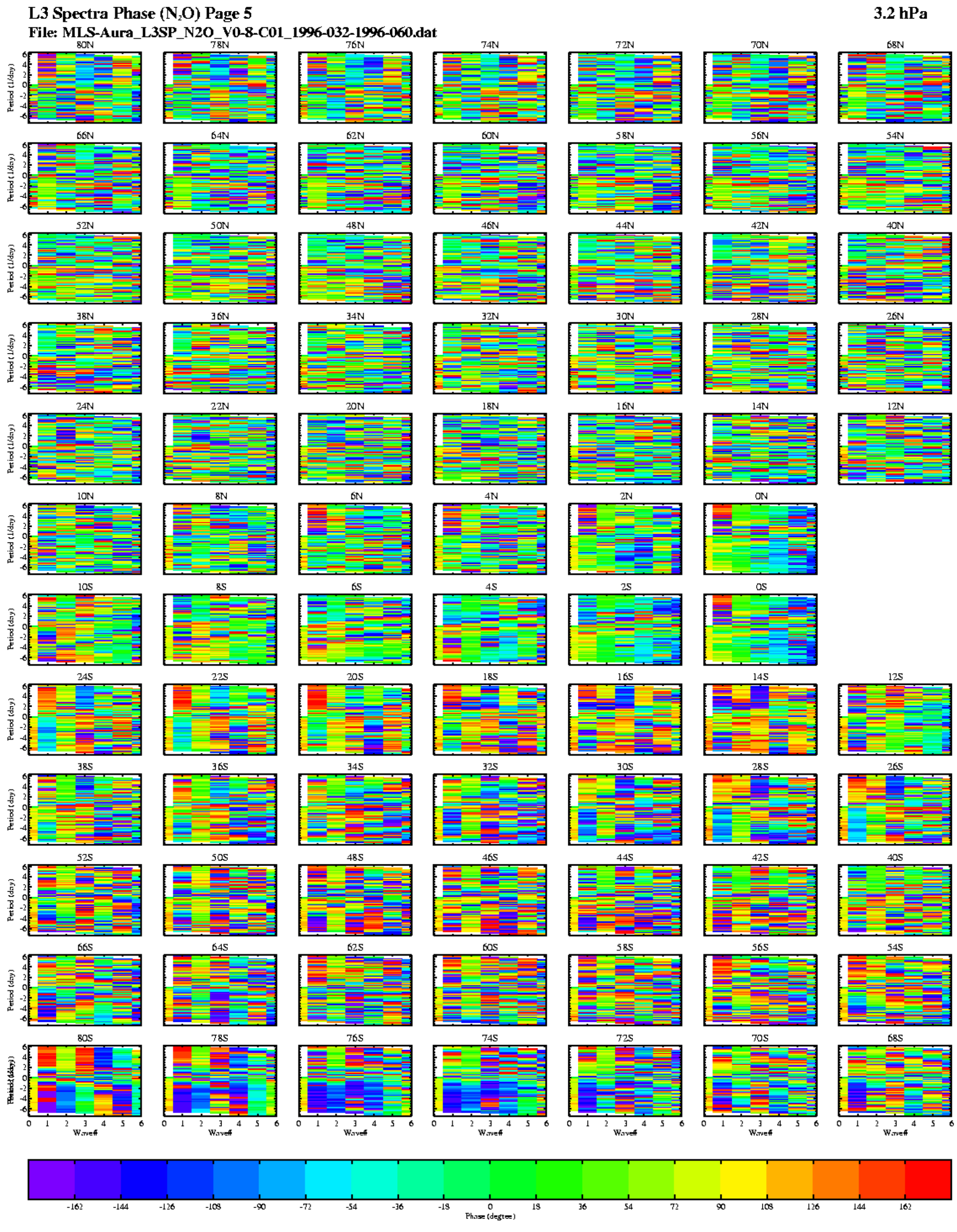

L3 Spectra Phase (N_2O) Page 5
3.2 hPa
File: MLS-Aura_L3SP_N2O_V0-8-C01_1996-032-1996-060.dat
Period (1/day)
Period (day)
Wave#
Phase (degree)
Produced on 7-May-2004, v1.0

Figure E8-5

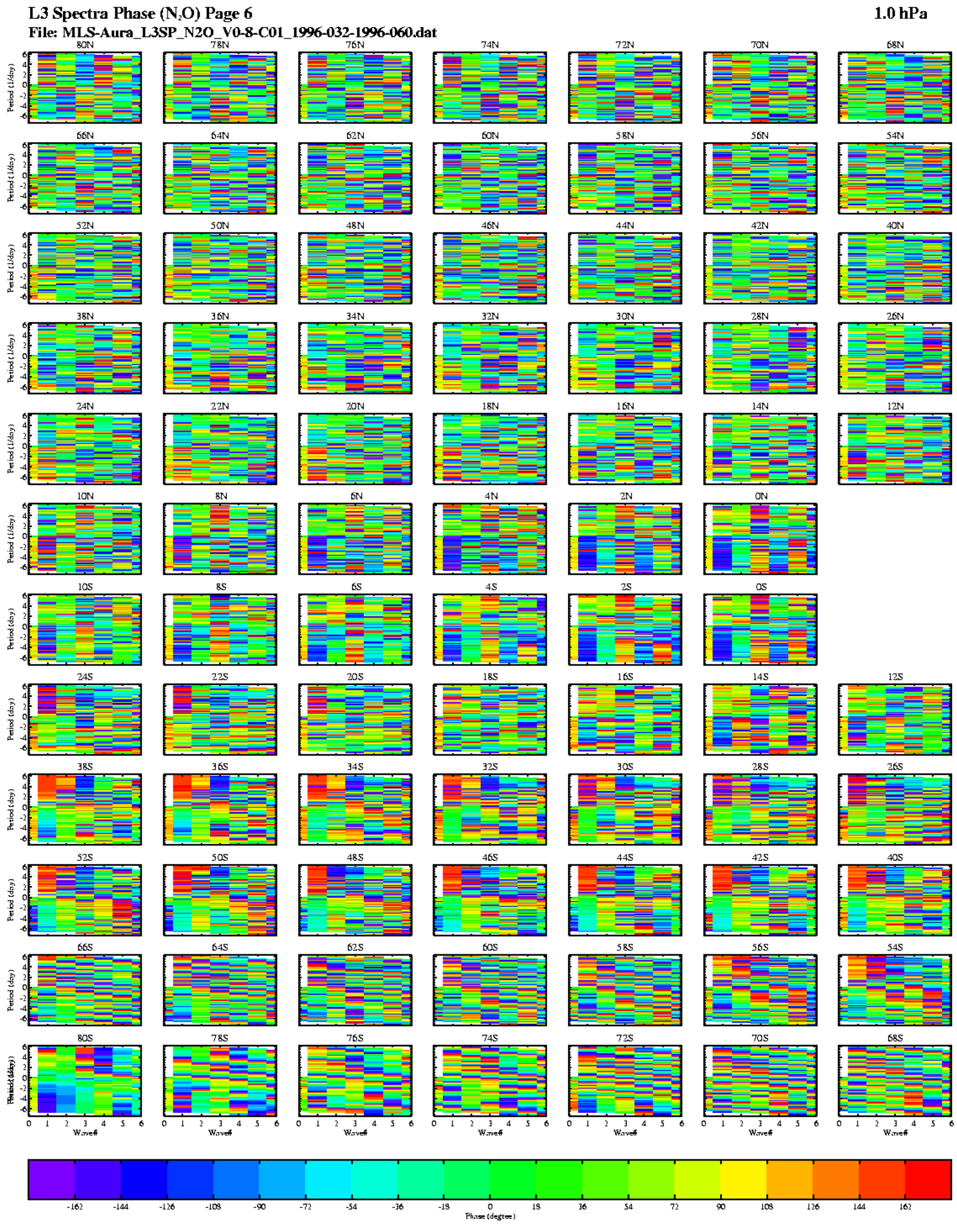

L3 Spectra Phase (N_2O) Page 6
1.0 hPa
File: MLS-Aura_L3SP_N2O_V0-8-C01_1996-032-1996-060.dat
Period (1/day)
Period (day)
Wave#
Phase (degree)
Produced on 7-May-2004, v1.0

Figure E8-6

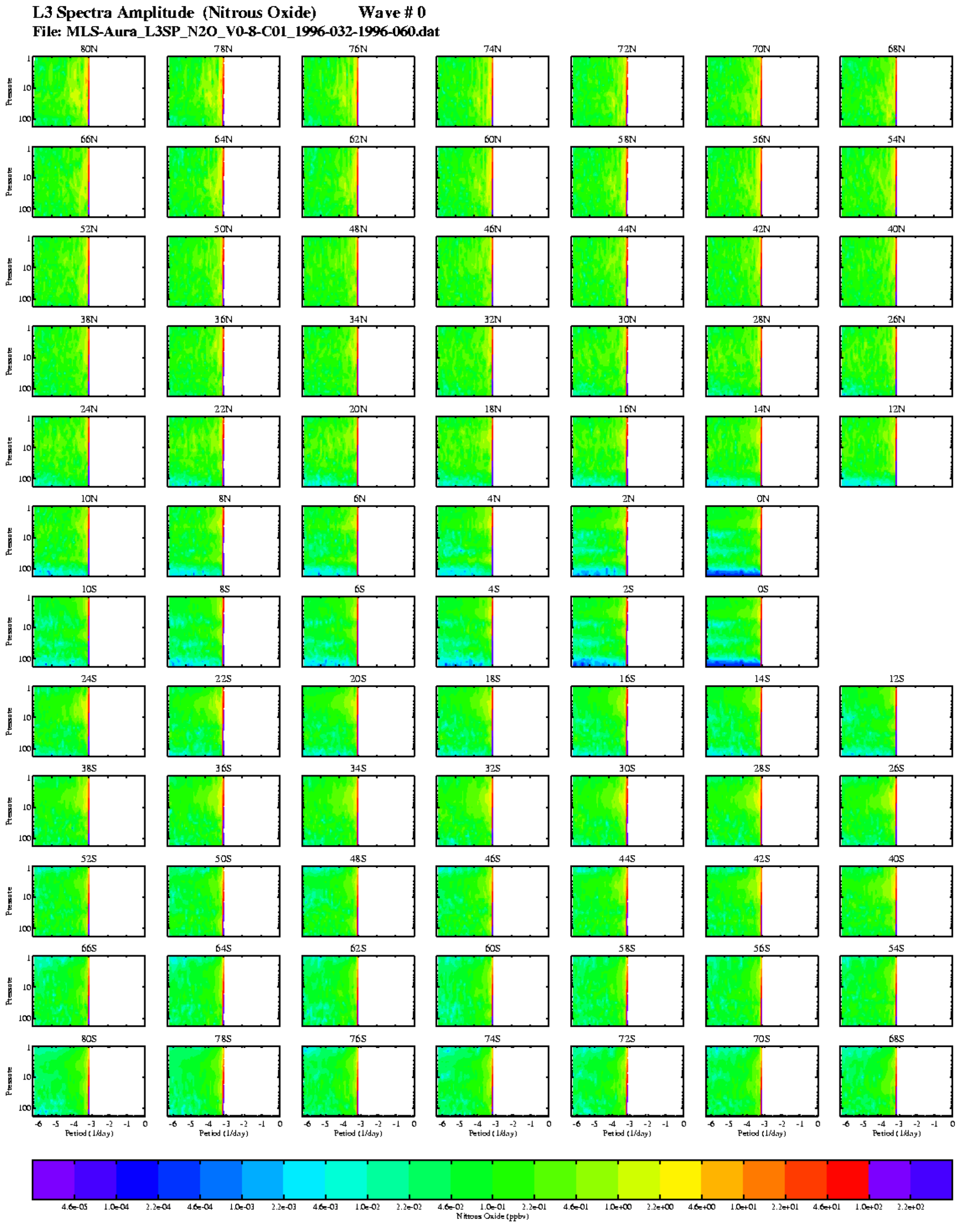
L3 Spectra Amplitude (Nitrous Oxide) Wave # 0
File: MLS-Aura_L3SP_N2O_V0-8-C01_1996-032-1996-060.dat
Pressure
Period (1/day)
Nitrous Oxide (ppbv)
Produced on 3-May-2004, v1.0

Figure E9-1

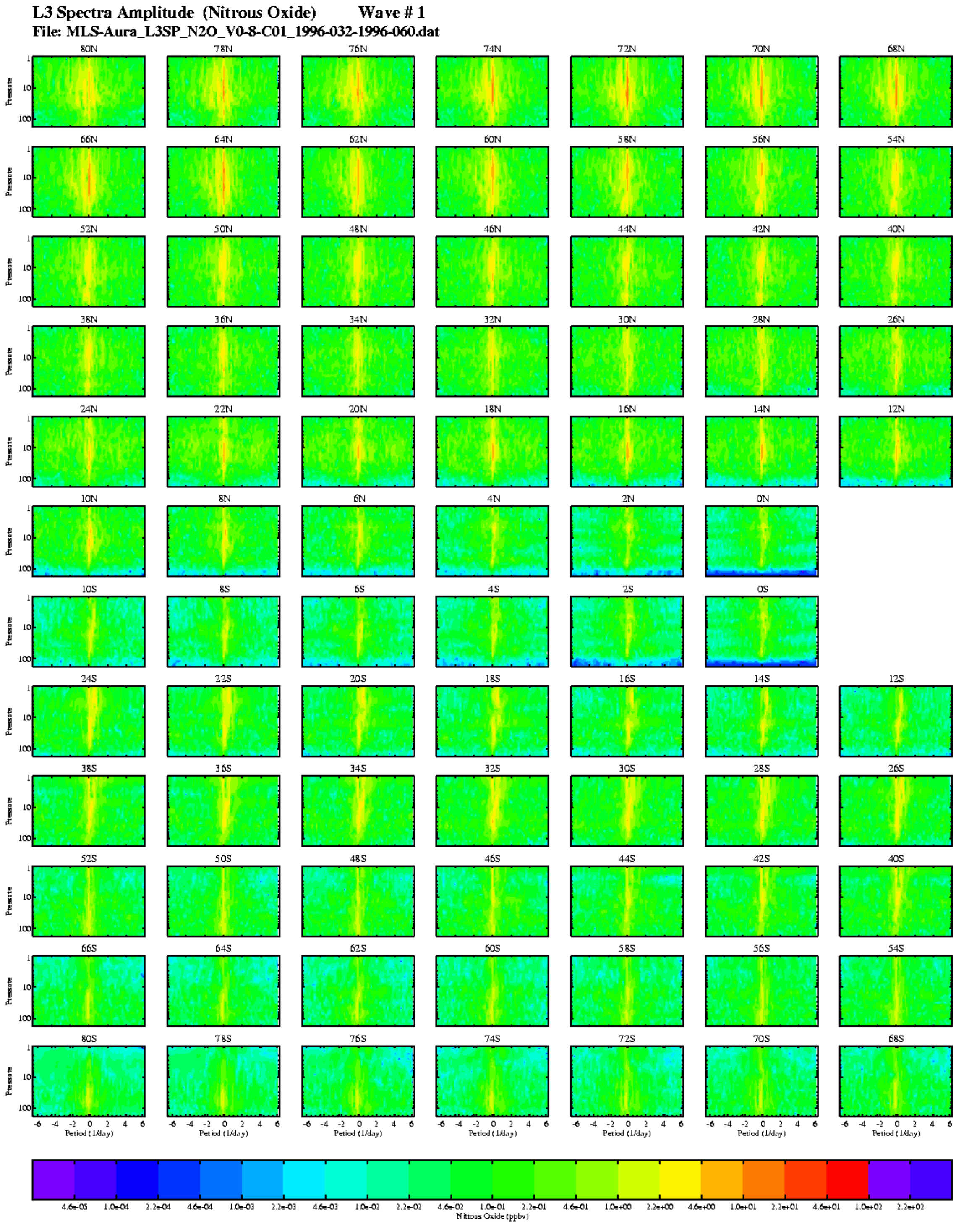
L3 Spectra Amplitude (Nitrous Oxide) Wave # 1
File: MLS-Aura_L3SP_N2O_V0-8-C01_1996-032-1996-060.dat
Pressure
Period (1/day)
Nitrous Oxide (ppbv)
Produced on 3-May-2004, v1.0

Figure E9-2

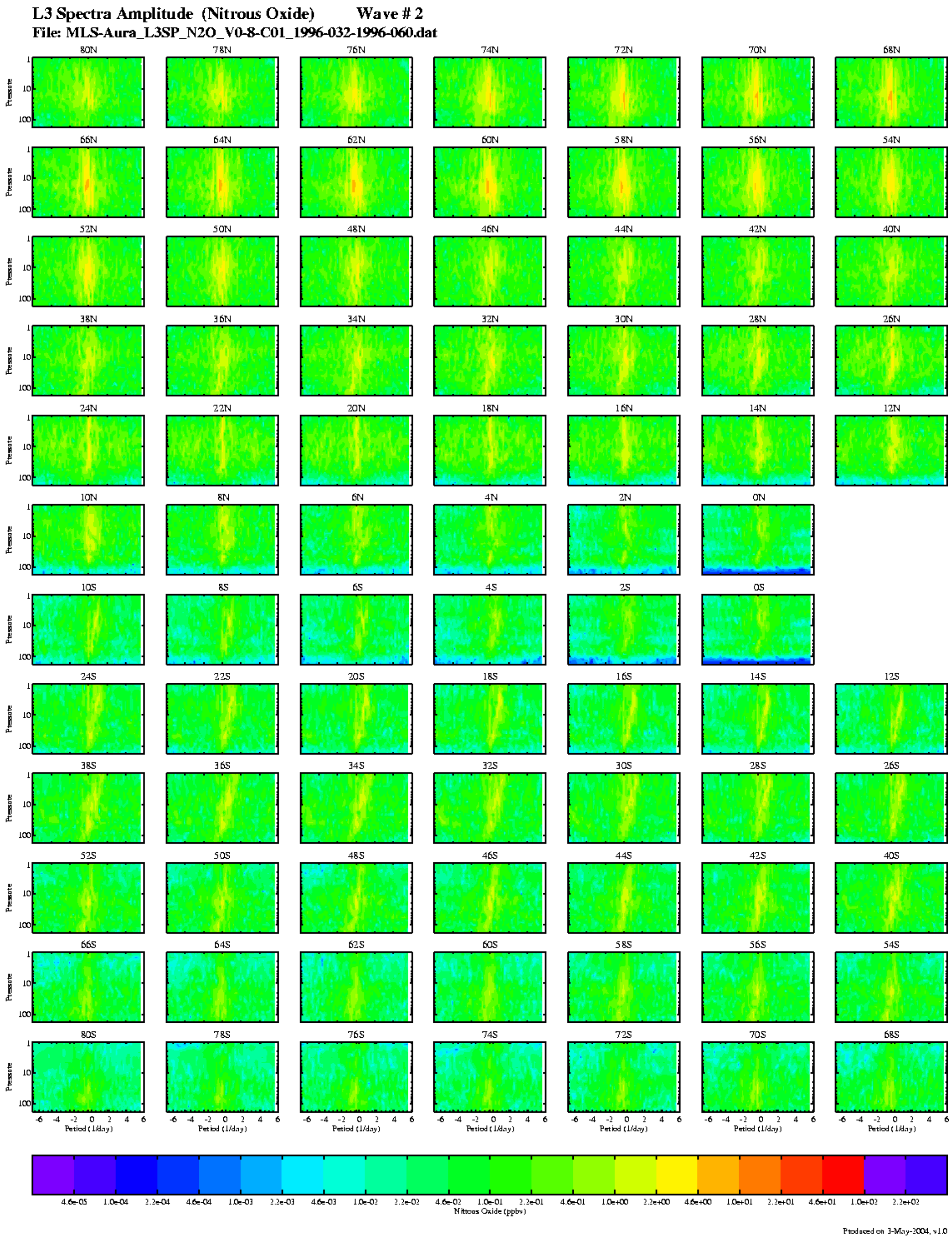
L3 Spectra Amplitude (Nitrous Oxide) Wave # 2
File: MLS-Aura_L3SP_N2O_V0-8-C01_1996-032-1996-060.dat
Pressure
Period (1/day)
Nitrous Oxide (ppbv)
Produced on 3-May-2004, v1.0

Figure E9-3

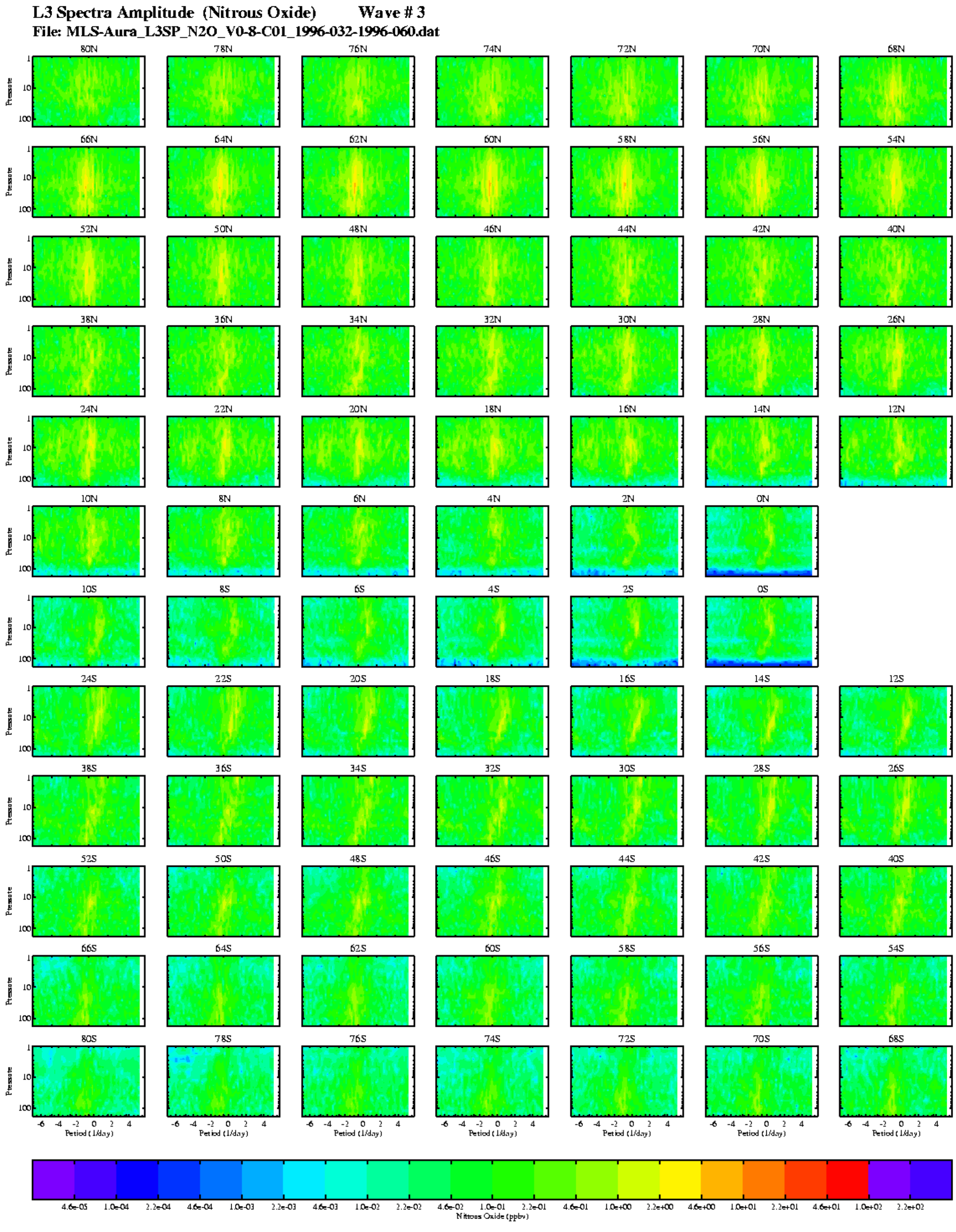
L3 Spectra Amplitude (Nitrous Oxide) Wave # 3
File: MLS-Aura_L3SP_N2O_V0-8-C01_1996-032-1996-060.dat
Pressure
Period (1/day)
Nitrous Oxide (ppbv)
Produced on 3-May-2004, v1.0

Figure E9-4

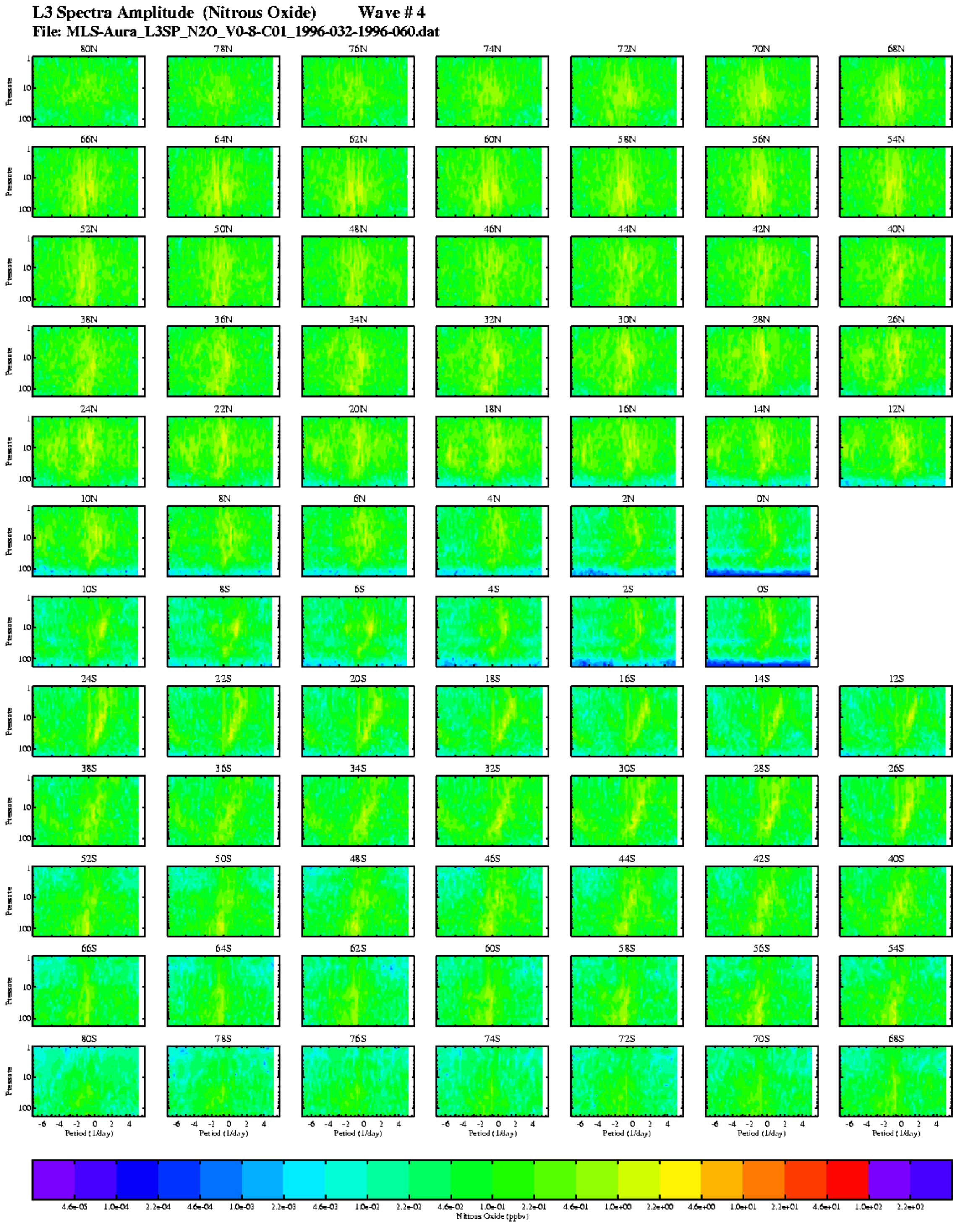
L3 Spectra Amplitude (Nitrous Oxide) Wave # 4
File: MLS-Aura_L3SP_N2O_V0-8-C01_1996-032-1996-060.dat
Pressure
Period (1/day)
Nitrous Oxide (ppbv)
Produced on 3-May-2004, v1.0

Figure E9-5

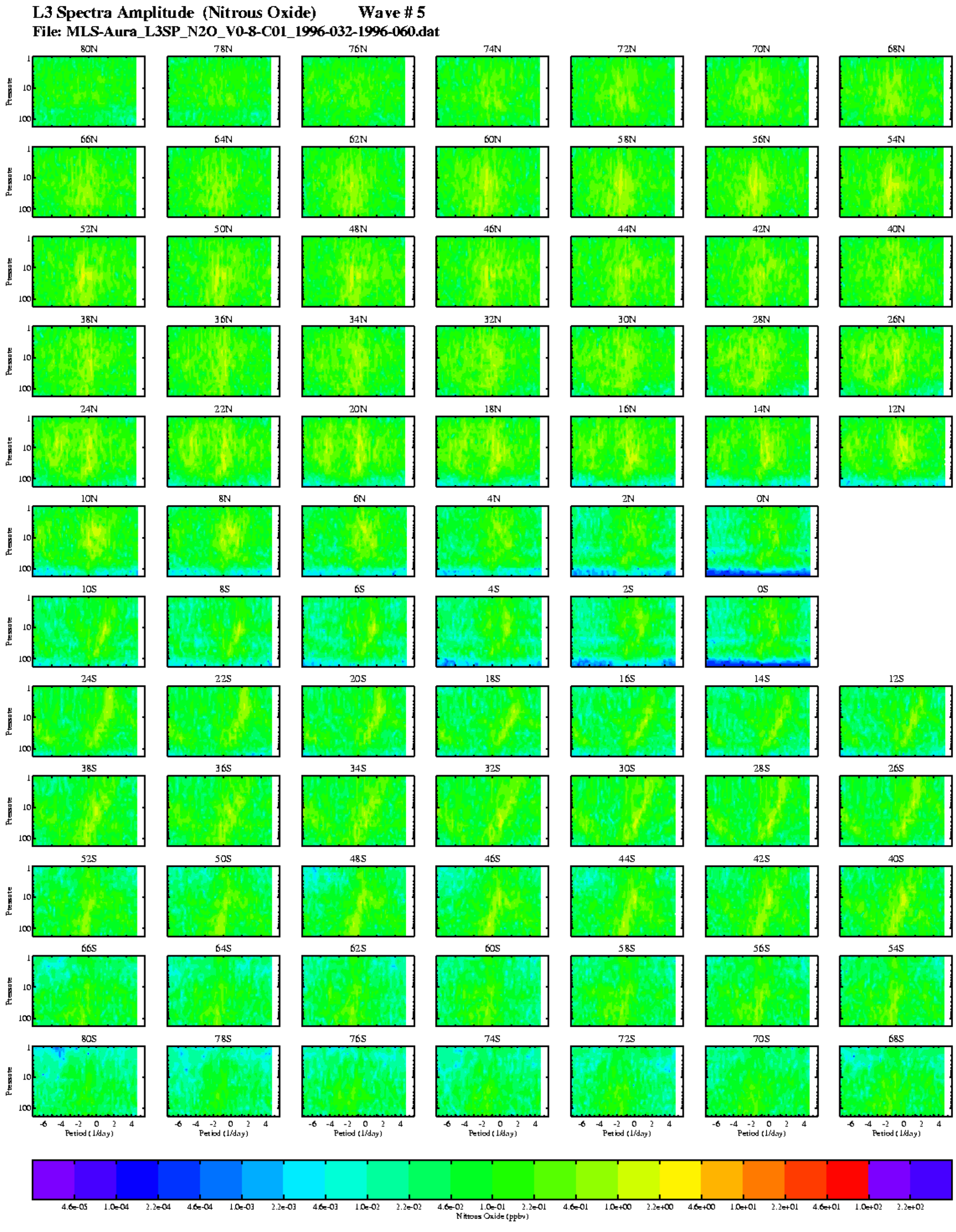
L3 Spectra Amplitude (Nitrous Oxide) Wave # 5
File: MLS-Aura_L3SP_N2O_V0-8-C01_1996-032-1996-060.dat
Pressure
Period (1/day)
Nitrous Oxide (ppbv)
Produced on 3-May-2004, v1.0

Figure E9-6

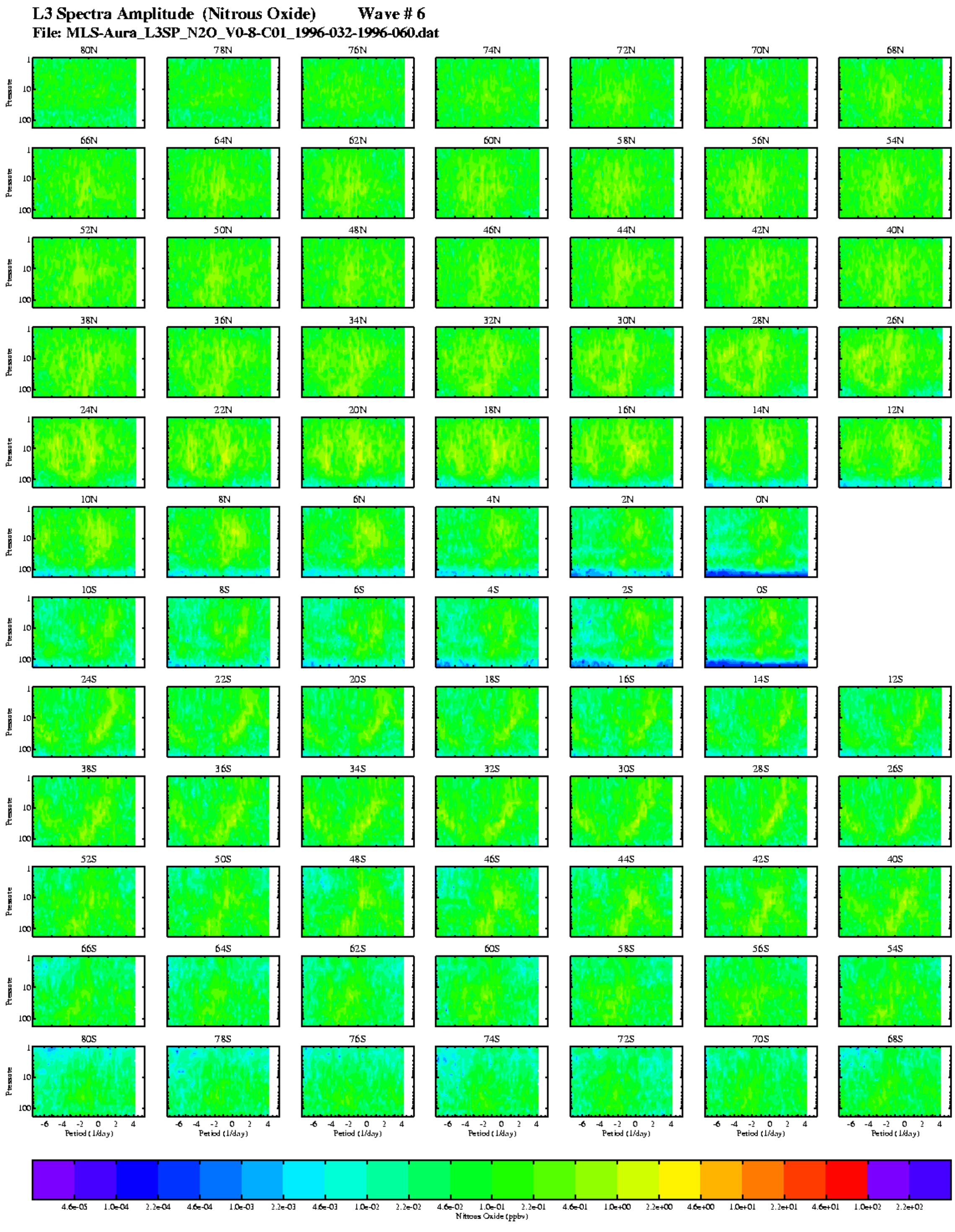
L3 Spectra Amplitude (Nitrous Oxide) Wave # 6
File: MLS-Aura_L3SP_N2O_V0-8-C01_1996-032-1996-060.dat
Period (1/day)
Nitrous Oxide (ppbv)
Produced on 3-May-2004, v1.0

Figure E9-7

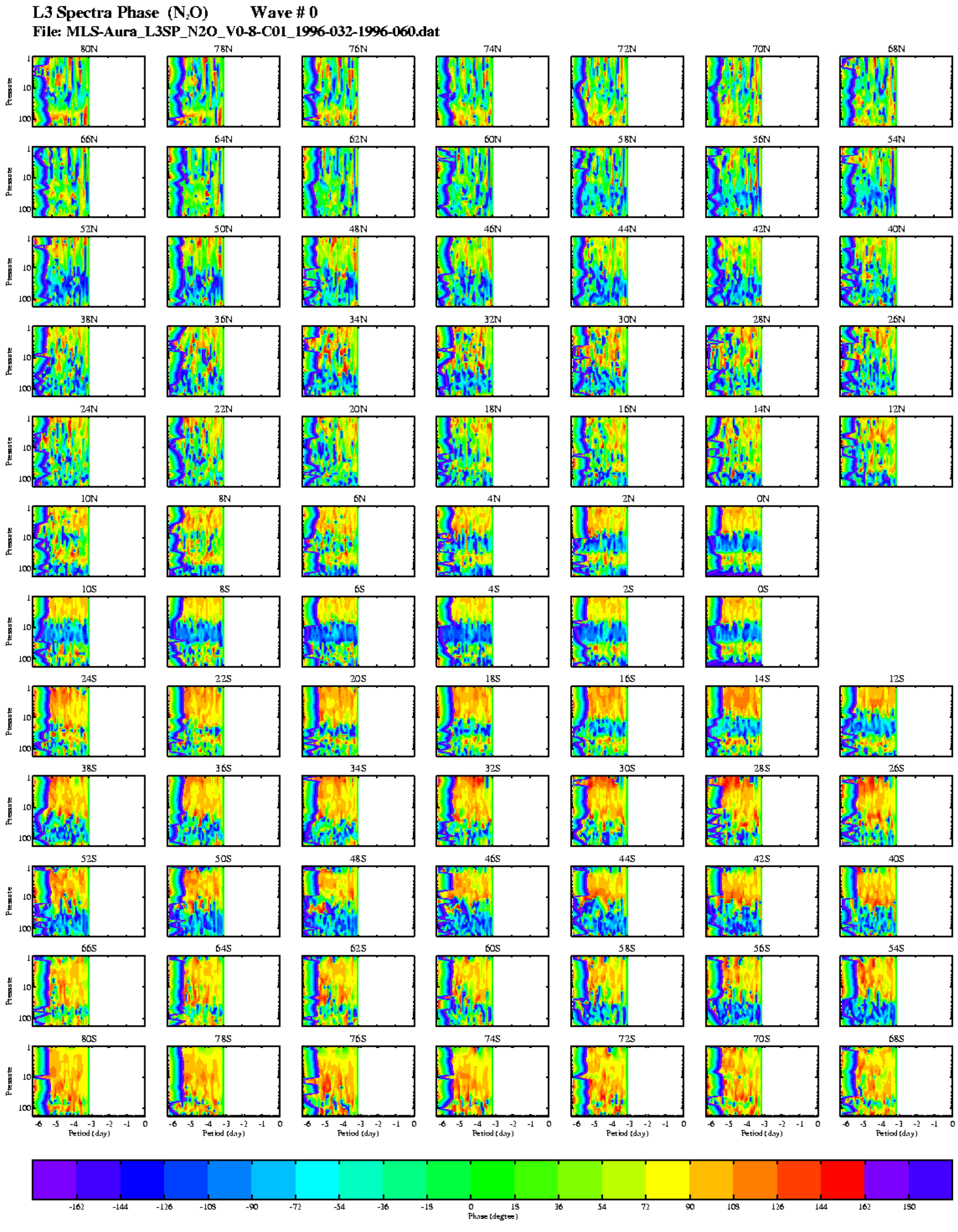
L3 Spectra Phase (N2O) Wave # 0
File: MLS-Aura_L3SP_N2O_V0-8-C01_1996-032-1996-060.dat
Pressure
Period (day)
Phase (degree)
Produced on 30-Apr-2004, v1.0

Figure E10-1

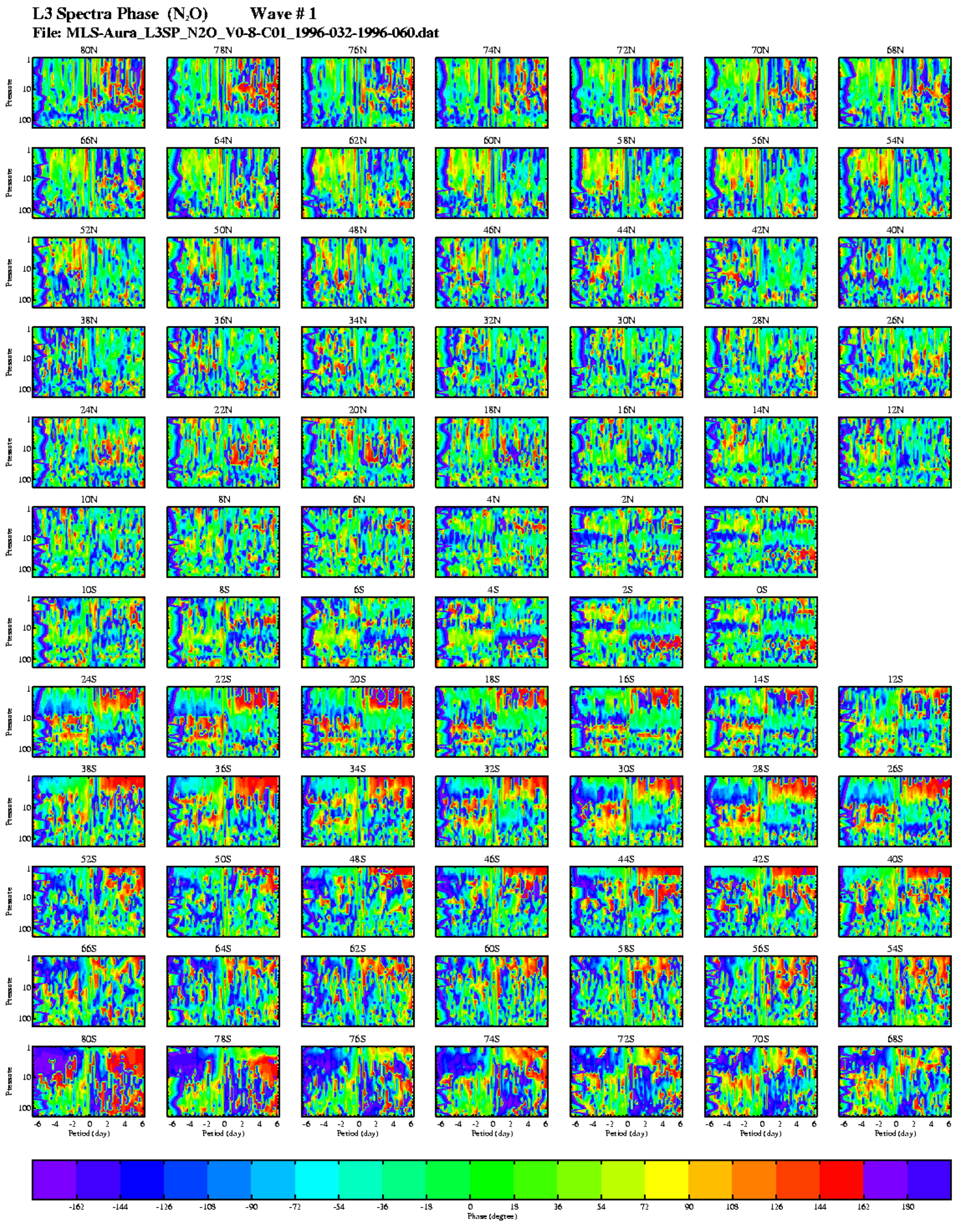
L3 Spectra Phase (N_2O) Wave # 1
File: MLS-Aura_L3SP_N2O_V0-8-C01_1996-032-1996-060.dat
Pressure
Period (day)
Phase (degree)
Produced on 30-Apr-2004, v1.0

Figure E10-2

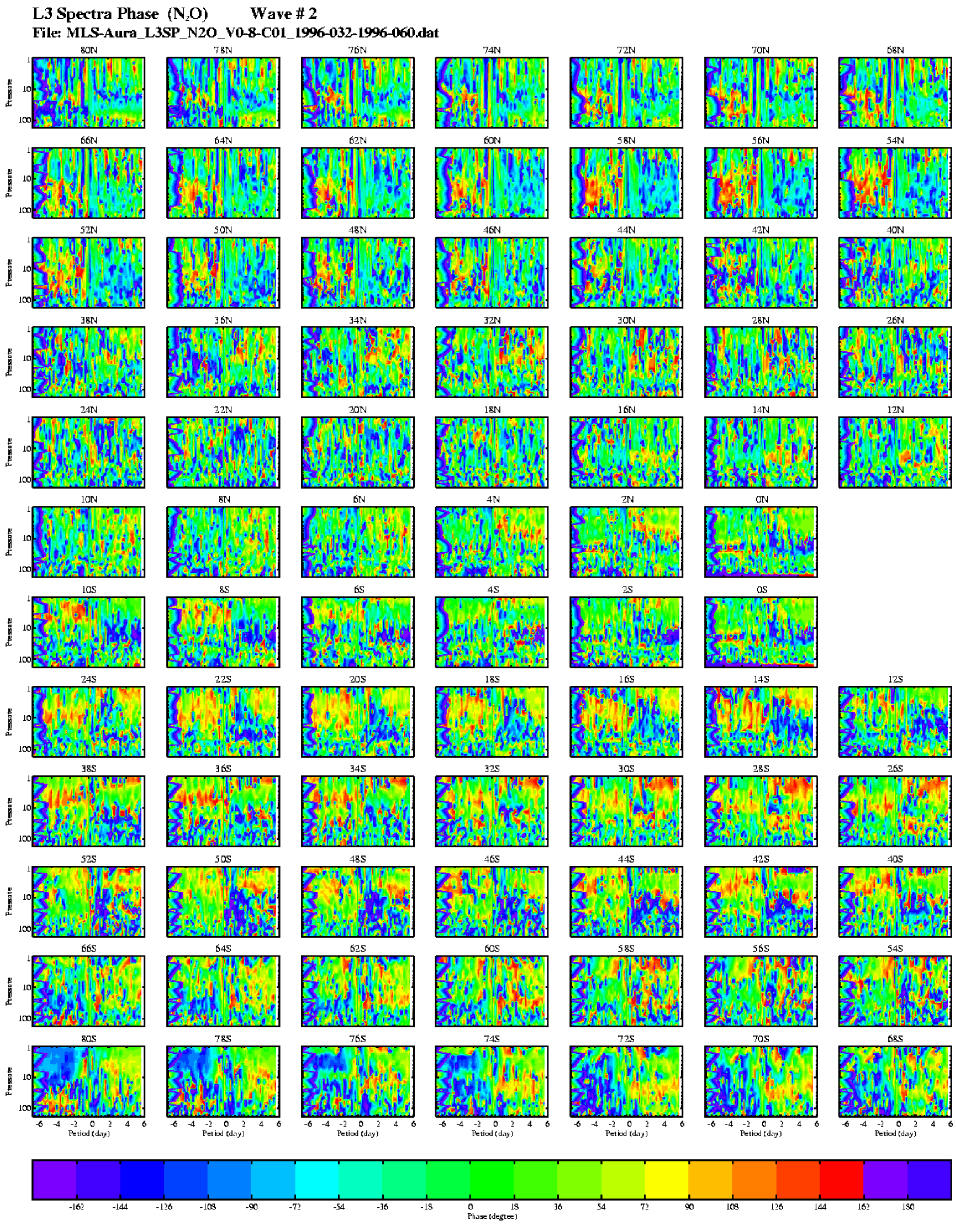
L3 Spectra Phase (N_2O) Wave # 2
File: MLS-Aura_L3SP_N2O_V0-8-C01_1996-032-1996-060.dat
Pressure
Period (day)
Phase (degree)
Produced on 30-Apr-2004, v1.0

Figure E10-3

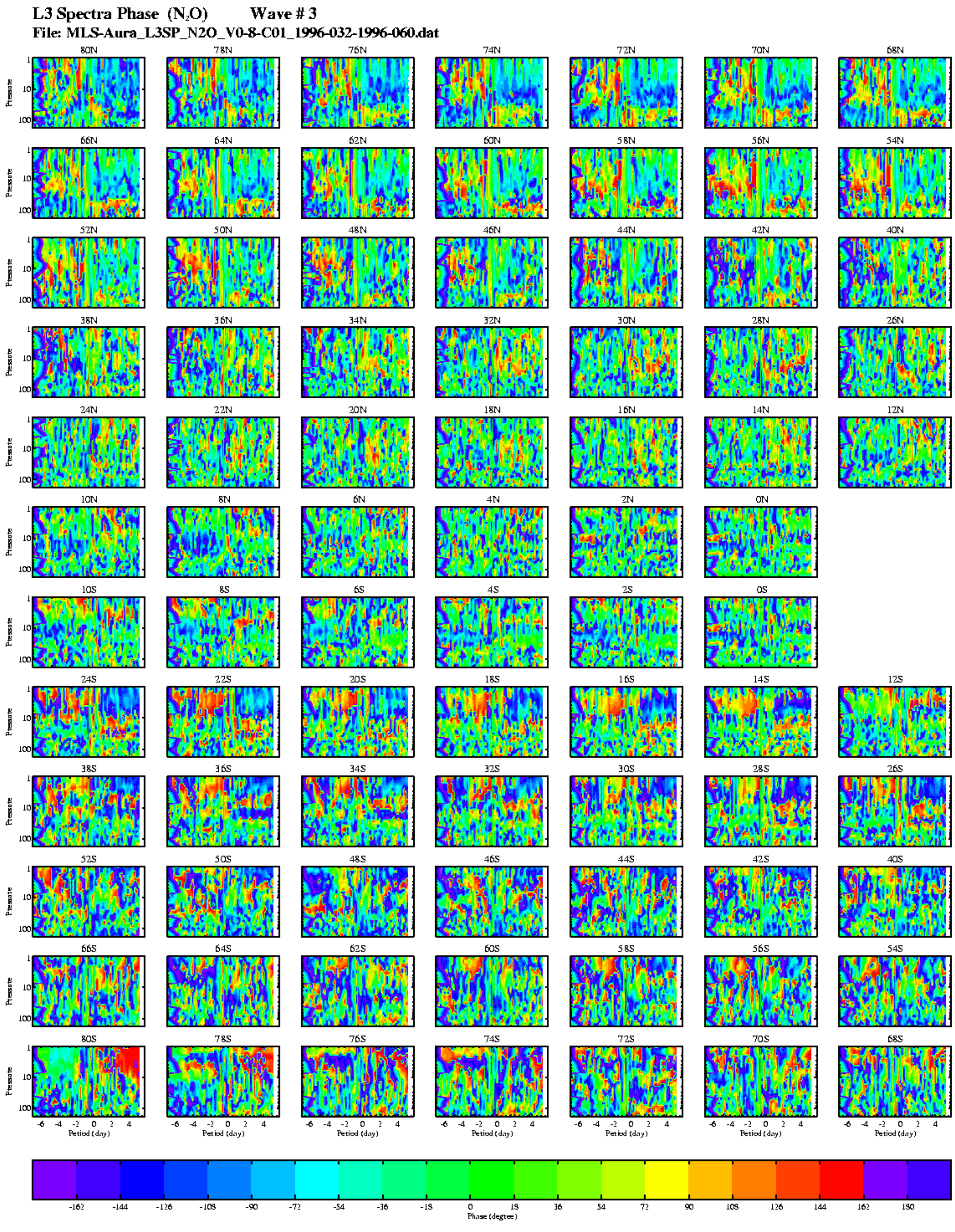

L3 Spectra Phase (N_2O) Wave # 3
File: MLS-Aura_L3SP_N2O_V0-8-C01_1996-032-1996-060.dat
Pressure
Period (day)
Phase (degree)
Produced on 30-Apr-2004, v1.0

Figure E10-4

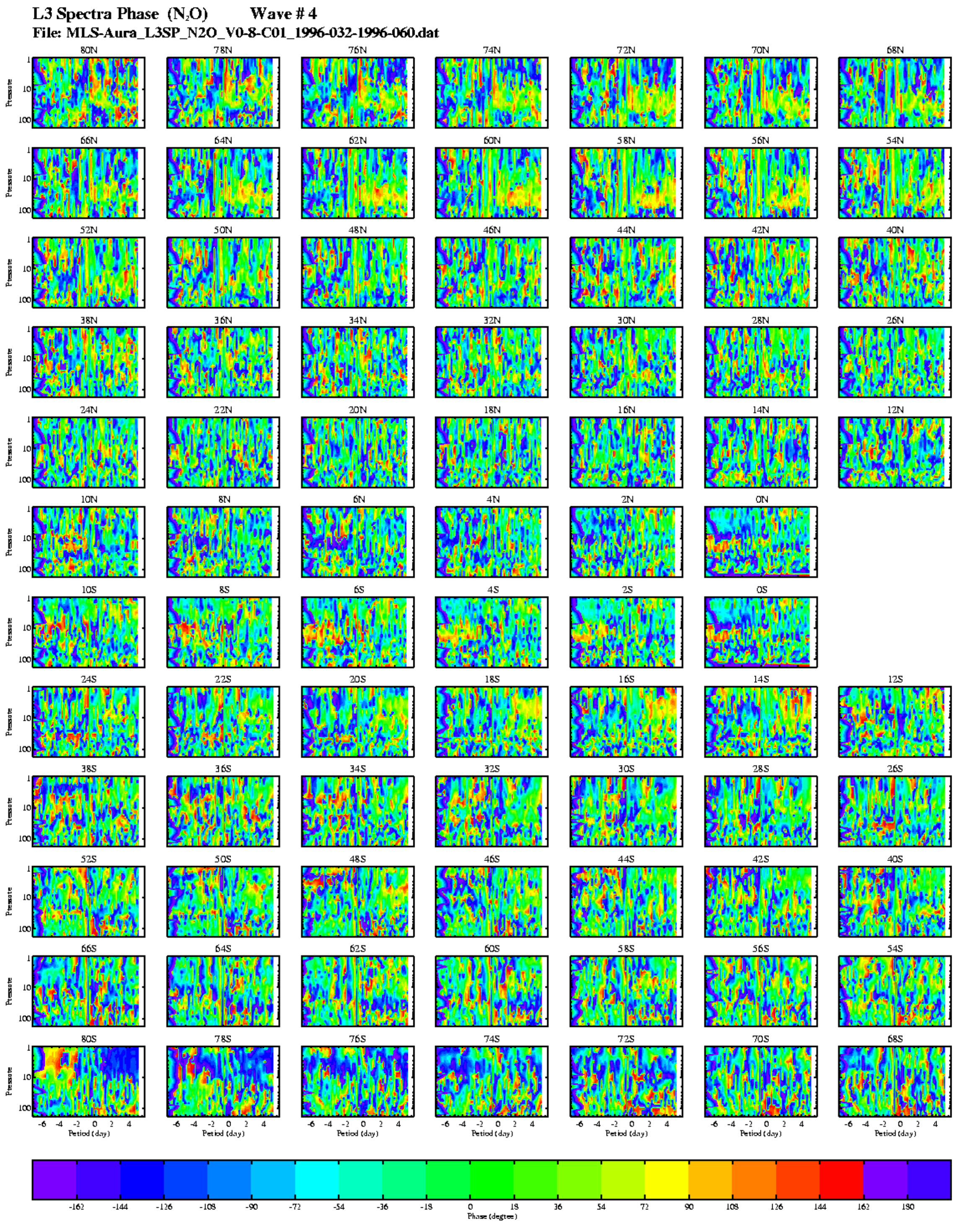

L3 Spectra Phase (N2O) Wave # 4
File: MLS-Aura_L3SP_N2O_V0-8-C01_1996-032-1996-060.dat
80N
78N
76N
74N
72N
70N
68N
66N
64N
62N
60N
58N
56N
54N
52N
50N
48N
46N
44N
42N
40N
38N
36N
34N
32N
30N
28N
26N
24N
22N
20N
18N
16N
14N
12N
10N
8N
6N
4N
2N
0N
10S
8S
6S
4S
2S
0S
24S
22S
20S
18S
16S
14S
12S
38S
36S
34S
32S
30S
28S
26S
52S
50S
48S
46S
44S
42S
40S
66S
64S
62S
60S
58S
56S
54S
80S
78S
76S
74S
72S
70S
68S
Pressure
1
10
100
-6 -4 -2 0 2 4
Period (day)
-162 -144 -126 -108 -90 -72 -54 -36 -18 0 18 36 54 72 90 108 126 144 162 180
Phase (degree)
Produced on 30-Apr-2004, v1.0

Figure E10-5

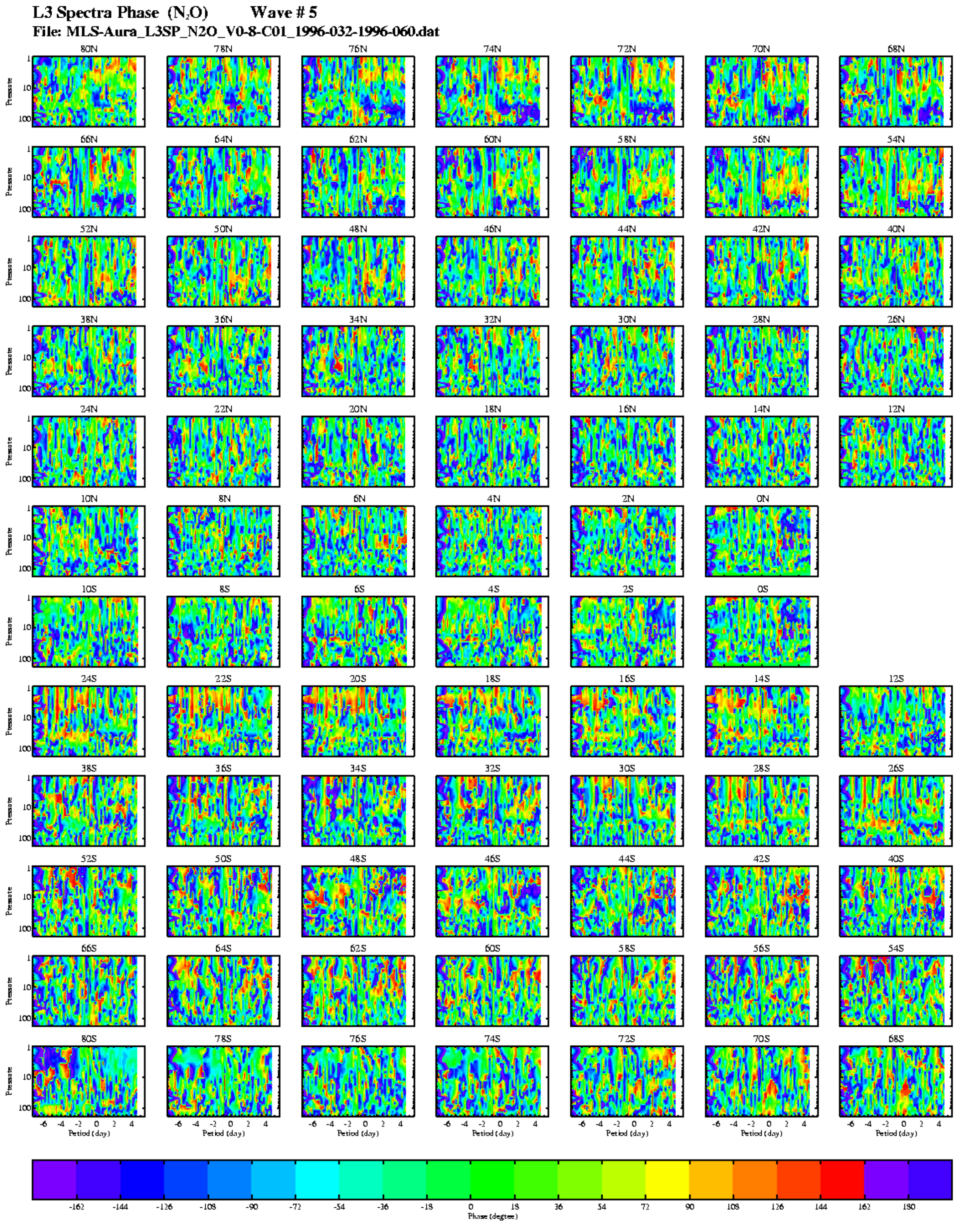
L3 Spectra Phase (N2O) Wave # 5
File: MLS-Aura_L3SP_N2O_V0-8-C01_1996-032-1996-060.dat
Pressure
Period (day)
Phase (degree)
Produced on 30-Apr-2004, v1.0

Figure E10-6

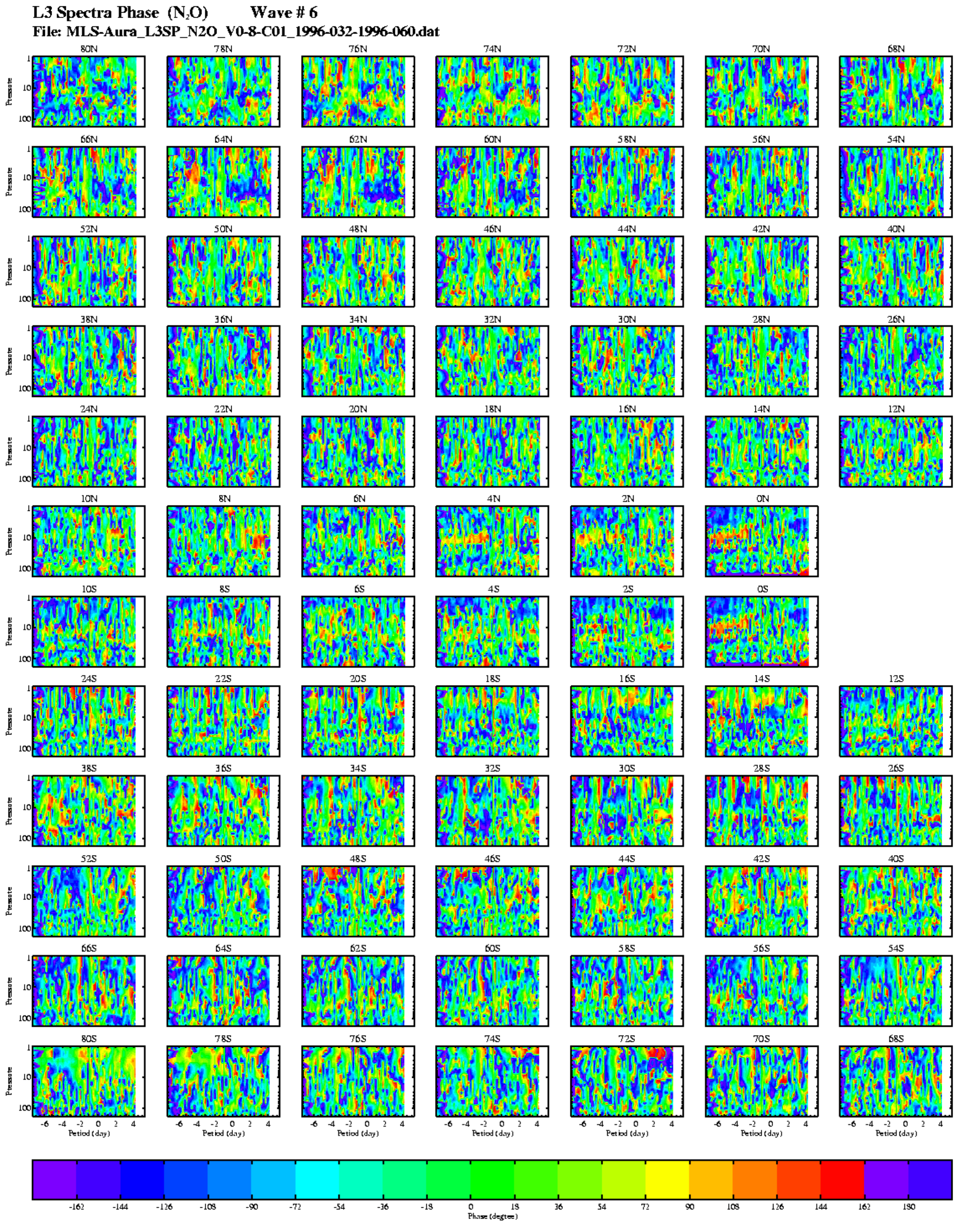
L3 Spectra Phase (N_2O) Wave # 6
File: MLS-Aura_L3SP_N2O_V0-8-C01_1996-032-1996-060.dat
Pressure
Period (day)
Phase (degree)
Produced on 30-Apr-2004, v1.0

Figure E10-7

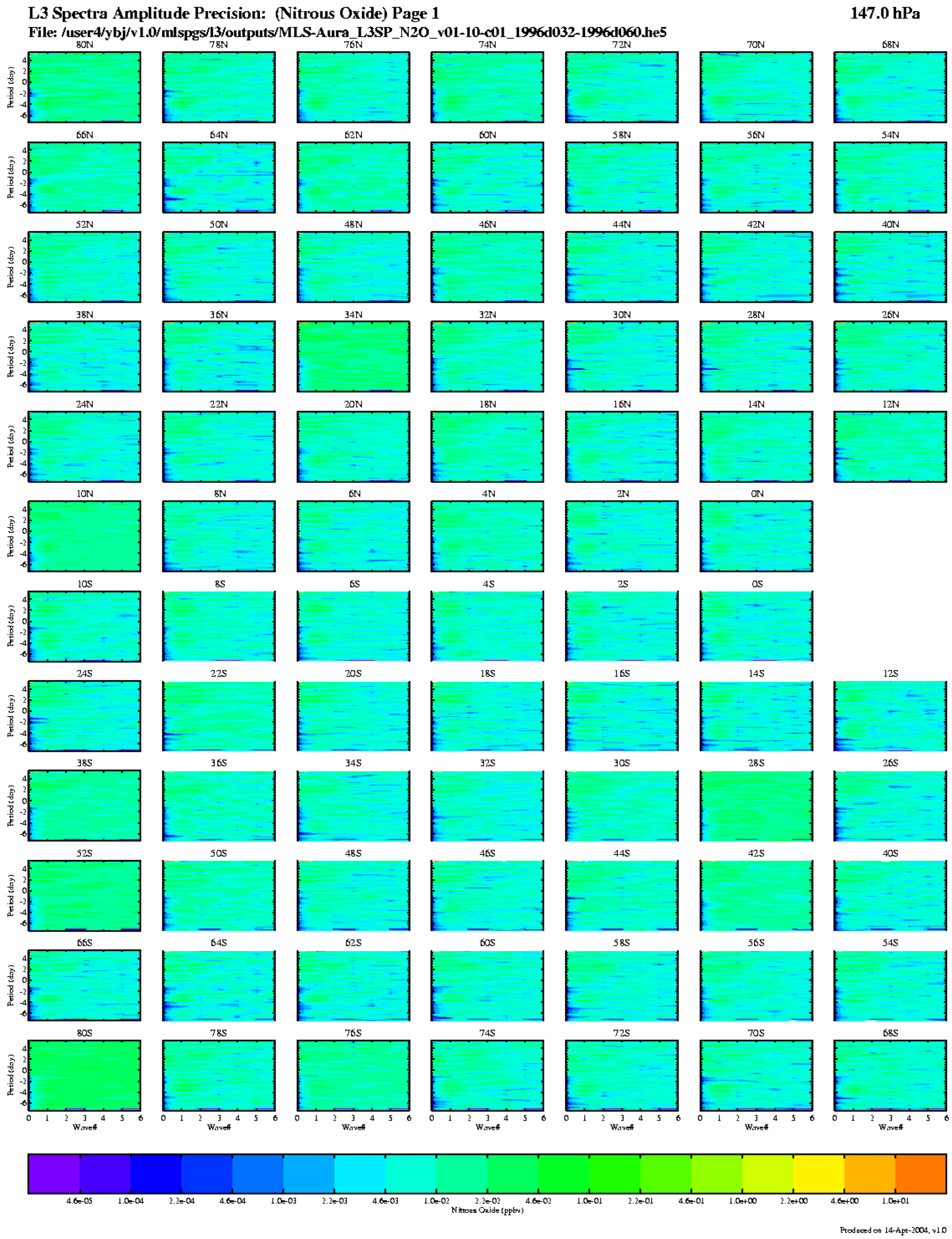
L3 Spectra Amplitude Precision: (Nitrous Oxide) Page 1
147.0 hPa
File: /user4/ybj/v1.0/mlspgs/l3/outputs/MLS-Aura_L3SP_N2O_v01-10-c01_1996d032-1996d060.he5
Period (day)
Wave#
Nitrous Oxide (ppbv)
Produced on 14-Apr-2004, v1.0

Figure E11-1

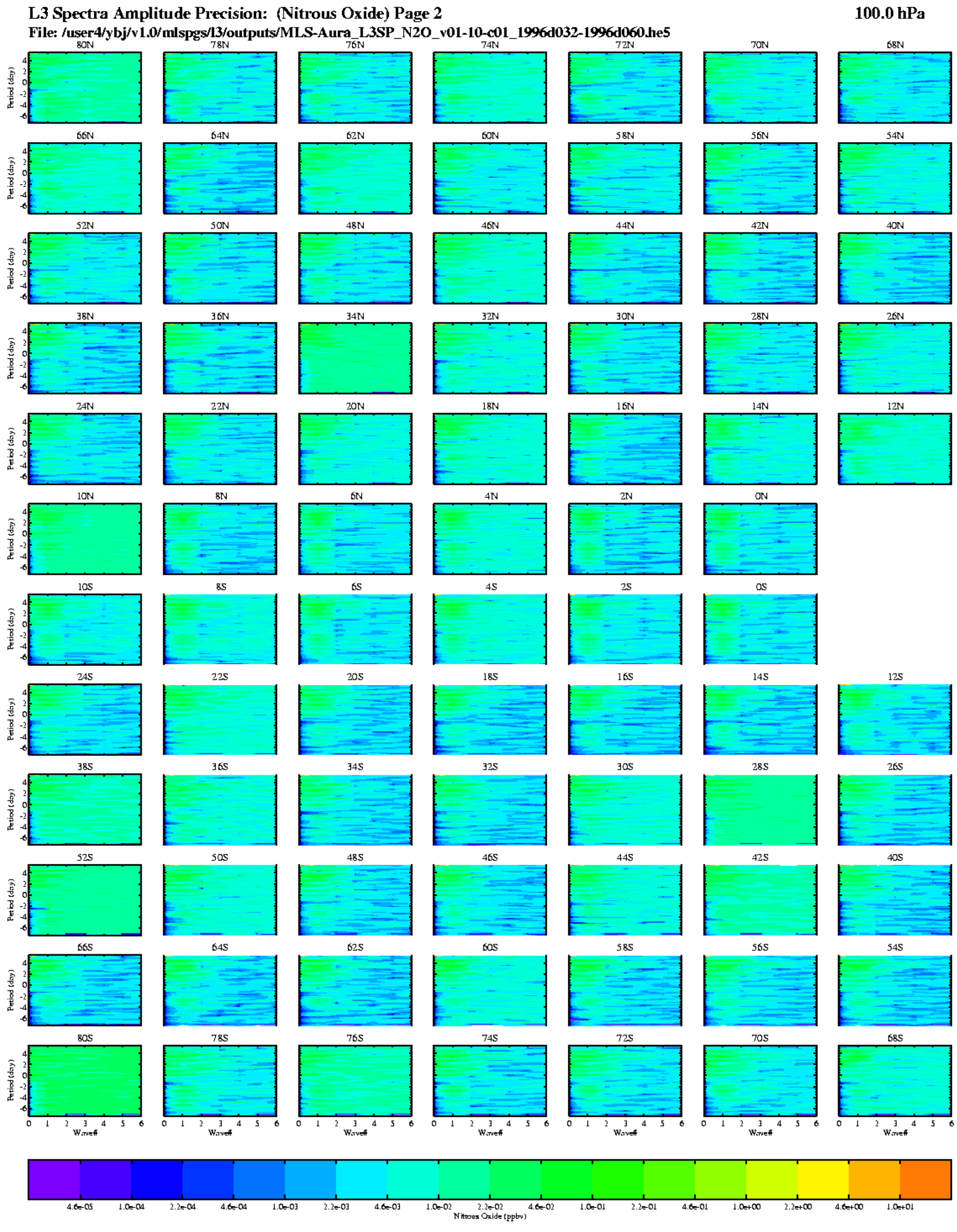

L3 Spectra Amplitude Precision: (Nitrous Oxide) Page 2
100.0 hPa
File: /user4/ybj/v1.0/mlspgs/l3/outputs/MLS-Aura_L3SP_N2O_v01-10-c01_1996d032-1996d060.he5
Period (day)
Wave#
Nitrous Oxide (ppbv)
Produced on 14-Apr-2004, v1.0

Figure E11-2

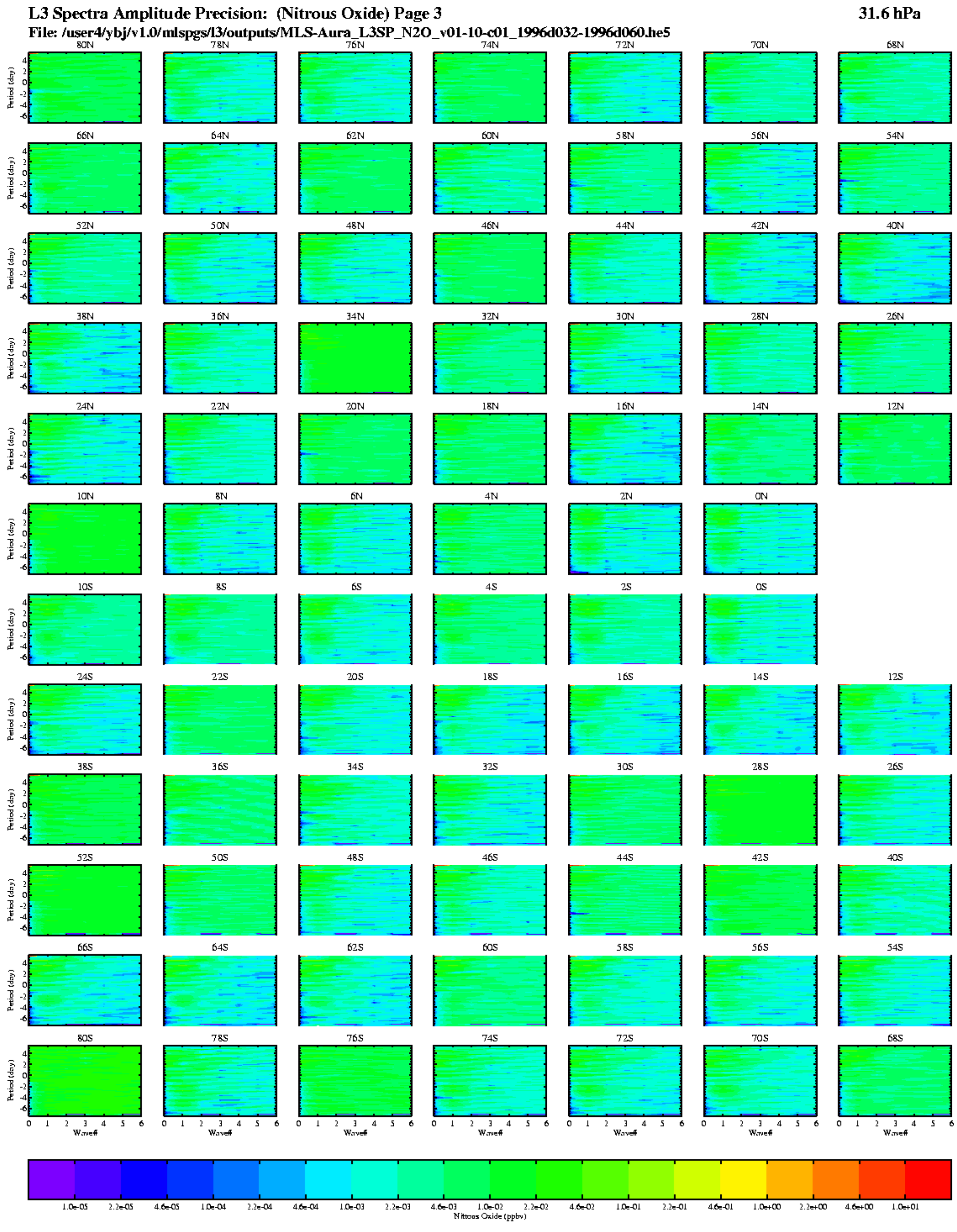
L3 Spectra Amplitude Precision: (Nitrous Oxide) Page 3
31.6 hPa
File: /user4/ybj/v1.0/mlspgs/l3/outputs/MLS-Aura_L3SP_N2O_v01-10-c01_1996d032-1996d060.he5
Period (day)
Wave#
Nitrous Oxide (ppbv)
Produced on 14-Apr-2004, v1.0

Figure E11-3

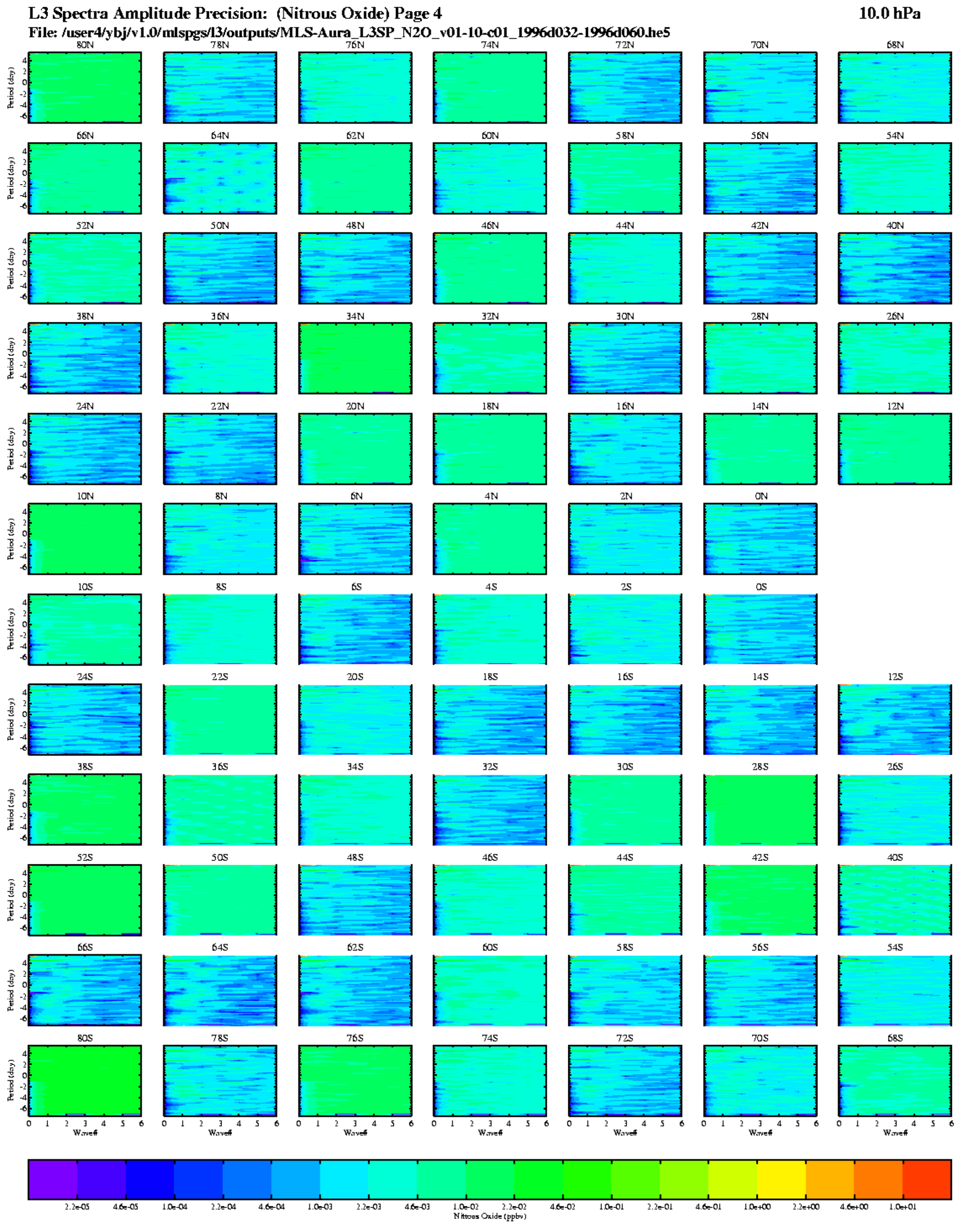
L3 Spectra Amplitude Precision: (Nitrous Oxide) Page 4
10.0 hPa
File: /user4/ybj/v1.0/mlspgs/l3/outputs/MLS-Aura_L3SP_N2O_v01-10-c01_1996d032-1996d060.he5
Period (day)
Wave#
Nitrous Oxide (ppbv)
Produced on 14-Apr-2004, v1.0

Figure E11-4

L3 Spectra Amplitude Precision: (Nitrous Oxide) Page 5 **3.2 hPa**

File: /user4/ybj/v1.0/mlspgs/l3/outputs/MLS-Aura_L3SP_N2O_v01-10-c01_1996d032-1996d060.he5

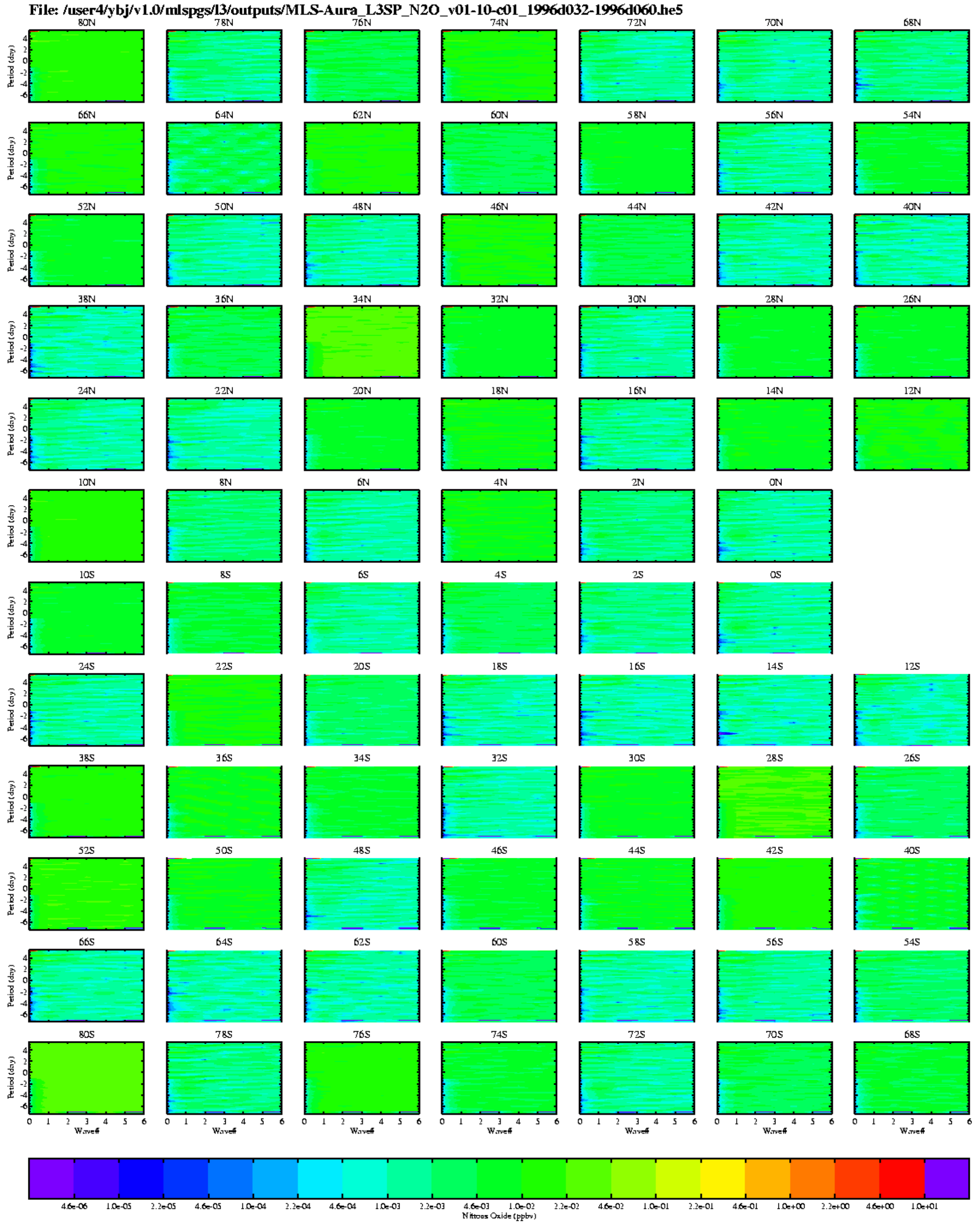

Figure E11-5

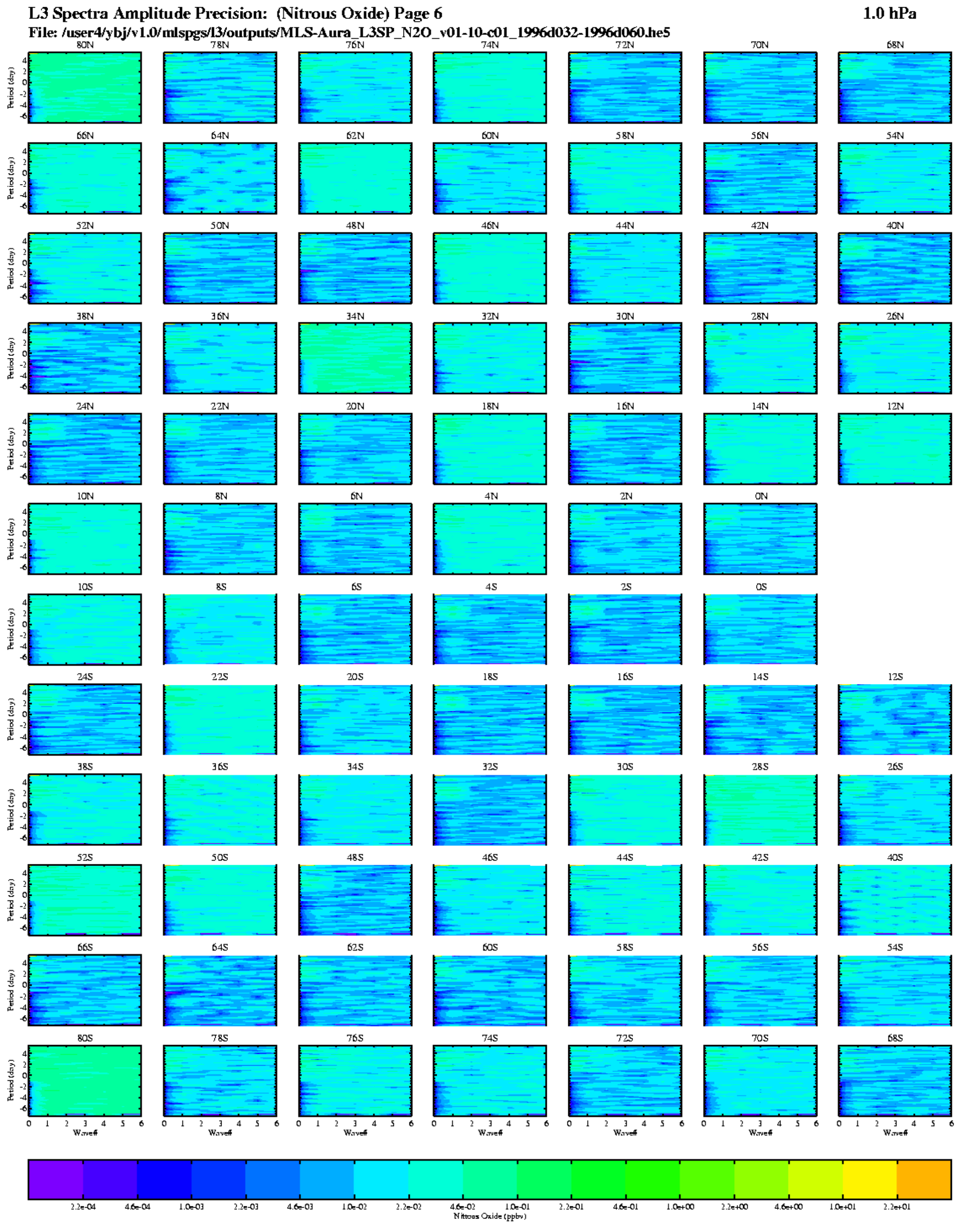
L3 Spectra Amplitude Precision: (Nitrous Oxide) Page 6
1.0 hPa
File: /user4/ybj/v1.0/mlspgs/l3/outputs/MLS-Aura_L3SP_N2O_v01-10-c01_1996d032-1996d060.he5
Period (day)
Wave#
Nitrous Oxide (ppbv)
Produced on 14-Apr-2004, v1.0

Figure E11-6

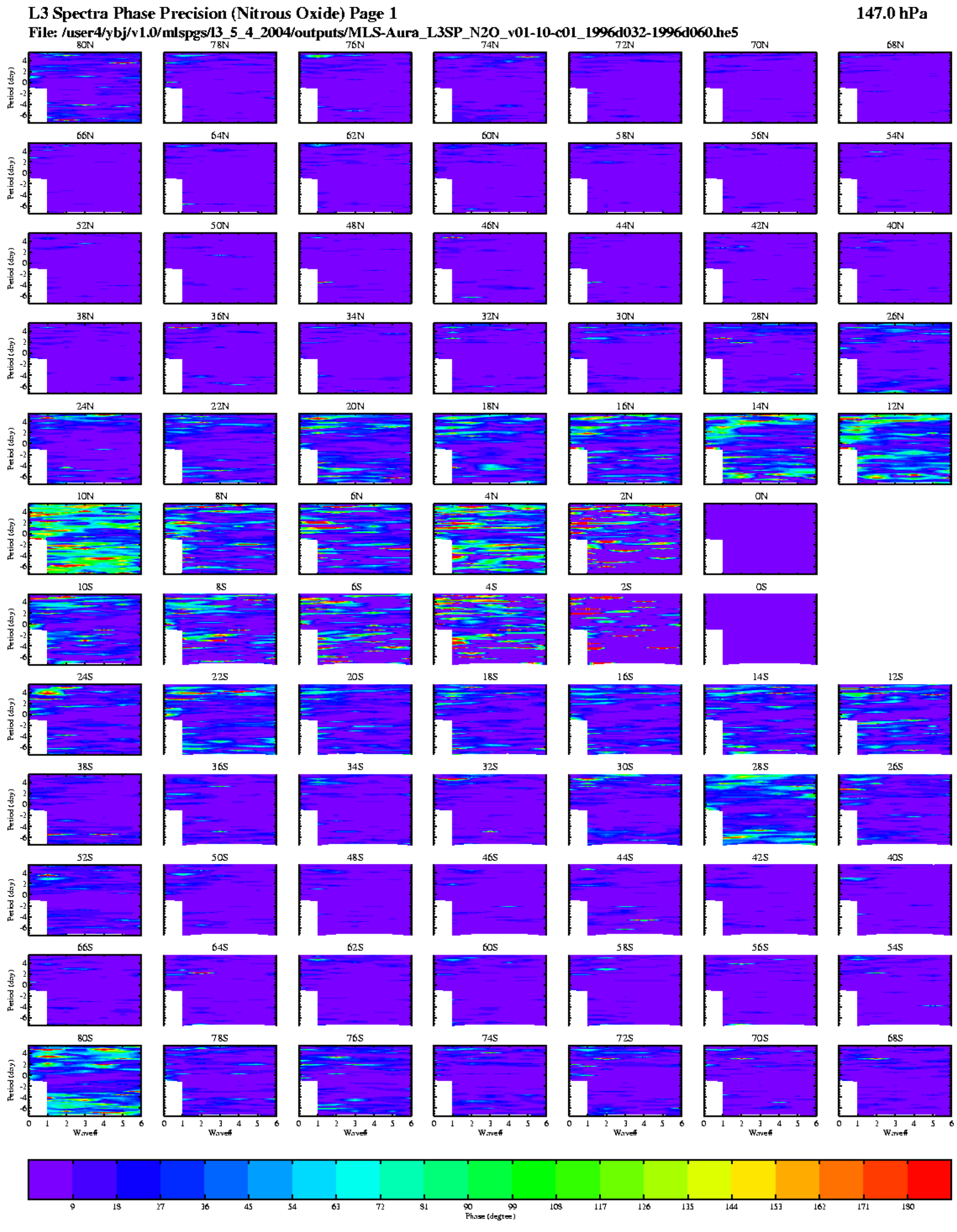
L3 Spectra Phase Precision (Nitrous Oxide) Page 1
147.0 hPa
File: /user4/ybj/v1.0/mlspgs/l3_5_4_2004/outputs/MLS-Aura_L3SP_N2O_v01-10-c01_1996d032-1996d060.he5
Period (day)
Wave#
Phase (degree)
Produced on 6-May-2004, v1.0

Figure E12-1

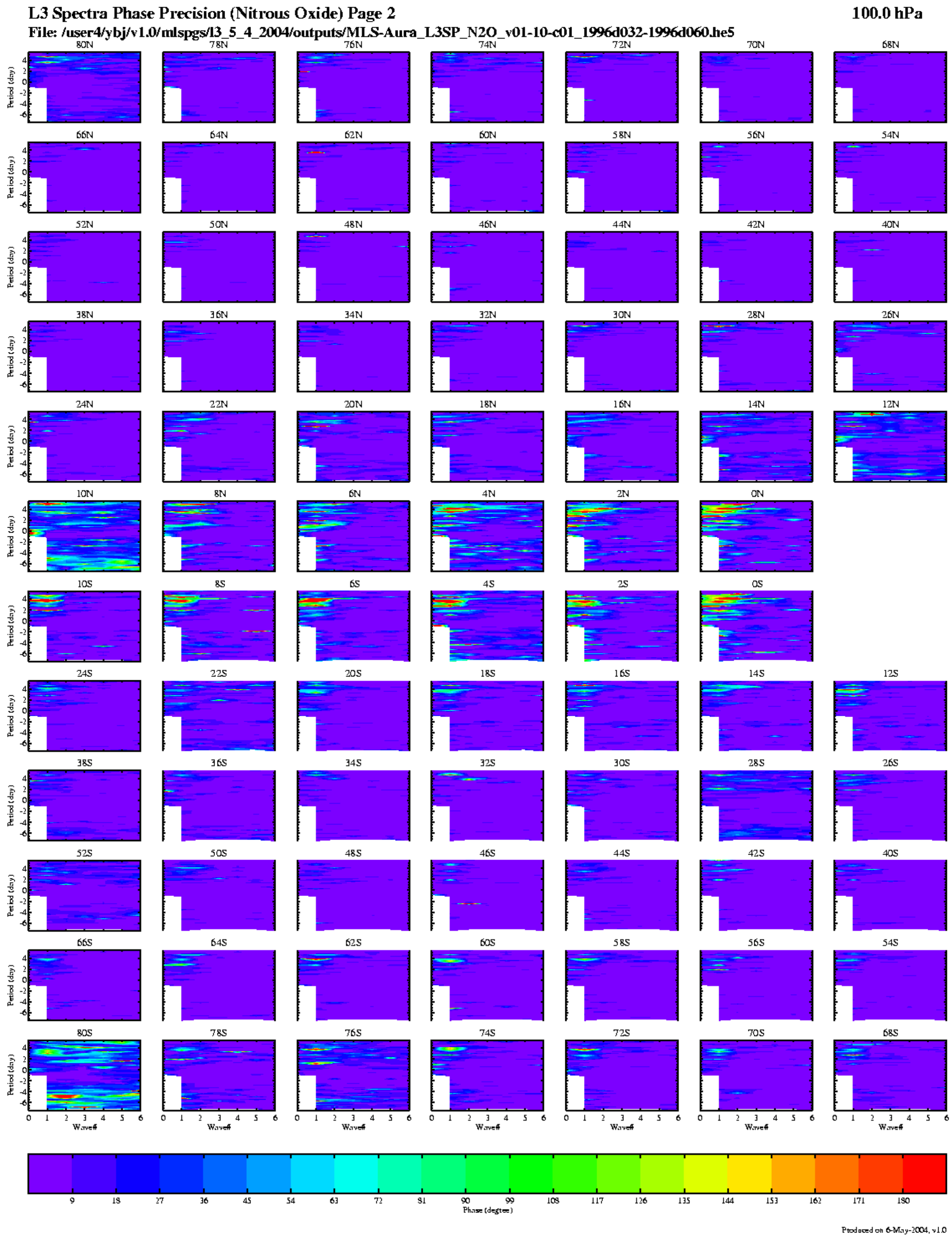
L3 Spectra Phase Precision (Nitrous Oxide) Page 2
100.0 hPa
File: /user4/ybj/v1.0/mlspgs/l3_5_4_2004/outputs/MLS-Aura_L3SP_N2O_v01-10-c01_1996d032-1996d060.he5
Period (day)
Wave#
Phase (degree)
Produced on 6-May-2004, v1.0

Figure E12-2

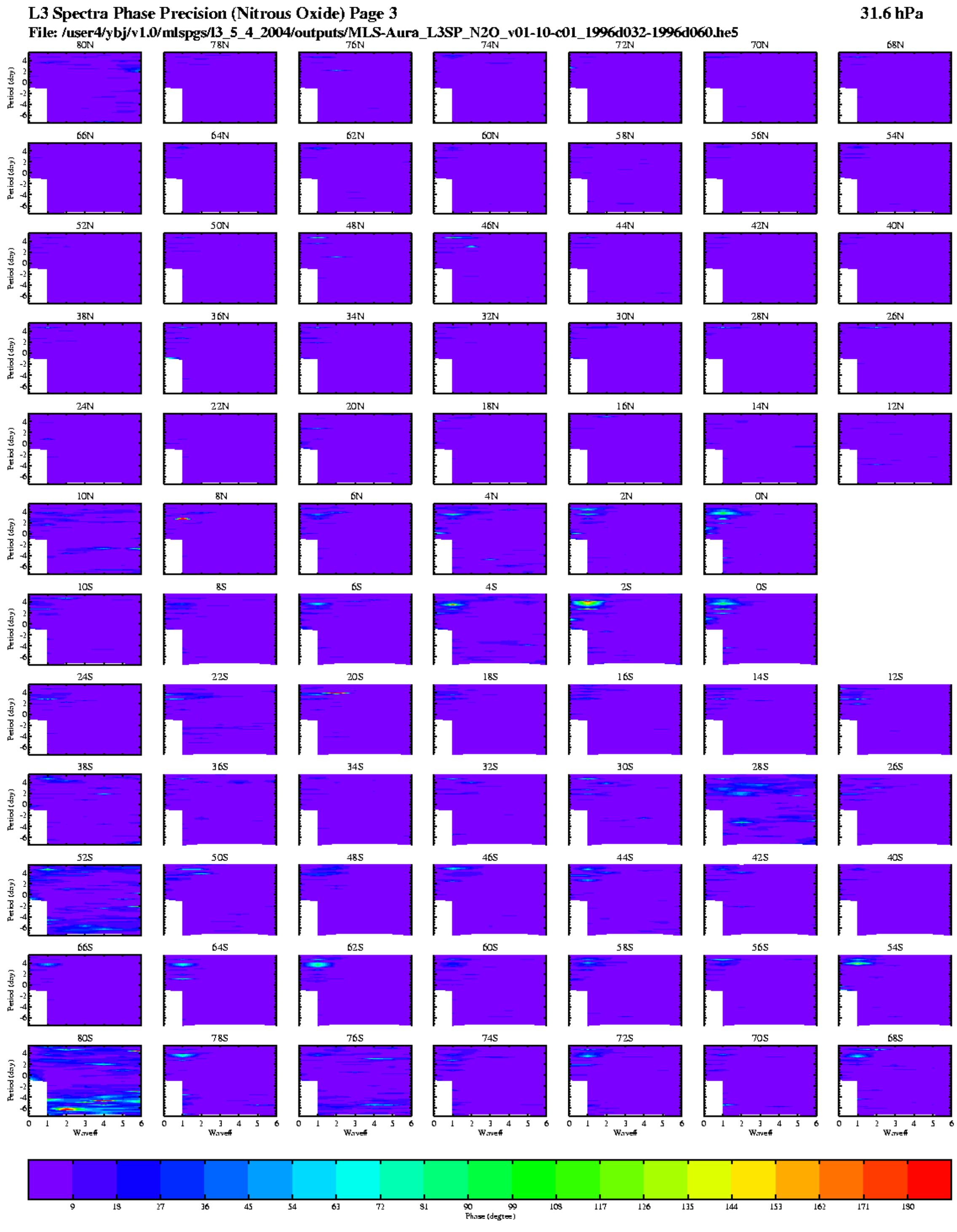
L3 Spectra Phase Precision (Nitrous Oxide) Page 3
31.6 hPa
File: /user4/ybj/v1.0/mlspgs/l3_5_4_2004/outputs/MLS-Aura_L3SP_N2O_v01-10-c01_1996d032-1996d060.he5
Period (day)
Wave#
Phase (degree)
Produced on 6-May-2004, v1.0

Figure E12-3

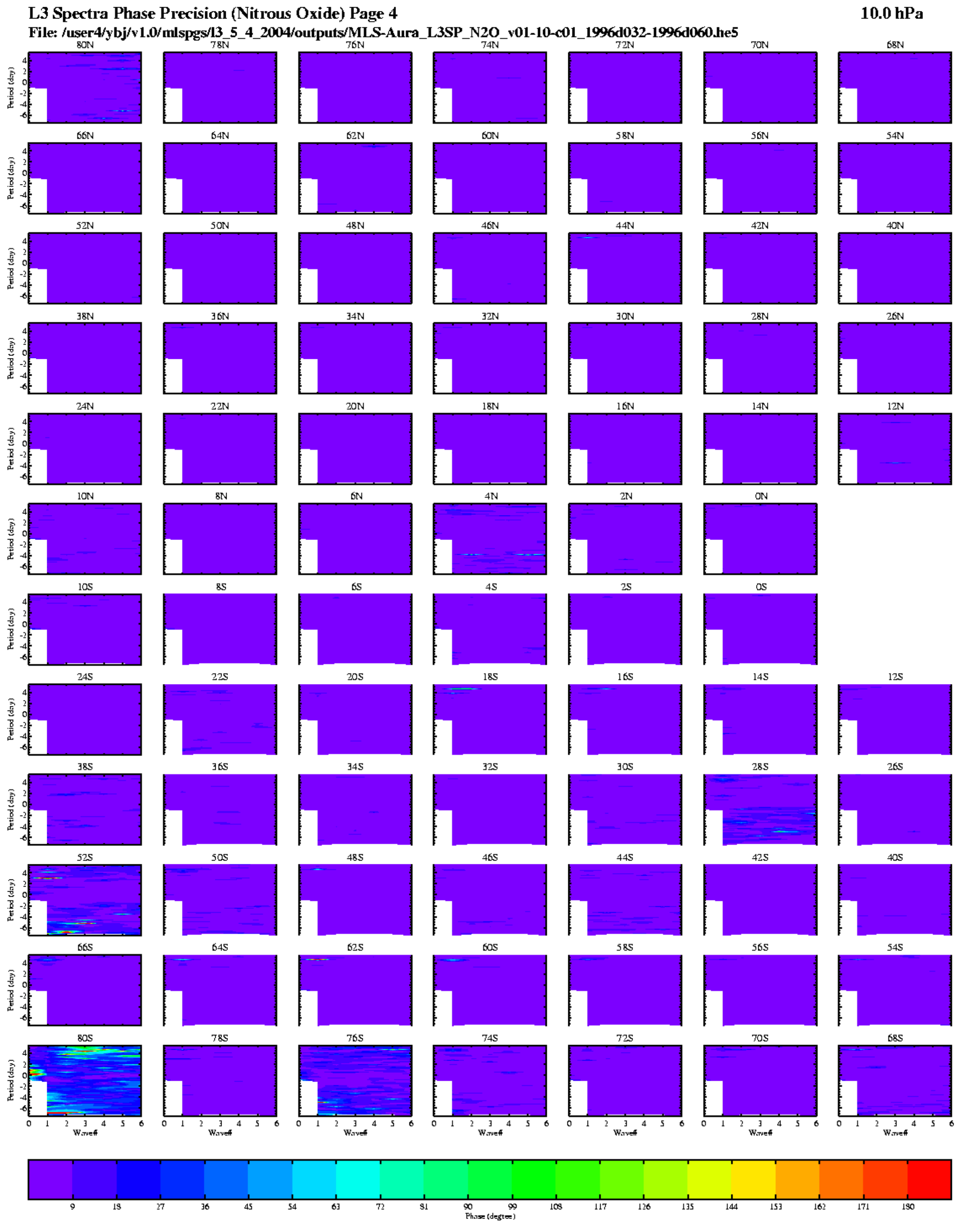
L3 Spectra Phase Precision (Nitrous Oxide) Page 4
10.0 hPa
File: /user4/ybj/v1.0/mlspgs/l3_5_4_2004/outputs/MLS-Aura_L3SP_N2O_v01-10-c01_1996d032-1996d060.he5
Period (day)
Wave#
Phase (degree)
Produced on 6-May-2004, v1.0

Figure E12-4

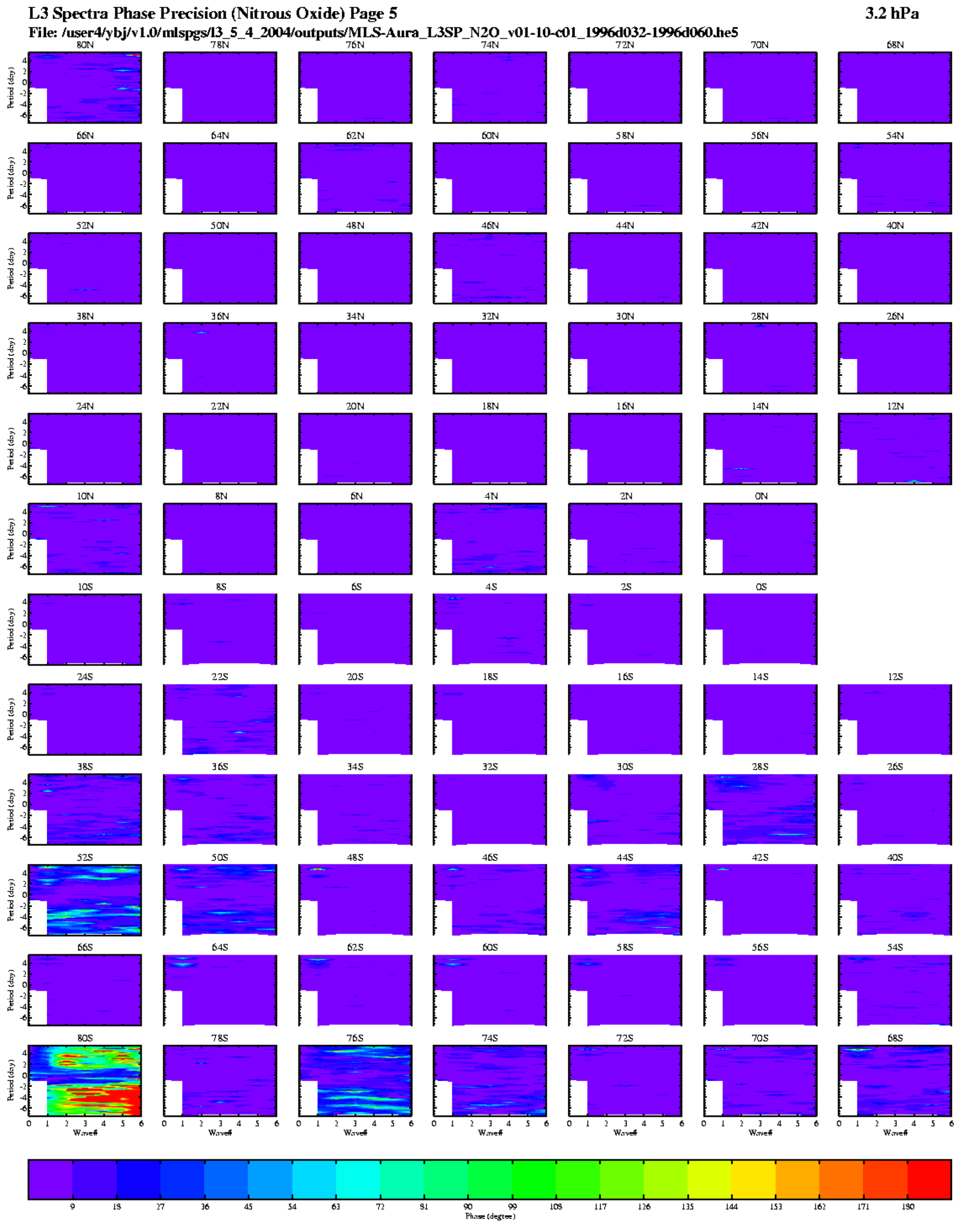
L3 Spectra Phase Precision (Nitrous Oxide) Page 5
3.2 hPa
File: /user4/ybj/v1.0/mlspgs/l3_5_4_2004/outputs/MLS-Aura_L3SP_N2O_v01-10-c01_1996d032-1996d060.he5
Period (day)
Wave#
Phase (degree)
Produced on 6-May-2004, v1.0

Figure E12-5

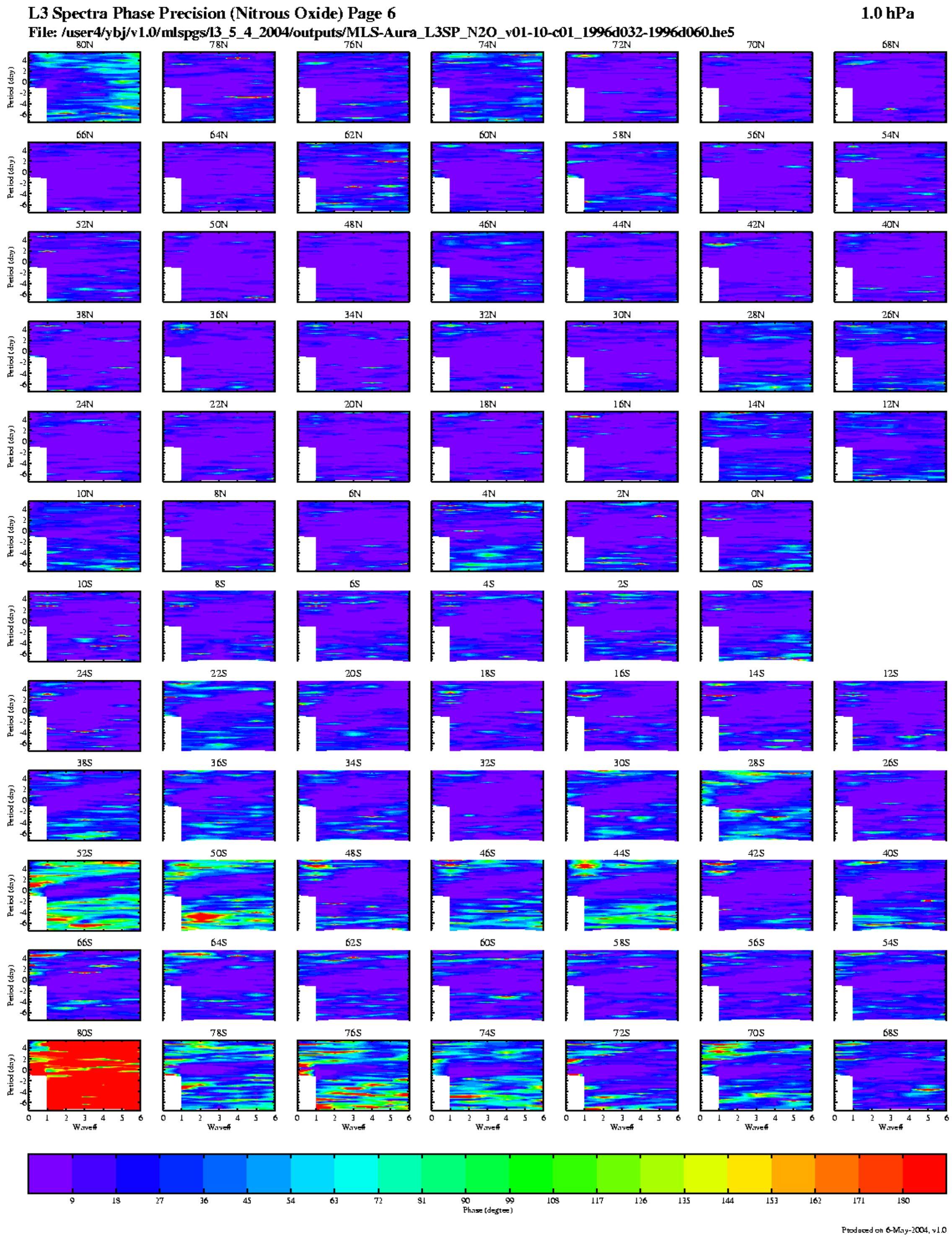
L3 Spectra Phase Precision (Nitrous Oxide) Page 6
1.0 hPa
File: /user4/ybj/v1.0/mlspgs/l3_5_4_2004/outputs/MLS-Aura_L3SP_N2O_v01-10-c01_1996d032-1996d060.he5
Period (day)
Wave#
Phase (degree)
Produced on 6-May-2004, v1.0

Figure E12-6

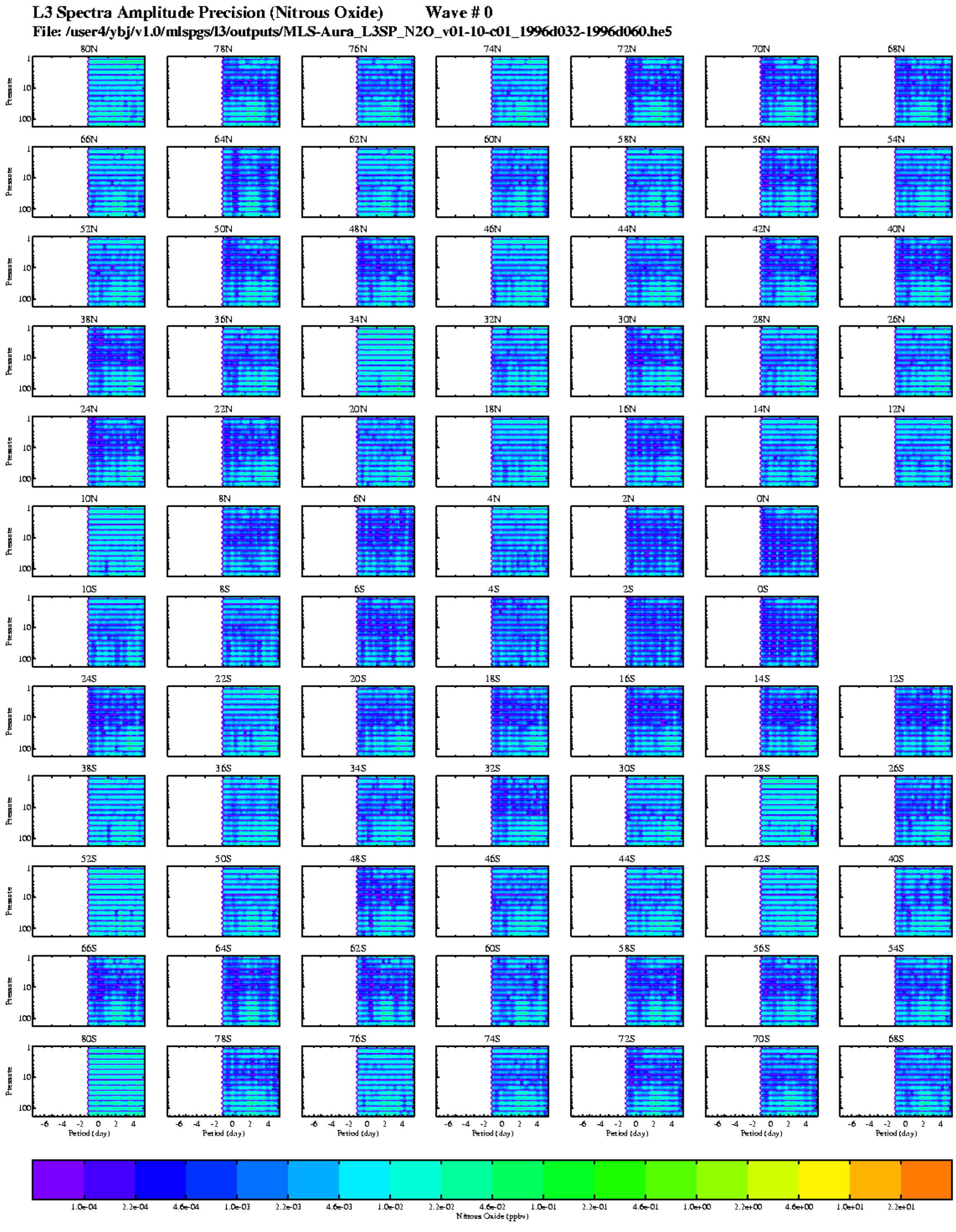
L3 Spectra Amplitude Precision (Nitrous Oxide) Wave # 0
File: /user4/ybj/v1.0/mlspgs/l3/outputs/MLS-Aura_L3SP_N2O_v01-10-c01_1996d032-1996d060.he5
Period (day)
Pressure
Nitrous Oxide (ppbv)
Produced on 15-Apr-2004, v1.0

Figure E13-1

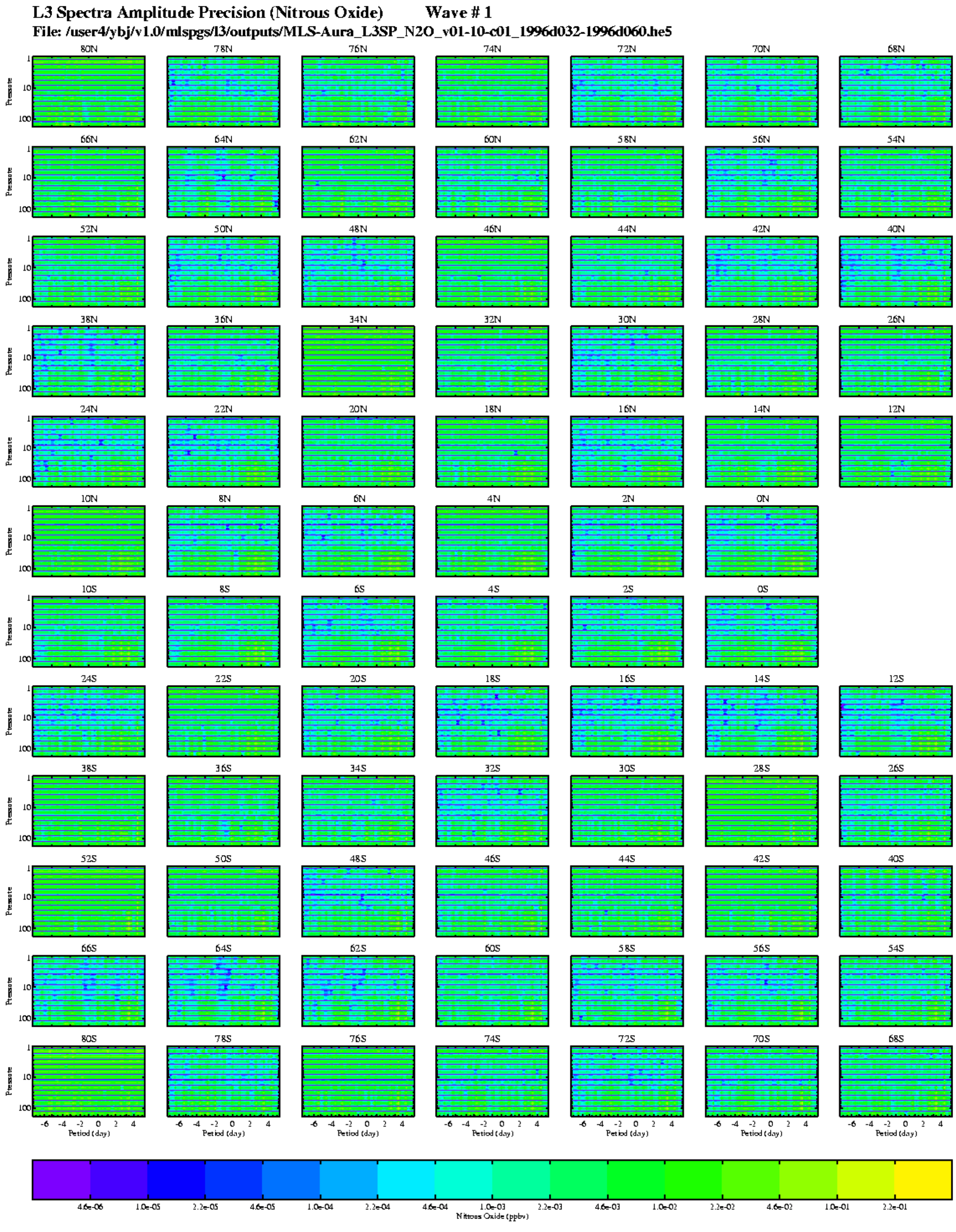
L3 Spectra Amplitude Precision (Nitrous Oxide) Wave # 1
File: /user4/ybj/v1.0/mlspgs/l3/outputs/MLS-Aura_L3SP_N2O_v01-10-c01_1996d032-1996d060.he5
Pressure
Period (day)
Nitrous Oxide (ppbv)
Produced on 15-Apr-2004, v1.0

Figure E13-2

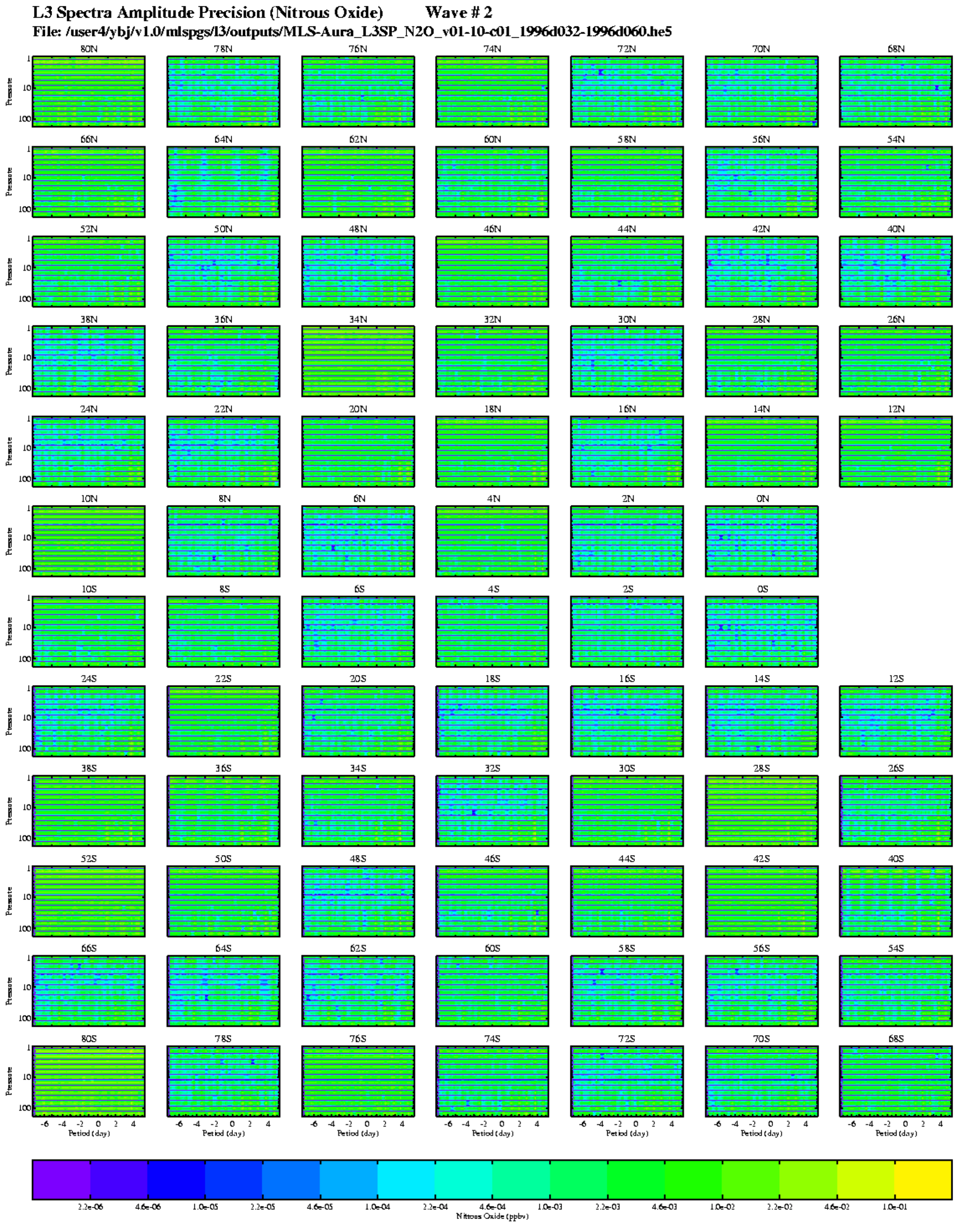
L3 Spectra Amplitude Precision (Nitrous Oxide) Wave # 2
File: /user4/ybj/v1.0/mlspgs/l3/outputs/MLS-Aura_L3SP_N2O_v01-10-c01_1996d032-1996d060.he5
Pressure
Period (day)
Nitrous Oxide (ppbv)
Produced on 15-Apr-2004, v1.0

Figure E13-3

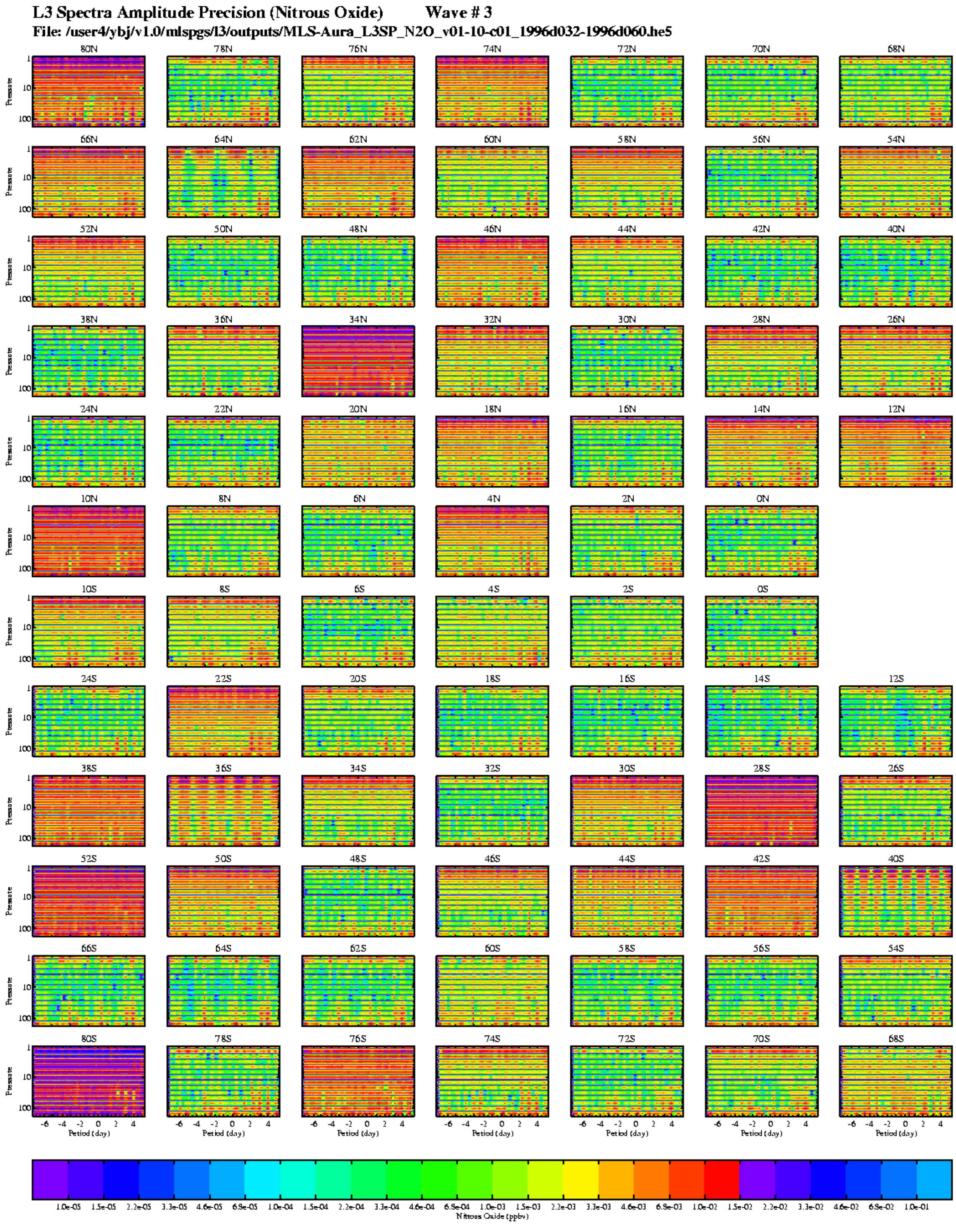
L3 Spectra Amplitude Precision (Nitrous Oxide) Wave # 3
File: /user4/ybj/v1.0/mlspgs/l3/outputs/MLS-Aura_L3SP_N2O_v01-10-c01_1996d032-1996d060.he5
Pressure
Period (day)
Nitrous Oxide (ppbv)
Produced on 15-Apr-2004, v1.0

Figure E13-4

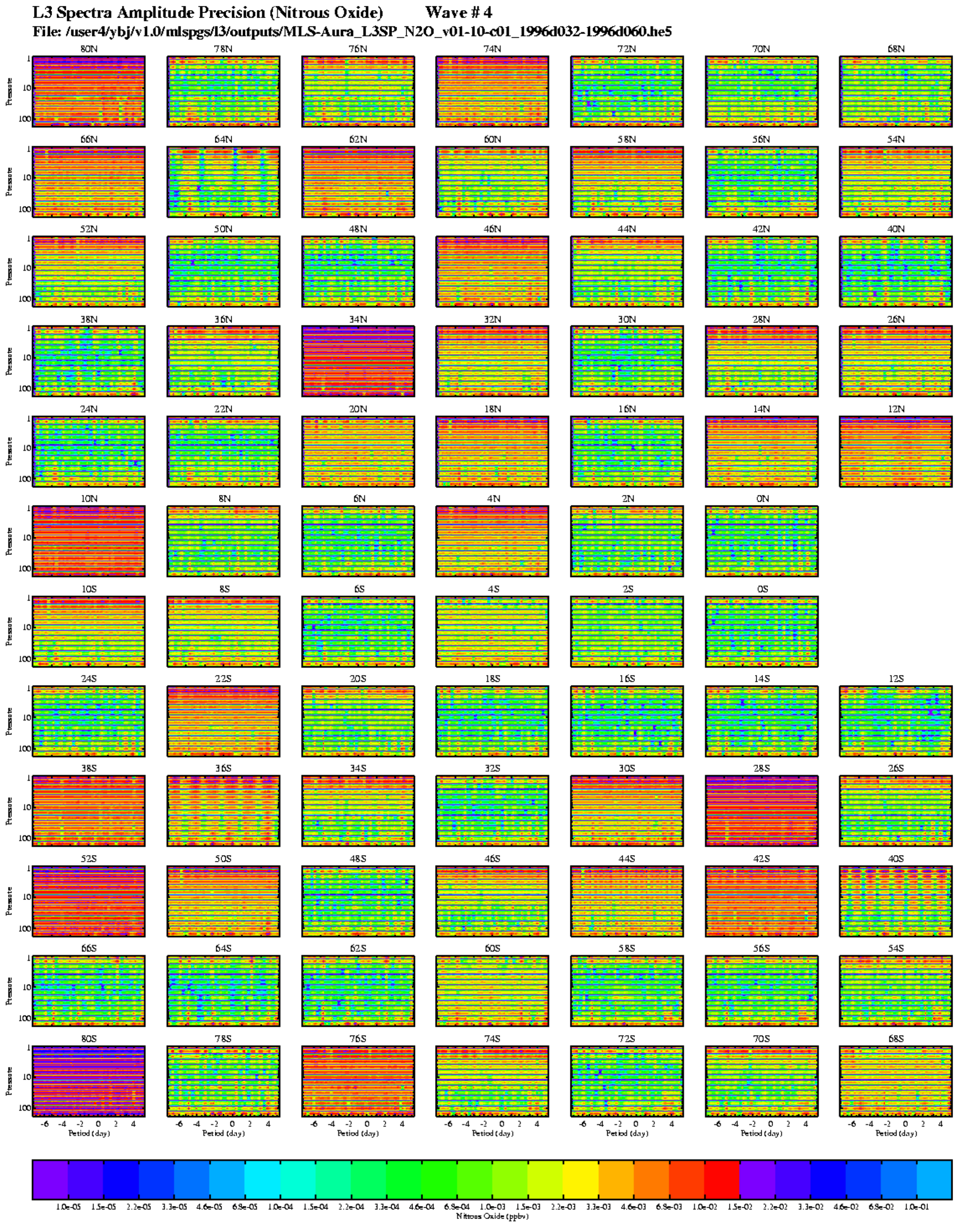
L3 Spectra Amplitude Precision (Nitrous Oxide) Wave # 4
File: /user4/ybj/v1.0/mlspgs/l3/outputs/MLS-Aura_L3SP_N2O_v01-10-c01_1996d032-1996d060.he5
Pressure
Period (day)
Nitrous Oxide (ppbv)
Produced on 15-Apr-2004, v1.0

Figure E13-5

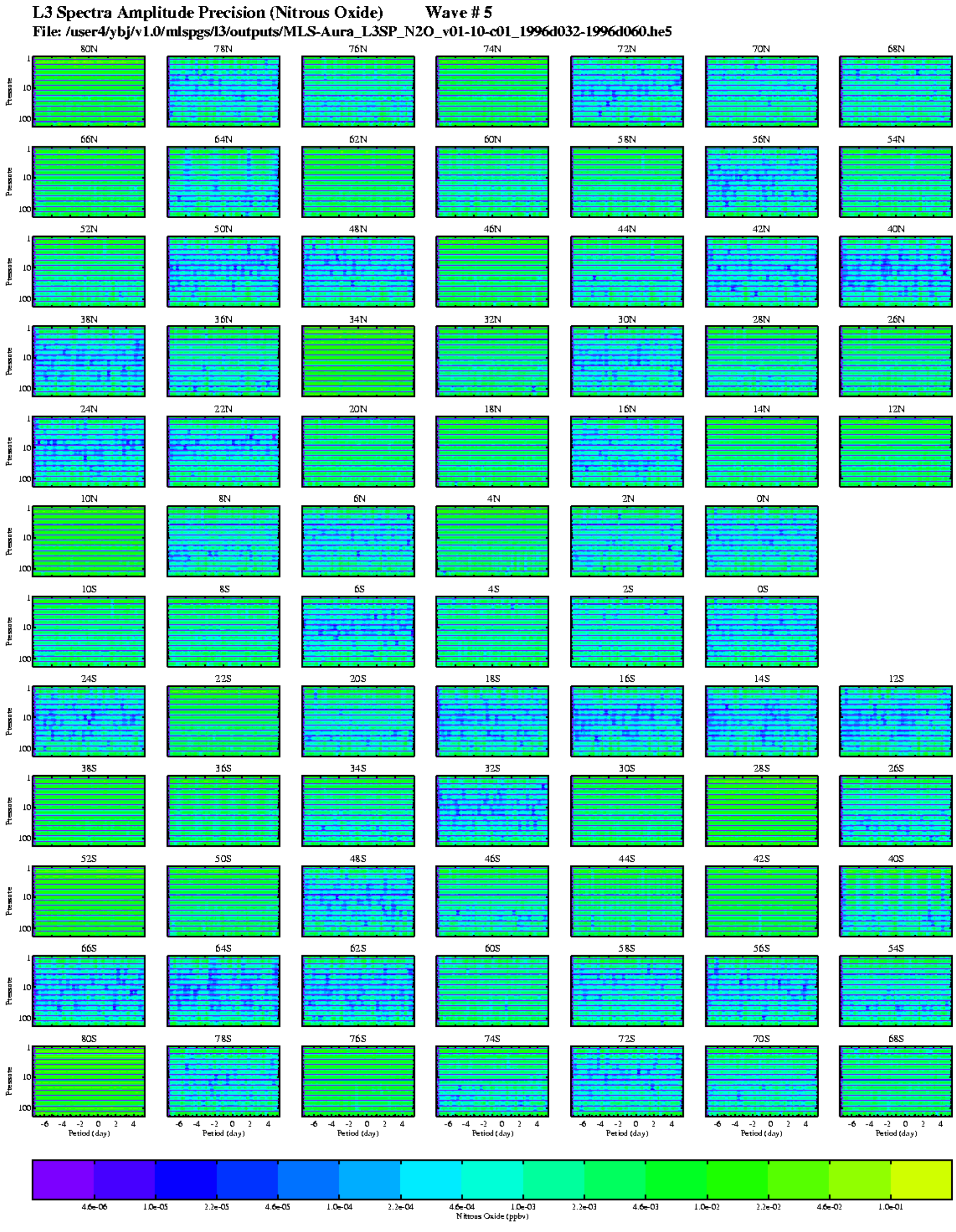

L3 Spectra Amplitude Precision (Nitrous Oxide) Wave # 5
File: /user4/ybj/v1.0/mlspgs/l3/outputs/MLS-Aura_L3SP_N2O_v01-10-c01_1996d032-1996d060.he5
Pressure
Period (day)
Nitrous Oxide (ppbv)
Produced on 15-Apr-2004, v1.0

Figure E13-6

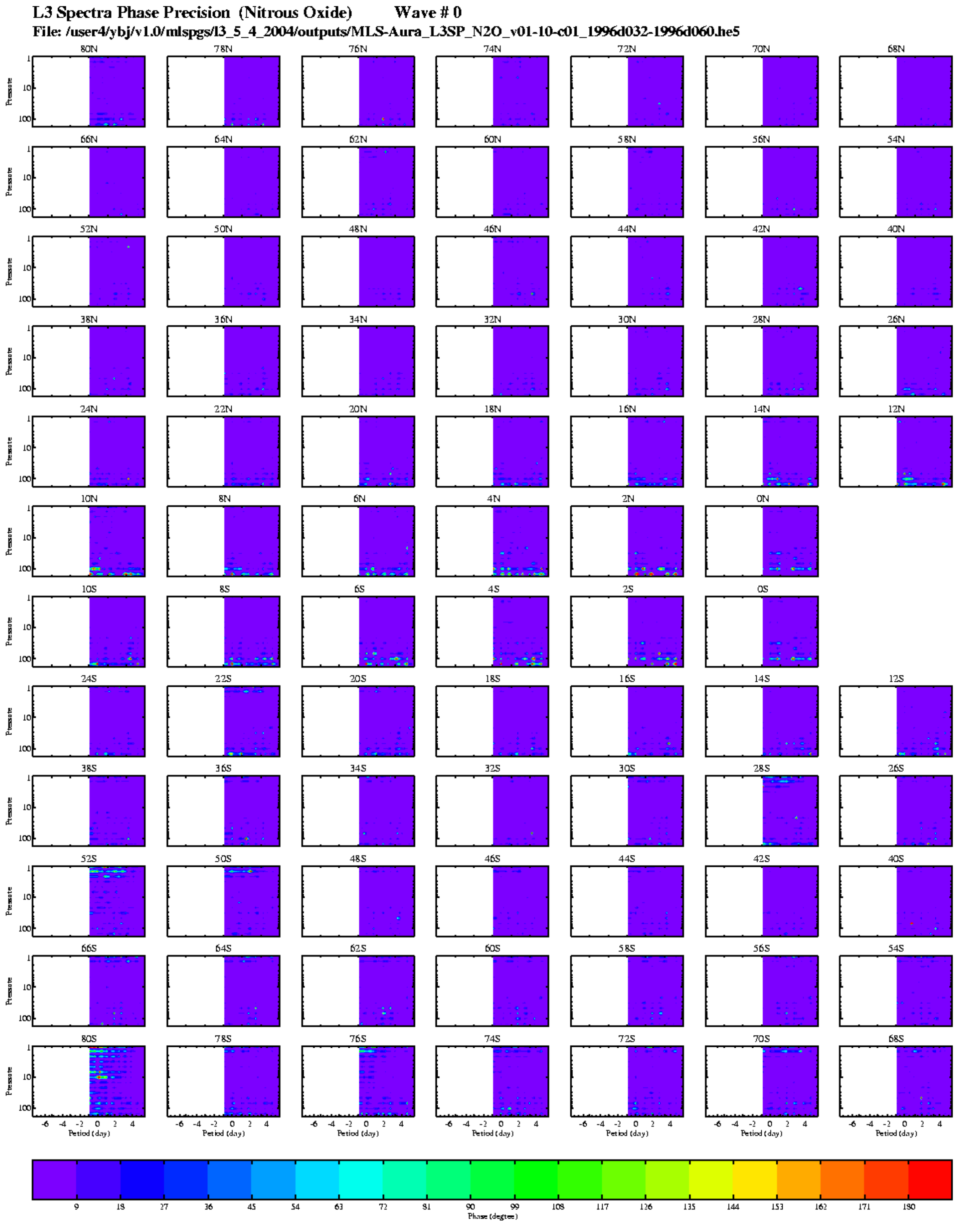
L3 Spectra Phase Precision (Nitrous Oxide) Wave # 0
File: /user4/ybj/v1.0/mlspgs/l3_5_4_2004/outputs/MLS-Aura_L3SP_N2O_v01-10-c01_1996d032-1996d060.he5
Pressure
Period (day)
Phase (degree)
Produced on 6-May-2004, v1.0

Figure E14-1

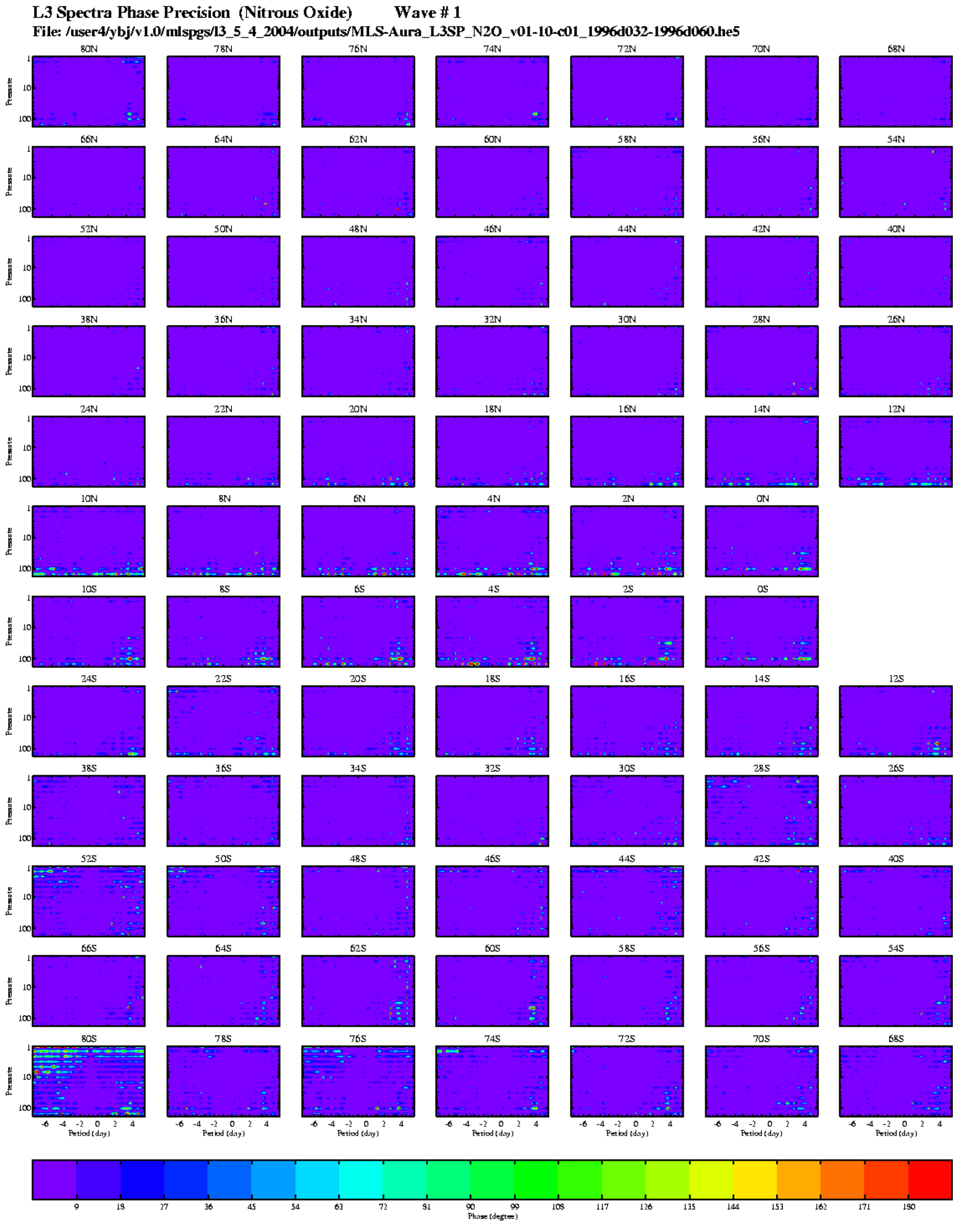
L3 Spectra Phase Precision (Nitrous Oxide) Wave # 1
File: /user4/ybj/v1.0/mlspgs/l3_5_4_2004/outputs/MLS-Aura_L3SP_N2O_v01-10-c01_1996d032-1996d060.he5
80N 78N 76N 74N 72N 70N 68N
66N 64N 62N 60N 58N 56N 54N
52N 50N 48N 46N 44N 42N 40N
38N 36N 34N 32N 30N 28N 26N
24N 22N 20N 18N 16N 14N 12N
10N 8N 6N 4N 2N 0N
10S 8S 6S 4S 2S 0S
24S 22S 20S 18S 16S 14S 12S
38S 36S 34S 32S 30S 28S 26S
52S 50S 48S 46S 44S 42S 40S
66S 64S 62S 60S 58S 56S 54S
80S 78S 76S 74S 72S 70S 68S
Pressure
1
10
100
-6 -4 -2 0 2 4
Period (day)
9 18 27 36 45 54 63 72 81 90 99 108 117 126 135 144 153 162 171 180
Phase (degree)
Produced on 6-May-2004, v1.0

Figure E14-2

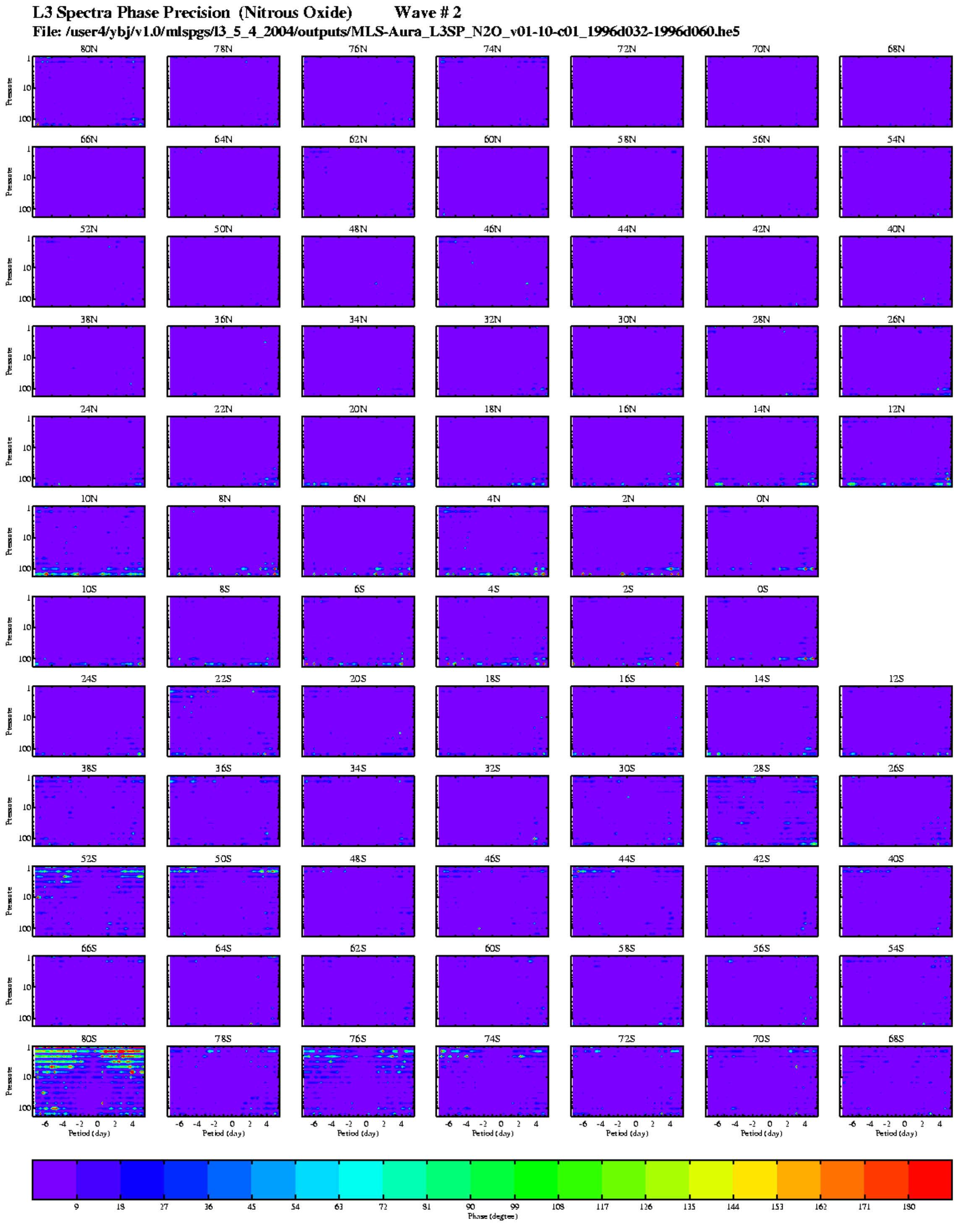
L3 Spectra Phase Precision (Nitrous Oxide) Wave # 2
File: /user4/ybj/v1.0/mlspgs/l3_5_4_2004/outputs/MLS-Aura_L3SP_N2O_v01-10-c01_1996d032-1996d060.he5
Pressure
Period (day)
Phase (degree)
Produced on 6-May-2004, v1.0

Figure E14-3

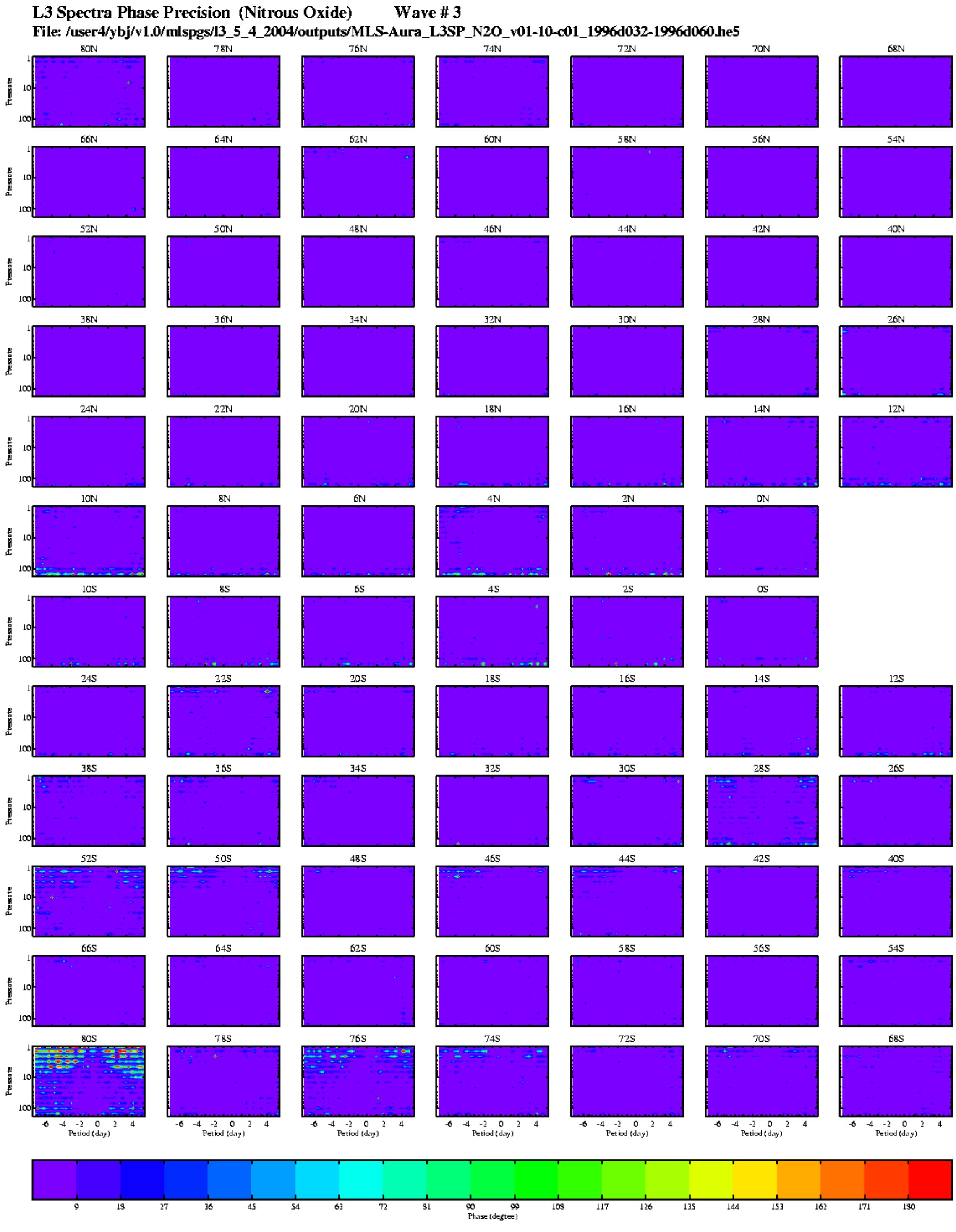
L3 Spectra Phase Precision (Nitrous Oxide) Wave # 3
File: /user4/ybj/v1.0/mlspgs/l3_5_4_2004/outputs/MLS-Aura_L3SP_N2O_v01-10-c01_1996d032-1996d060.he5
Pressure
Period (day)
Phase (degree)
Produced on 6-May-2004, v1.0

Figure E14-4

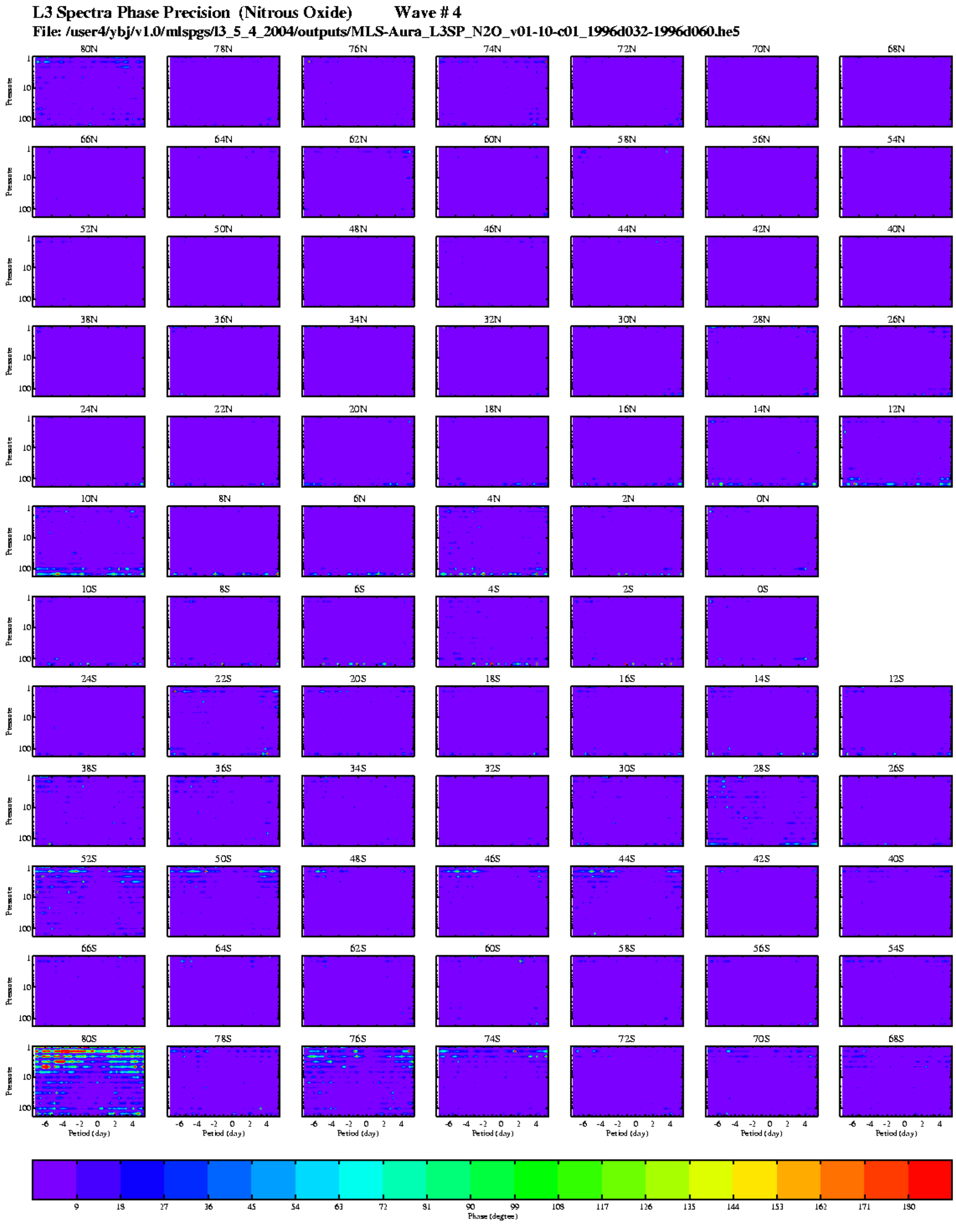
L3 Spectra Phase Precision (Nitrous Oxide) Wave # 4
File: /user4/ybj/v1.0/mlspgs/l3_5_4_2004/outputs/MLS-Aura_L3SP_N2O_v01-10-c01_1996d032-1996d060.he5
Pressure
Period (day)
Phase (degree)
Produced on 6-May-2004, v1.0

Figure E14-5

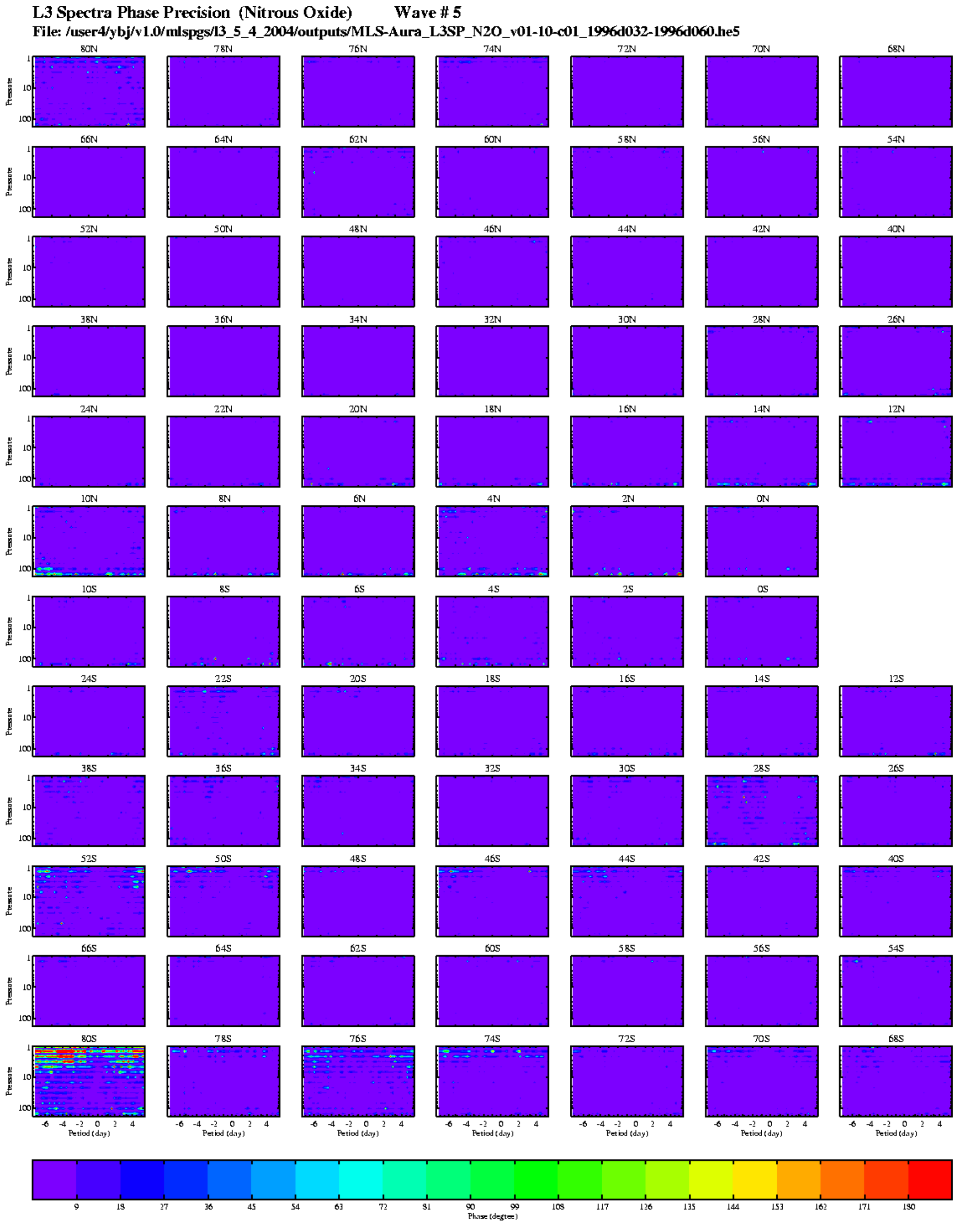
L3 Spectra Phase Precision (Nitrous Oxide) Wave # 5
File: /user4/ybj/v1.0/mlspgs/l3_5_4_2004/outputs/MLS-Aura_L3SP_N2O_v01-10-c01_1996d032-1996d060.he5
Pressure
Period (day)
Phase (degree)
Produced on 6-May-2004, v1.0

Figure E14-6

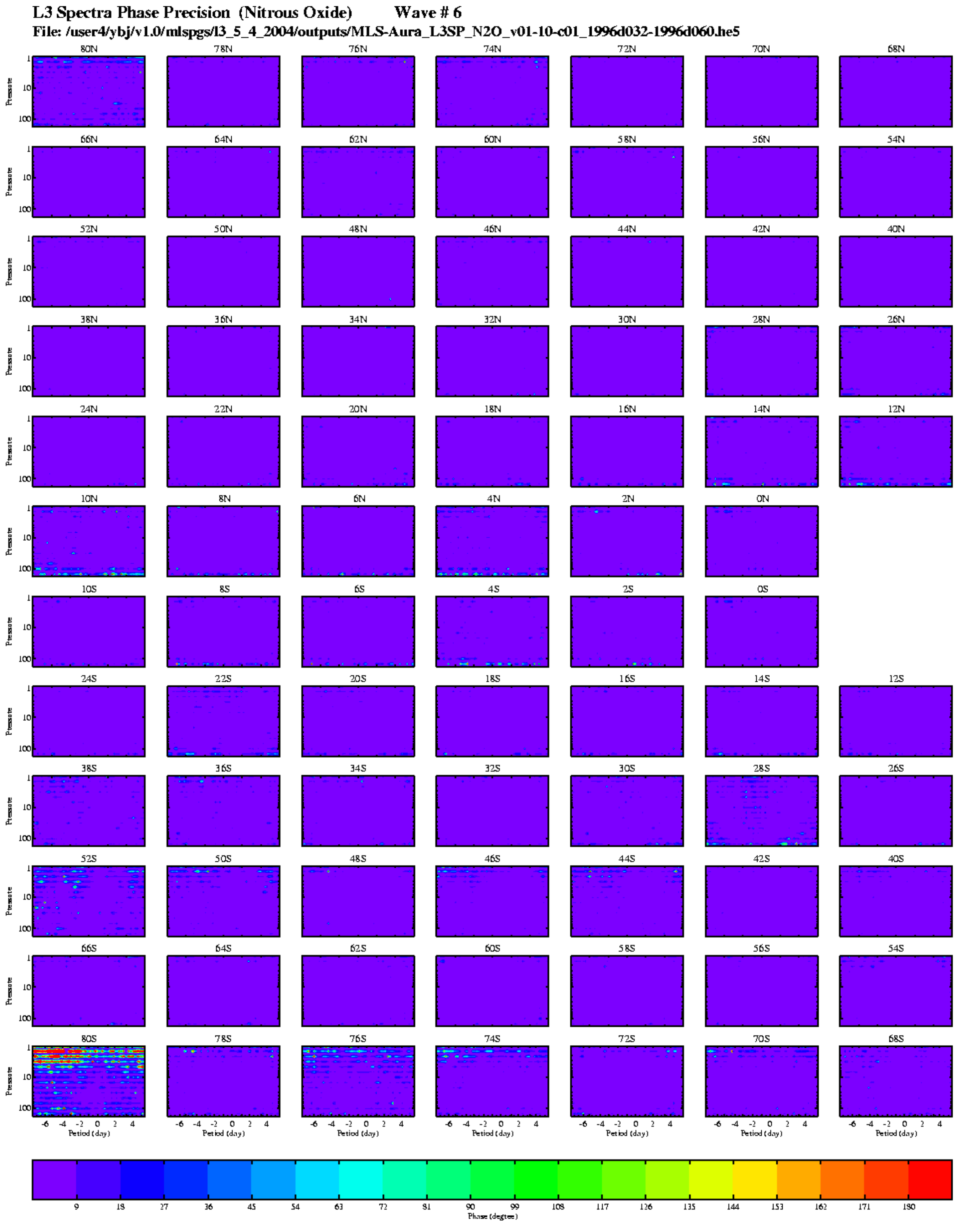
L3 Spectra Phase Precision (Nitrous Oxide) Wave # 6
File: /user4/ybj/v1.0/mlspgs/l3_5_4_2004/outputs/MLS-Aura_L3SP_N2O_v01-10-c01_1996d032-1996d060.he5
Pressure
Period (day)
Phase (degree)
Produced on 6-May-2004, v1.0

Figure E14-7

L3 Monthly Map: (Nitrous Oxide)
File: MLS-Aura_L3MM_Standard_V0-8-C01_1996-032-1996-060.dat

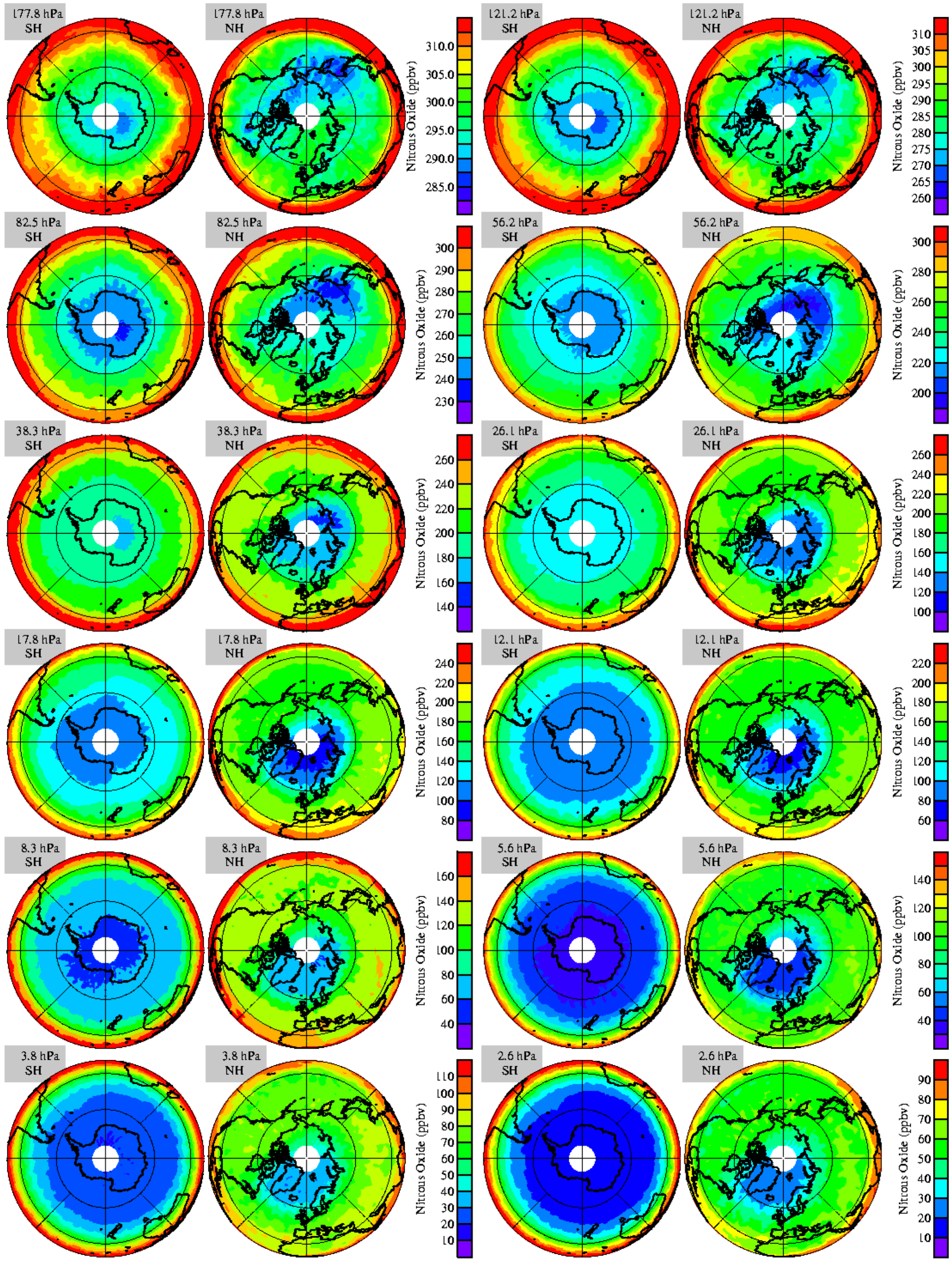

Figure E15

Produced on 15-Apr-2004, v1.0

L3 Monthly Map: (Nitrous Oxide)
File: MLS-Aura_L3MM_Standard_V0-8-C01_1996-032-1996-060.dat

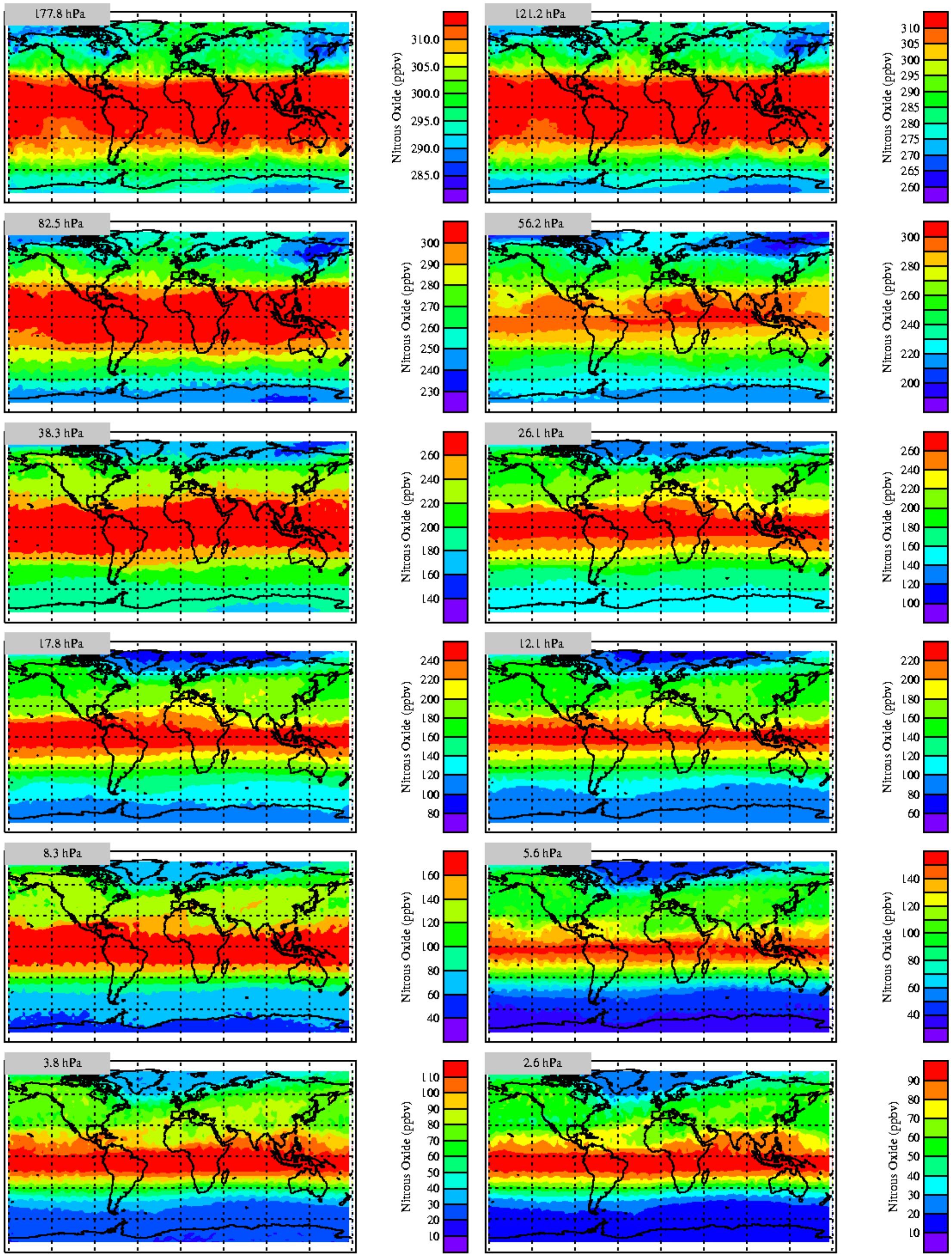

Figure E16

Produced on 15-Apr-2004, v1.0


L3 Monthly Longitude-Height Cross-Section Plot: (Nitrous Oxide)
File: MLS-Aura_L3MM_Standard_V0-8-C01_1996-032-1996-060.dat
Longitude
Nitrous Oxide (ppbv)
Produced on 15-Apr-2004, v1.0

Figure E17

L3 Daily Zonal Mean: (Nitrous Oxide)
File: MLS-Aura_L3DM_N2O_V0-7-C01_1996-050.dat

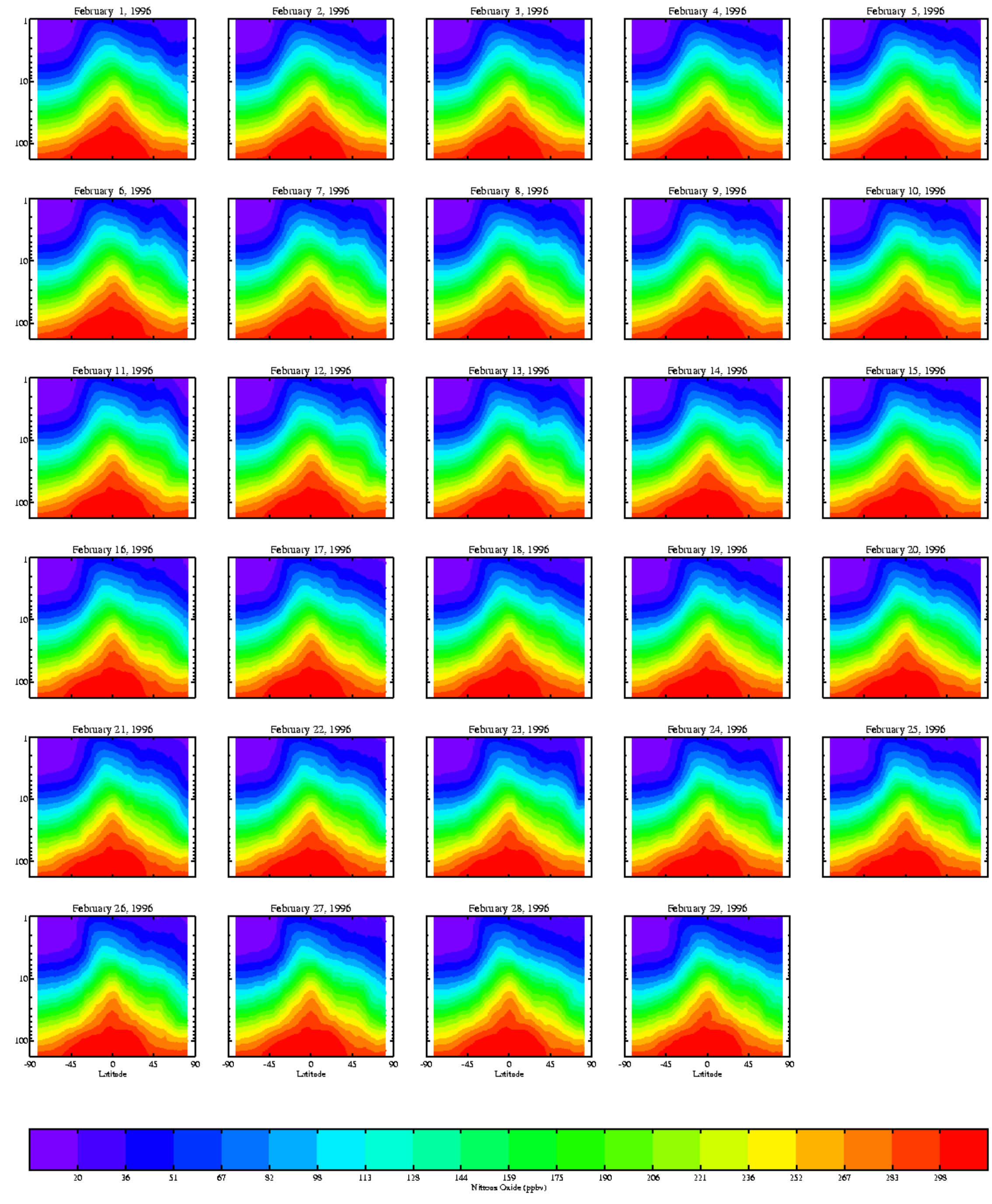

Figure E18

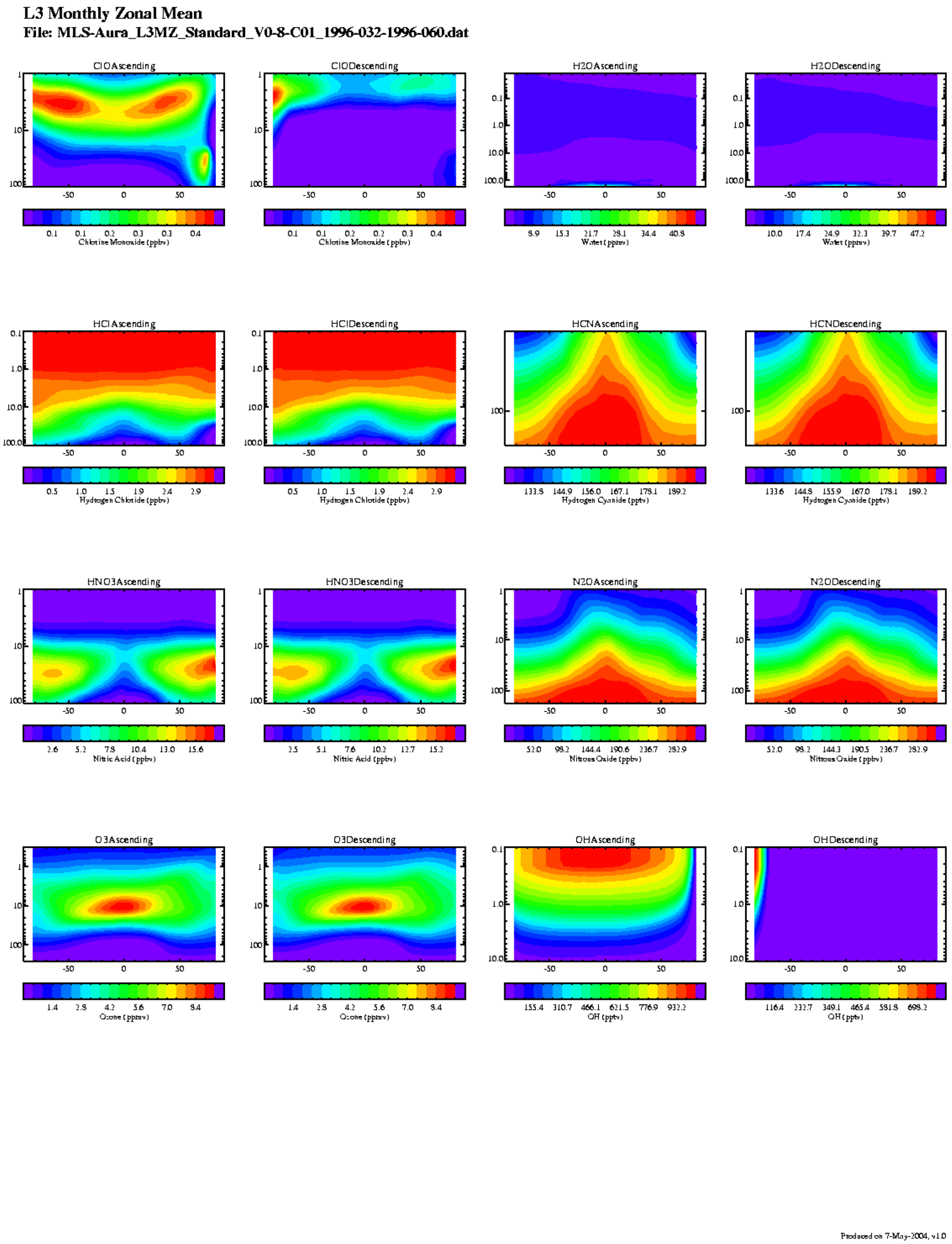
L3 Monthly Zonal Mean
File: MLS-Aura_L3MZ_Standard_V0-8-C01_1996-032-1996-060.dat
ClOAscending
ClODescending
H2OAscending
H2ODescending
Chlorine Monoxide (ppbv)
Water (ppmv)
HClAscending
HClDescending
HCNAscending
HCNDescending
Hydrogen Chloride (ppbv)
Hydrogen Cyanide (pptv)
HNO3Ascending
HNO3Descending
N2OAscending
N2ODescending
Nitric Acid (ppbv)
Nitrous Oxide (ppbv)
O3Ascending
O3Descending
OHAscending
OHDescending
Ozone (ppmv)
OH (pptv)
Produced on 7-May-2004, v1.0

Figure E19

References

Båth, M., 'Spectral Analysis in Geophysics,' *Elsevier*, Amsterdam, p95, 1974.

Brigham, O. E., 'The fast Fourier transform and its applications,' *Prentice Hall*., Englewood Cliffs, New Jersey 07632, 1988.

Canziani, P. O., J. R. Holton, E. Fishbein, L. Froidevaux, and J. W. Waters, 'Equatorial Waves: A UARS MLS view,' *J. Atmos. Sci*., **51**, 3053, 1994.

Chapman, W. A., M. J. Cross, D. A. Flower, G. E. Peckham and S. D. Smith, 'A spectral analysis of global atmospheric temperature fields observed by the selective chopper radiometer on the Nimbus 4 satellite during the year 1970-1,' *Proc. Roy. Soc. London*, A, **338**, 57, 1974.

Chapman, W. A., and J. McGregor, 'Application of complex demodulation to meteorological satellite data,' *Quart. J. Roy . Meteor. Soc*, 104, 213-223, 1978.

Elson, L. S., and L. Froidevaux, 'Use of fourier transforms for asynoptic mapping: Application to the Upper Atmosphere Research Satellite Microwave Limb Sounder,' *J. Geophys. Res*., **98**, 23039, 1993.

Elson, L. S., G. L. Manney, L. Froidevaux, and J. W. Waters, 'Large-scale variations in ozone from the 1st 2 years of UARS MLS data,' *J. Atmos. Sci*., **51**, 2867, 1994.

Hartmann, D., 'The structure of the stratosphere in the Southern Hemisphere during late winter 1973 as observed by satellite,' *J. Atmos. Sci*. **33**, 1141, 1976.

Hayashi, Y., 'Modified methods of estimating space-time spectra from polar-orbiting satellite data. Part I: The frequency transform method,' *J. Meteor. Soc. Japan*., **98**, 23039, 1983.

Jarnot, R.F., H. M. Pickett, and M. Schwartz,'EOS MLS Level 1 Data Processing Algorithm Theoretical Basis,' Jet Propulsion Laboratory Document D-15210**,** Version 2.0, April 8, 2004. (available on the MLS web site, http://mls.jpl.nasa.gov)

Lait, L. R. and J. L. Stanford, 'Applications of asynoptic space-time Fourier Transform Methods to scanning satellite measurements,' *J. Atmos. Sci*., **45**, 3784, 1988a.

Lait, L. R. and J. L. Stanford, 'Fast, long-lived features in the polar stratosphere,' *J. Atmos. Sci*., **45**, 3800, 1988b.

Limpasuvan V., and D.L. Wu, 'Two-day wave observations of UARS Microwave Limb Sounder mesospheric water vapor and temperature,' *J. Geophys. Res*., **108**(D10),4307, doi:10.1029/2002JD002903, 2003.

Livesey, N.J., and W. V. Snyder, 'EOS MLS Retrieval Processes Algorithm Theoretical Basis,' JPL Document D-16159, Version 1.3, June 21, 2004. (available on the MLS web site, http://mls.jpl.nasa.gov)

Rodgers, C., 'Evidence for the 5-day wave in the upper stratosphere,' *J. Atmos. Sci*. **37**, 237, 1976.

Salby, M.L., 'Sampling theory for asynoptic satellite observations. Part I: Space-time spectra, resolution and aliasing,' *J. Atmos. Sci*. **39**, 2577, 1982a.

Salby, M.L., 'Sampling theory for asynoptic satellite observations. Part I: Fast Fourier synoptic mapping,' *J. Atmos. Sci*. **39**, 2601, 1982b.

Salby, M.L., 'Climate monitoring from space: Asynoptic sampling considerations,' *Amer Meteor. Soc* 2, 1091, 1989.

Salby, M.L., and F. Sassi, 'Synoptic mapping of convective structure from undersampled satellite observations,' *J. Climate*, **14**, 2281-2295, 2001.

Sassi, F., and M.L. Salby, 'Fast Fourier synoptic mapping of UARS data,' *J. Geophys. Res*, **103**, 10885-10898, 1998.

Waters, J.W., 'An Overview of the EOS MLS Experiment,' JPL Document D-15745, Version 2.0, April 2, 2004. (available on the MLS web site, http://mls.jpl.nasa.gov)